Applied Materials Today 42 (2025) 102574

Contents lists available at ScienceDirect

Applied Materials Today

journal homepage: www.elsevier.com/locate/apmt

Nanomaterial advanced smart coatings: Emerging trends shaping the future

Vishnu V. Pillai [a], Brindha Ramasubramanian [b], Olivia Sequerth [c], Srikanth Pilla [c,d,e,f], Tao Wang [g], Amar K Mohanty [g,h], Premika Govindaraj [a], Saeed M. Alhassan [j], Nisa Salim [a], Peter Kingshott [a], Franz Konstantin Fuss [i], Seeram Ramakrishna [b], Nishar Hameed [a,*]

[a] Swinburne University of Technology, Australia
[b] National University of Singapore, Singapore
[c] Center for Composite Materials, University of Delaware, Newark, DE 19716, United States
[d] Department of Mechanical Engineering, University of Delaware, Newark, DE 19716, United States
[e] Department of Materials Science and Engineering, University of Delaware, Newark, DE 19716, United States
[f] Department of Chemical and Biomolecular Engineering, University of Delaware, Newark, DE 19716, United States
[g] Bioproducts Discovery and Development Centre, Department of Plant Agriculture, Crop Science Building, University of Guelph, 50 Stone Road East, Guelph, Ontario, Canada
[h] School of Engineering, Thornabrough Building, University of Guelph, 50 Stone Road East, Guelph, Ontario, Canada
[i] Chair of Biomechanics, Faculty of Engineering Science, University of Bayreuth, Germany
[j] Department of Chemical Engineering, Khalifa University of Science and Technology, P.O. Box 127788, Abu Dhabi, United Arab Emirates

ARTICLE INFO

Keywords:
Nanomaterials
Internet of Things
Real-Time Sensing
Electronic skin
Sustainability

ABSTRACT

Advancements in nanotechnology have positioned coatings as a pivotal field with the potential to significantly impact both industry and society. This review delves into nanomaterials and their potential to create smart coatings capable of real-time monitoring and flexible electronics applications. The mechanisms of conductivity and sensing capabilities within these coatings are emphasized to highlight their importance in the context of artificial intelligence. Furthermore, the current trends shaping the coatings industry are summarized, such as the concept of electronic skin (E-skin) and increasing focus on sustainability. In the digital era, the integration of the Internet of Things (IoT) is set to transform the future of coatings, enhancing their intelligence and environmental interactivity. Smart coatings are poised to revolutionize our interaction with the environment, spanning applications from consumer goods to robotics and sensors. The ongoing development of these materials and technologies promises to unlock new and exciting possibilities. By discussing the above aspects in detail, this review positions itself as a forward-looking contribution that summarizes the state-of-the-art and anticipates future directions for smart coatings, offering insights into how ongoing advancements can unlock new possibilities for both industrial applications and societal impact.

1. COATINGS: an overview of state-of-the-art

Coatings have played a significant role throughout history, from prehistoric cave paintings to advanced coatings in various industries. It is a crucial topic in the scientific community, and the reasons for this widespread attention are its potential to combine the bulk properties of a substrate with the tailored capabilities of a layer at the surface and the availability of various deposition techniques [1,2]. Coatings can provide enhanced functionality by incorporating functional additives in low concentrations. By utilising these additives, the properties of the coatings are improved significantly, making them versatile and suitable for a wide range of applications. In addition, coatings reduce maintenance costs and extend the lifetime of products. Stimuli-responsive materials in coatings enable them to sense and react to environmental alterations, including temperature, force, sound, pH, electric and magnetic field (Fig. 1) [3]. Though the selection of strategy for the synthesis of coatings depends highly on the desired application, the most common methods used for the fabrication of coatings include electrochemical plating, conversion coatings, chemical and physical vapour depositions, thermal spray coating, sol-gel coatings, micro- and nanocapsule based coatings. Amongst, *electrochemical plating* is the simplest and most cost-effective method for coating metals to a substrate [4,5]. Aoki et al. reported a

* Corresponding author.
E-mail address: nisharhameed@swin.edu.au (N. Hameed).

https://doi.org/10.1016/j.apmt.2024.102574
Received 24 September 2024; Received in revised form 15 December 2024; Accepted 23 December 2024
Available online 30 December 2024

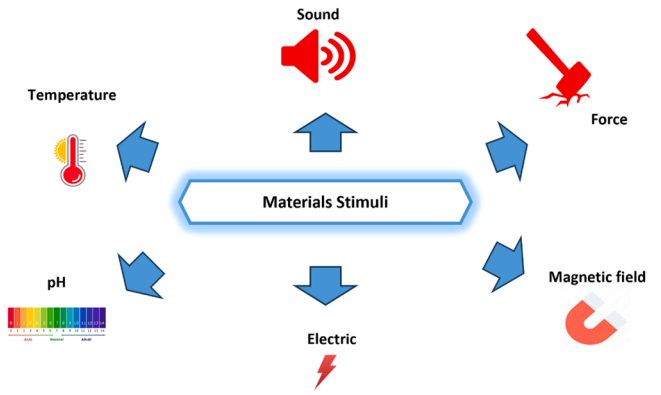

Fig. 1. Schematic representation of stimuli-responsive materials.

reversible electrochromic mirror for smart window applications by utilising the electroplating method to coat a film of Ag onto a transparent ITO electrode [6]. Kim et al. employed the electroplating technique to deposit nickel nanocones and zinc oxide nanosheets onto fabric, producing multifunctional materials that are wearable, stretchable, washable, hydrophobic, and antibacterial. Additionally, these materials exhibited sensing, heating, and supercapacitive properties [7]. They are widely used in self-cleaning [8], optically active [9], anti-corrosion [10], anti-bacterial, and anti-fouling applications [11] in various industries, such as automotive, military, biomedical, building, and construction (Fig. 2). The introduction of nanotechnology boosted the coating industry by creating novel coating formulations, resulting in the development of multifunctional coating systems [12]. Carbon nanotubes (CNTs) are used for enhancing physical reinforcement and conductivity properties; nanoclays for improved barrier properties and low cost; titanium, cerium, and zinc oxide nanoparticles for UV absorption properties due to their combination of efficiency and lack of migration from the film are few examples of such nanomaterials [13–15].

There is an emerging trend in shifting electronic components and circuits from rigid substrates to more flexible and stretchable materials like thin plastics, textiles, and foams. To achieve this transition, there is a need for advanced formulations/coatings that are smart, cost effective and sustainable [25]. Similarly, due to urbanization, there is a huge demand for mass transport, building infrastructure, and renewable energy industries. Traditional structural health monitoring (SHM) methods include visual inspection, destructive testing, and static monitoring. However, these conventional methods can be capital-intensive due to the associated operational and maintenance costs. Therefore, real time SHM is critical for these sectors to maintain safety and long-term performance. The use of fibre reinforced polymer composites (FRP) is rapidly increasing in the afore mentioned industries to achieve lightweight, strength, and long-term durability [26]. FRP composites traditionally struggle with inadequate out-of-plane properties, which can compromise their overall structural integrity. Additionally, FRP materials' inherent lack of conductivity poses challenges when incorporating sensing and data transmission systems into composite structures [27]. Coating reinforcements with nanofillers can improve the mechanical and physical properties of the composite while imparting sensing abilities and endowing multifunctional properties to the final structure [28,29]. Smart coatings have the potential to provide a lightweight and cost-effective solution by being applied to various structural elements, including complex three-dimensional shapes. These coatings can also be highly customizable and offer sensing capability. Compared to individual strain gauges that are adhered and wired separately, smart coatings require fewer and less complex installation steps and are less likely to fail [30]. Smart coatings allow real-time data analysis by integrating advanced sensor technology with intelligent algorithms. The field of smart coatings for SHM is experiencing a swift evolution marked by continuous research and development efforts. Unlike previous reviews [25,31–38], which often provide a broad overview of smart coatings or focus on a single aspect, this work distinguishes itself by offering a focused analysis of the integration of nanomaterials in smart coatings. It emphasises advancements in conductivity mechanisms and sensing capabilities specifically tailored for SHM applications and flexible electronics. This review serves as a one-stop resource for readers interested in smart coatings, presenting an amalgamation of emerging trends and advancements in the field. By the end of this review, readers will gain a comprehensive understanding of the latest developments in smart coatings, including a deep dive into emerging trends such as electronic skin (E-skin) and sustainability, which are transforming the coatings industry. Furthermore, this review highlights the pivotal role of smart coatings in the Internet of Things (IoT) era, exploring their potential to enhance environmental interactivity and revolutionise sectors ranging from consumer goods to robotics and sensors.

In this review, we will focus on the following key points:

- A detailed analysis of different nanomaterials in smart coatings, exploring their properties, synthesis methods, and applications.
- Discussing the integration of smart coatings for developing electronic skin with enhanced functionalities.

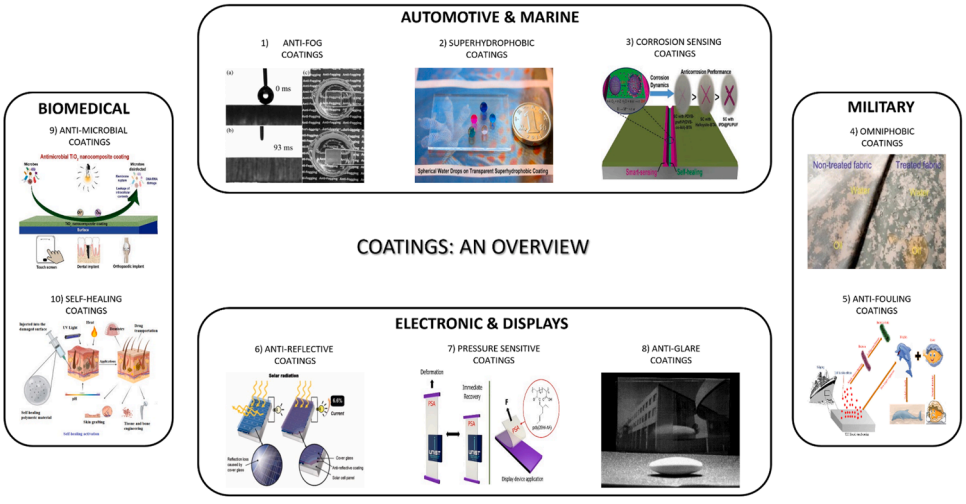

Fig. 2. An overview of smart coatings [11,16–24].
Reproduced with Permission

- Delving into the sustainability aspects of smart coatings and their environmental implications.

By the end of this review, readers will have a comprehensive understanding of the latest developments in smart coatings.

2. Nanomaterials for smart coatings

2.1. Carbonaceous materials: CNTs & graphene

The utilization of carbon-based materials has generated significant interest in the development of smart coatings. Carbon, the fundamental element for life on Earth, plays a crucial role in a multitude of technological applications. This is due to carbon's exceptional ability to bind to itself and all other elements in countless ways. The two natural allotropes of elemental carbon are diamond and graphite, which consist of extended networks of sp3- and sp2-hybridized carbon atoms, respectively. Both forms exhibit unique physical properties such as hardness, thermal conductivity, lubrication behavior, and electrical conductivity. The discovery of fullerenes in 1985 by Kroto et al. marked the beginning of a growing family of synthetic carbon allotropes, including the synthesis of CNTs in 1991 and graphene in 2004 (Fig. 3) [39].

One-dimensional (1D) tubes, known as CNTs, are remarkable materials with a high aspect ratio ranging from 30 to 1000. In addition, CNTs possess unique properties such as high mechanical strength, excellent electrical conductivity, and remarkable thermal conductivity. CNTs have shown immense potential for various applications, including developing lightweight and strong materials, high-performance electronic devices, and efficient energy storage devices [40]. However, challenges still need to be solved in synthesizing and processing CNTs, such as the production of defects in the nanotube structure and difficulties in achieving uniform dispersion in composites. Over the years, various techniques have been developed for the fabrication of CNTs that can be tailored to suit specific applications. Each synthesis process results in CNTs with varying electrical, mechanical, and thermal properties. Among the different techniques used for CNTs fabrication, the three most employed methods are chemical vapor deposition (CVD), laser ablation, and arc discharge. Despite the advantages of laser ablation and arc discharge techniques, CVD has become the industry's most standardized and widely used technique. This is due to its simplicity, low cost of fabrication, and ability to produce CNTs on a large scale. In terms of yield, defects, and characteristics, the three production techniques for single-walled (SWCNTs) and multi-walled (MWCNTs) differ in several ways (Table 1). Notably, high yields of both SWCNTs and MWCNTs can be obtained using all three fabrication techniques. However, the physical properties of the resulting CNTs, such as their length and diameter, vary depending on the specific synthesis process employed. Therefore, the selection of a CNTs fabrication technique must be based solely on the specific properties required for the intended application of the resulting CNTs [41,42].

Table 1
Comparing CVD, laser ablation, and arc discharge techniques for fabrication of SWCNTs and MWCNTs: yield, defects, and characteristics analysis [43].

PARAMETERS	ARC DISCHARGE	CHEMICAL VAPOR DEPOSITION	LASER ABLATION
ADVANTAGES	Inexpensive; Easy fabrication process; Few structural defects particularly on SWCNTs	Simple process; High Purity; Easy scaling up	Good diameter of CNTs Few defects
DEFECTS	Need a lot of purification	Often riddled with defects	Fewer defects but the technique is expensive
DISADVANTAGES	Nanotubes are short and randomly oriented; Requirement of post-processing steps	Many Defects	Very Expensive; High power requirement
MWCNTs	Short tubes with inner diameter of 1 – 3 nm and outer diameter of approx.10 nm	Long tubes with a diameter of 10 – 240 nm	Synthesis is possible, but due to higher cost – not used often
SWCNTs	Short tubes with a diameter of 0.6 – 1.4 nm	Long tubes with a diameter of 0.6 – 4 nm	Long bundles of tubes with Individual diameter of 1 – 2 nm
YIELD (%)	3090	20100	≤70

CNTs have exceptional electrical properties, making them perfect for creating flexible electronic devices like sensors, transistors, and biological sensing labels. SWCNTs and MWCNTs have been widely used as processing materials to develop piezoresistive strain sensors. Due to the high interfacial bonding of CNTs with most polymers, they are often embedded in polymeric substrates, which are functionalized to increase their ability to link with the associated substrates. Researchers have been working to enhance the efficiency of piezoresistive sensors using various methods, including modifying CNTs-based electrodes with other

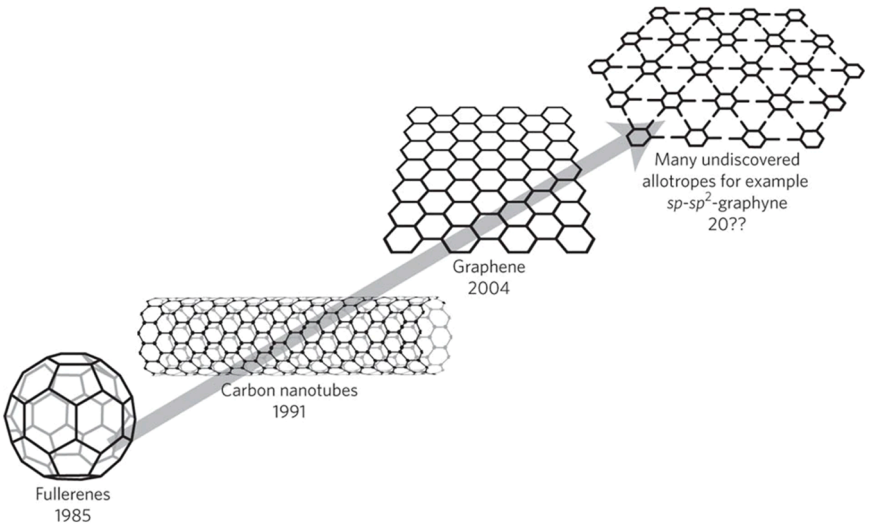

Fig. 3. The genesis of synthetic carbon allotropes [39] Reproduced with Permission.

polymers and nanomaterials to increase their efficiency in reduced recovery and response times toward the tested application. As a result, various prototypes have been developed for piezoresistive strain sensing, contributing to the development of flexible wearable electronic devices and healthcare monitoring units [41]. Tang et al. developed a highly conductive CNTs/TPU composite nanofiber yarn by simply dip-coating CNTs ink (Fig. 4), which shows a resistance of 1.02 kΩ/cm. The study has explored the effects of coating methods on strain sensing performance and mechanism. This yarn-based strain sensor showed a 440 % relative resistance change at a 140 % strain, with satisfactory linearity and repeatability of 1250 cycles. A smart sports bandage was developed using this yarn to detect the motion of the wrist, elbow, knee, abdomen and chest, which could assist in training for badminton, basketball, and running and applied in medical monitoring for heart rate and respiratory rate. This paper provides a new strategy for developing flexible strain sensors based on yarn that can be directly integrated into fabrics. Overall, this strain sensor technology has immense possibilities in developing wearable technology that is both efficient and comfortable, thereby revolutionizing the field of healthcare and sports (Fig. 5) [44].

Novel coating formulations with carbonaceous nanofillers (Table 2), can improve the interfacial bonding and enhance the matrix's stiffness and strength, leading to improved flexural properties [45]. Two approaches are commonly used to incorporate nanomaterials into composites: (1) by mixing the nanomaterials in the resin and (2) by directly coating the nanomaterials onto the reinforcement. Previous studies have reported that fillers, such as carbon nanomaterials, were mixed into resin before composite manufacturing. This mixing aimed to disperse the nanofillers evenly within the resin, enhancing the properties of the composite, such as electrical conductivity and mechanical strength (Fig. 6). Graphene has emerged as a highly promising carbonaceous nanofiller for enhancing these properties. Despite its ability to enhance the structural properties of FRPs, integrating graphene-based materials into composites has been shown to significantly enhance various functional properties. These include electrical and thermal conductivity, sensing and surveillance, actuation, energy harvesting and storage, self-healing capability, electromagnetic interference (EMI) shielding, reusability, and environmental degradation [46–48].

The incorporation of CNTs into polymer composites presents several challenges, including low yield production, high production costs, and complex processing requirements, which currently hinder their widespread practical application in various industries [10]. Graphene, with its distinct properties arising from a single layer of carbon atoms arranged in a two-dimensional honeycomb lattice, has garnered significant interest as a potential carbon-based nanomaterial. Due to graphene's outstanding electrical conductivity(1738 siemens/m) [59], strong mechanical properties(Young's Modulus ~1100 GPa & Fracture strength ~125 GPa) [60], high thermal conductivity (~5000 $Wm^{-1}K^{-1}$) [61] and large surface area, it is highly sought after for numerous applications in electronics, energy storage, and biomedical devices [62]. Additionally, graphene's comparatively simpler production process and scalability have made it a more practical option for large-scale industrial applications [63,64]. Graphene functionalization fast-tracked the development of various composites and hybrid materials with enhanced properties, leading to potential applications such as water purification [65], energy storage [66], coatings [34], electronics [67], etc. Top-down and bottom-up are the two ways to synthesize graphene, which determines the number of layers, thickness, nature, and the average size of graphene materials. Mechanical exfoliation [68], chemical exfoliation [69], and chemical synthesis [70] are categorized under the former graphene synthesis approach. In contrast, epitaxial growth [71], pyrolysis [72], and chemical vapor deposition(CVD) [73] are the bottom-up methods for the synthesis of graphene (Fig. 7).

There are several methods for producing graphene, each with its own advantages and limitations in terms of quality and scalability potential. The scalability potential and quality of various common methods of graphene production are summarized in (Fig. 8). Two primary techniques for producing graphene on a large scale are liquid-phase exfoliation and reduction of GO. The former method entails dispersing particles of pristine or graphite expanded in a solvent, which weakens the van der Waals forces that bind the graphene layers. External forces, such as ultrasonication, shearing, or an electric field, are subsequently applied to separate the graphite into individual sheets of graphene. During the reduction of GO, pristine graphite is first oxidized to produce GO, which is then stirred or exposed to ultrasonication in a liquid medium. The GO is subsequently reduced to graphene, resulting in a restored graphene network. This method involves several chemical, thermal, and electrochemical processes and is typically performed in a specific sequence to produce reduced GO (rGO) [63]. GO, rGO, GNPs, graphene nanoribbons (GNRs), and graphene quantum dots (GQDs) are other derivatives of graphene that can be integrated with polymers to develop novel materials with enhanced properties. Low-cost, large-scale production, biocompatibility, and oxygenated functional groups make GO a perfect candidate for coating applications [74,75]. A commonly used method for synthesizing GO is the Hummers method; strong oxidizing agents used in this method will exfoliate and functionalize each sheet or the detached group of sheets from graphite [76]. Marcano et al. reported an improved Hummers method with higher hydrophilic oxidized graphitic material through an oxidation procedure with increased $KMnO_4$ (exclusive of $NaNO_3$) and concentrated mixture of H_2SO_4/H_3PO_4 in the ratio of 9:1 with zero emission of toxic gases such as NO_2, N_2O_4, etc. [77]. Yu et al. proposed an improved Hummers method by partly replacing $KMnO_4$ with K_2FeO_4 and controlling the amount of concentrated sulfuric acid to synthesize GO that reduced the

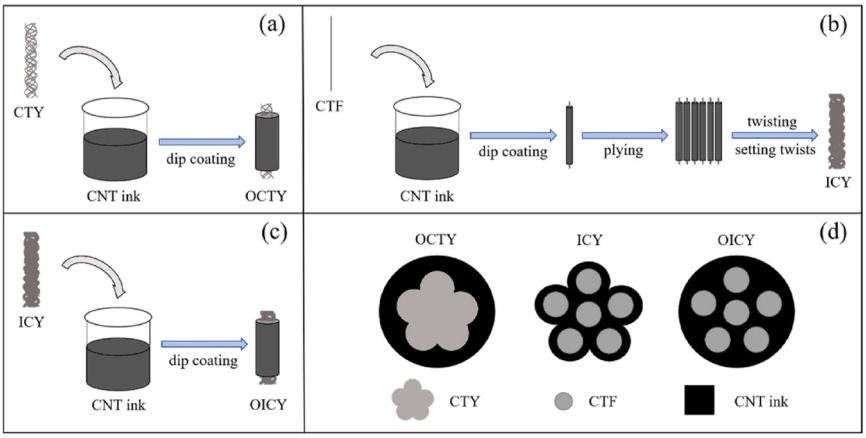

Fig. 4. Schematics of highly conductive CNTs/TPU composite nanofiber yarn fabrication by simply dip-coating CNTs [44].

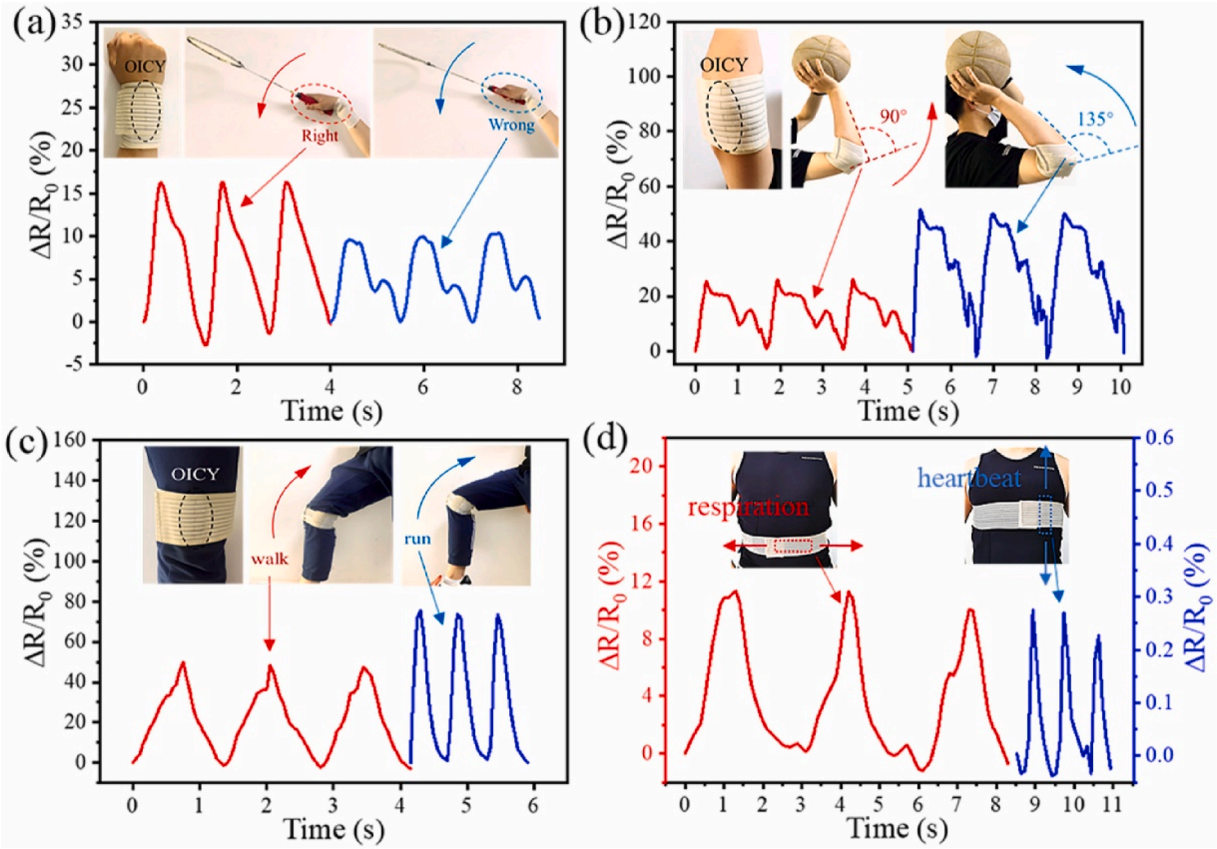

Fig. 5. The smart sports bandage can be utilised in various sports and healthcare settings, as depicted in the following images: (a) badminton, (b) basketball, (c) walking and running, and (d) monitoring respiration and heartbeat. Reproduced with Permission [44].

Table 2
:Carbonaceous nanofiller with glass and carbon fibres.

CARBONACEOUS NANOFILLER	FIBRE TYPE	MATRIX	METHOD & APPLICATION	REF.
CNTs	GF	Epoxy	CVD Cure self-monitoring and load self-sensing of FRPs	[49]
CNTs	GF	Epoxy	Flame synthesis Enhance interface properties	[50]
CNTs	GF	Epoxy	Layer by layer deposition Strain sensor for Structural health monitoring	[51]
CNTs	CF	Polydimethylsiloxane (PDMS)	Spray Process Multifunctional wearable electronics	[52]
CNTs	CF	Polyimide (PI)	Ultrasonic dispersion Improved interlaminar properties	[53]
Graphene	GF	Epoxy	Blade coating Strain sensing	[34]
GO	GF	Epoxy	Compression moulding Improved thermomechanical properties	[54]
LIG	GF	Epoxy	Transfer printing Structural health monitoring	[55]
GNPs/CNTs	GF	Epoxy	Dispersion process In situ damage monitoring of composites	[56]
GNPs	CF	Epoxy	Infusion process Structural applications	[57]
Graphene	CF	Polypropylene	Melt blending Transport Industry	[58]

GNPs – graphene nanoplatelets; LIG- Laser induced graphene; GO- graphene oxide, CNTs- Carbon nanotubes.

consumption of reactants and enabled a scalable production [78].

Graphene-based stimuli-responsive materials spontaneously response to external stimulations due to their sensitivity to different types of stimuli. For example, they can change their mechanical, electrical, or optical properties when exposed to other environmental conditions [80]. Multifunctional graphene coatings are developed by combining different derivatives of graphene nanomaterials with suitable polymer chemistry. Graphene-reinforced waterborne epoxy nanocomposites were reported to limit the water molecules' diffusion to the metal and reduce the corrosion rate significantly compared to the neat epoxy coatings [88]. Hu et al. developed a composite coating using functional GO and CNTs in epoxy. The coating showed improved

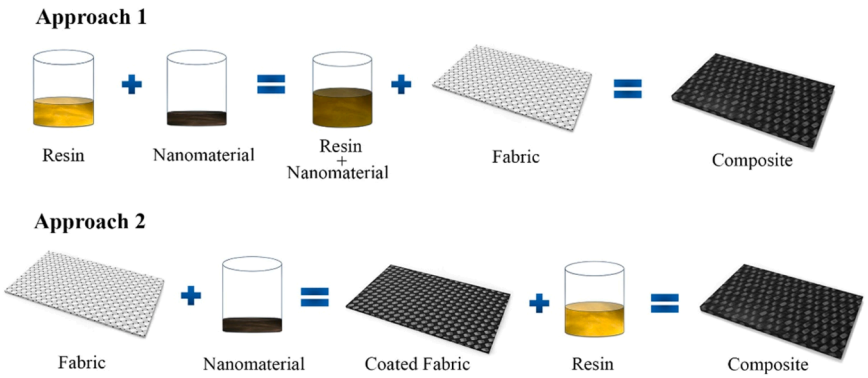

Fig. 6. Incorporation strategies of nanomaterials into composites [37] Reproduced with Permission.

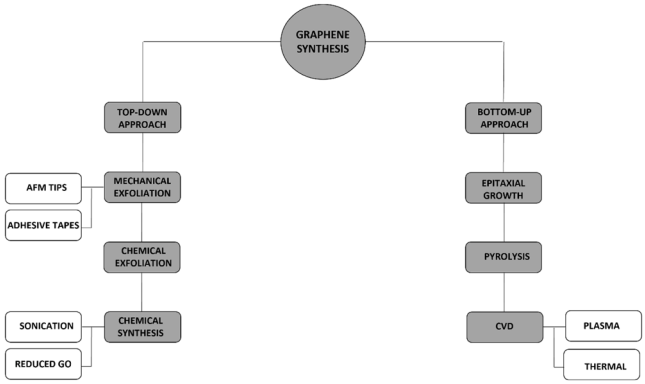

Fig. 7. Schematic representation of different approaches in graphene synthesis.

anticorrosion performance due to the synergistic effect of CNTs and GO. CNTs acted as a bridge, connecting GO sheets, and blocking corrosion. Functional GO enhanced compatibility and dispersion, providing a better barrier against corrosion. Overall, the composite coating demonstrated enhanced corrosion resistance [81]. Feng et al. developed GO-based Epoxy nanocomposites with BTA-loaded mesoporous silica nanocontainers that endowed the coating system with anti-corrosive and self-healing properties. BTA-SiO_2-GO exhibited good dispersibility in the epoxy coatings, contributing to better pH responsiveness and physical barrier properties [89]. These materials' sensitivity ranges from stimuli such as pH value, mechanical strain, thermal, electrical field, optical excitation, and gaseous or biological molecules [82] (Table 3).

Graphene dispersion refers to the process of uniformly dispersing graphene flakes or their derivatives in a solvent, binder or polymer matrix. This process is essential for achieving homogeneous graphene distribution and ensuring the graphene's desirable properties are maintained in the final product. The ability of graphene to disperse depends on the properties of both the solvent and graphene, including their solubility and surface tension parameters (Hildebrand and Hansen solubility parameters). The interactions between the solvent and graphene can be classified into three categories: dispersive (D), polar (P), and hydrogen bonding. Ensuring optimal graphene dispersion is imperative for enhancing composite materials' mechanical strength, thermal conductivity, and electrical conductivity [102,103]. In-situ sensors made with nanomaterials are becoming promising for process monitoring and self-sensing applications in composites. These sensors have several advantages, including mechanical robustness, non-invasive application, interfacial conformability, and controllable piezoresistive sensitivity. Graphene is an interesting material, not only because it is the thinnest known material with unique electrical and mechanical properties but also due to its linear change of resistance versus strain, making it a good candidate for piezoresistive sensor applications. When graphene-based nanomaterials are deposited on reinforcements using various methods, they form an electrically conductive network. Any disruption in the conductive path created by these nanomaterials due to external forces can change the overall electrical resistance of the system, which can be correlated to the physical phenomenon being monitored. The integration of graphene-based nanomaterials into FRP composites has resulted in significant improvements in structural and non-structural functionalities. As a result, a variety of smart composites for emerging novel applications have been developed. The integration of graphene-based nanomaterials into FRP composites has significantly improved structural and non-structural functionalities. As a result, various smart composites for emerging novel applications have been developed. The proper integration of graphene materials into FRP composites has been shown to significantly improve their functional properties, including electrical and thermal conductivity, sensing and monitoring, actuation, energy harvesting and storage, self-healing capability, EMI shielding, recyclability, and biodegradability [26,104,105]. Bathusha et al. reported a novel approach for in-situ monitoring of crack propagation and fracture behaviour in glass fibre-reinforced polymer (GFRP) composites using embedded rGO-coated fabrics and highly conductive GnP paper. The GFRP was manufactured through a vacuum-assisted resin infusion process, allowing piezoresistivity to be monitored at each stage. Two piezoresistive sensors, rGO-coated fabric and GnP paper, were embedded in GFRP laminates to enable in-situ monitoring of crack propagation and fracture behavior under both in-plane and out-of-plane loadings. Tensile tests on rGO-coated sensors showed that piezoresistivity varied inversely with the load rate. Additionally, the rGO-coated fabric sensors gradually increased piezoresistivity, followed by a steep, exponential rise. SEM analysis of fractured surfaces indicated that crack propagation in both pristine and rGO-coated laminates was driven by brittle matrix fracture and fibre/-matrix de-cohesion. Laminates with 50 μm GnP paper showed the highest sensitivity under Mode-I loading, although their interlaminar fracture toughness was reduced by 70 % compared to pristine laminates [106] (Fig. 9).

2.2. *Transition metal dichalcogenides*

The development of graphene and its distinctive properties have led to the discovery of a new category of nanomaterials called 2D transition metal dichalcogenides (TMDs). TMDs, due to their strong strain-induced bandgap modification and thereby large gauge factors, are widely explored in high-performance piezoresistive sensors. TMDs exhibit tunable optical and physical properties due to their nanosized thickness and quantum size effect. As a result, the transport of photons, phonons, and charge carriers can be confined to the 2D plane, leading to significant changes in their electronic and optical properties. 2D TMDs display a variety of properties, ranging from metals (e.g., $NbTe_2$, TaS_2), semimetals (e.g., $TiSe_2$, WTe_2), and superconductors (e.g., NbS_2, $PdTe_2$), to

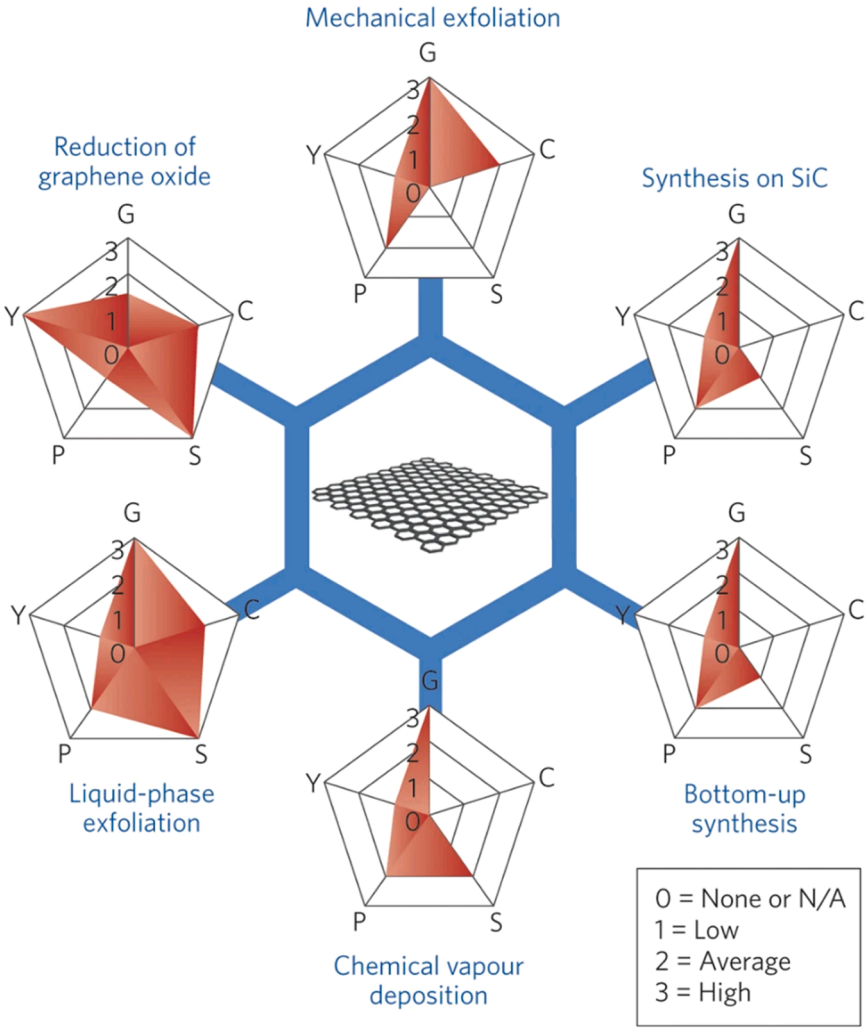

Fig. 8. A schematic illustration of commonly employed techniques to produce graphene. [79] Reproduced with Permission.
Each method has been assessed based on the quality of graphene (G), the cost aspect (C); where a low value corresponds to a high cost of production), scalability (S), purity (P), and yield (Y) of the overall production process.

Table 3
Graphene smart materials and their different stimuli responses.

STIMULI RESPONSE TYPE	GRAPHENE SMART MATERIAL	PREPARATION METHODOLOGY	APPLICATION	REF.
THERMAL	GO-PVA/PNIPA nancomposites	In situ free-radical polymerization Covalent modifications	Drug delivery, micro lenses, sensors, and artificial organ	[83–87]
	GO dispersions	Low-temperature chemical exfoliation	Sensor	
	rGO		Field-Effect Transistor	
LIGHT	mfGO	In situ Polymerization	Shape memory and self-healing materials	[88–90]
	PNIPAM-GO nanocomposite	Free-radical polymerization Co-precipitation	Artificial muscles and actuators Drug delivery	
	GO-PAH composites			
MECHANICAL	Graphene film	Vacuum filtration	Strain Sensors	[91–93]
	GWFs	Atmospheric pressure	Strain Sensors	
	Graphene Ripples	CVD Mechanical cleavage	Flexible Strain Sensors	
CHEMICAL	Graphene	Micromechanical cleavage	Chemical sensors	[94–96]
	g-GOF	Moisture/electric field	Humidity generator	
	GO films	Drop casting	Humidity sensor	
ELECTRICAL	GO sheets	Solvent exchange method	Microfluidics	[97–99]
	GO/PAM-PAA	In situ Polymerization	Sensors, artificial muscles, and switches	
	PPy/ Graphenes	Electro-polymerization	Actuators	
MAGNETIC	Fe_3O_4/rGO	Ultra-sonication treatment	Targeted drug delivery, magnetic resonance imaging	[100,101]
	Fe_3O_4/rGO composites	Chemical Deposition	Water treatment	

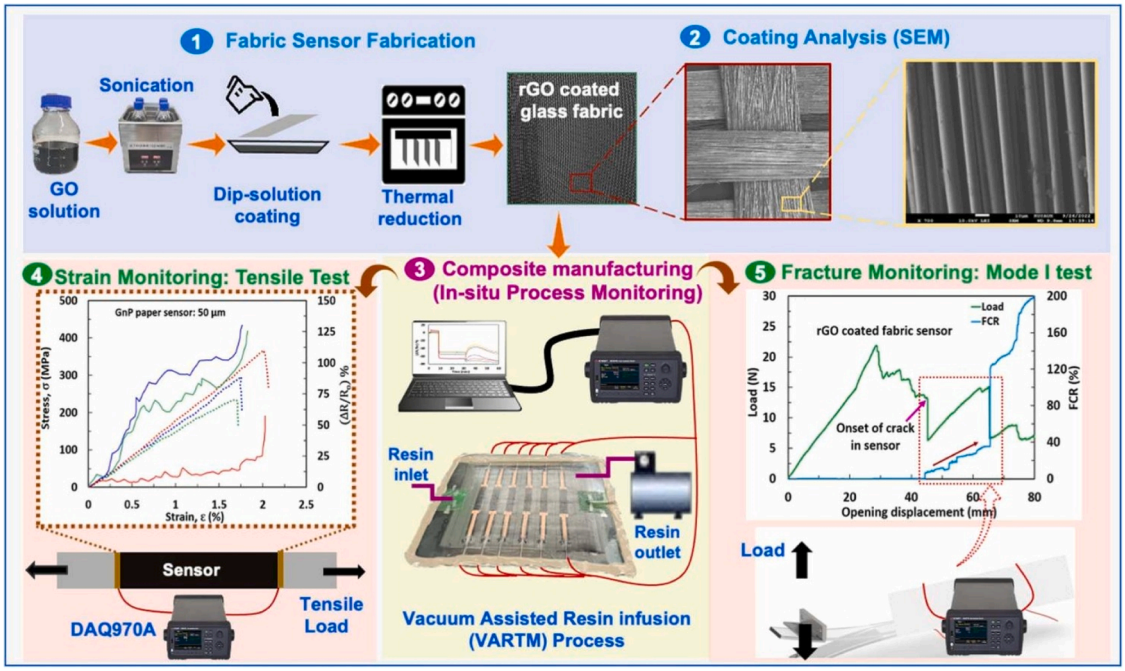

Fig. 9. Schematic of the manufacturing process for GFRP laminates with embedded rGO and GnP sensors for in-situ strain monitoring. Key stages include (1) Fabric Sensor Fabrication, (2) Coating Analysis via SEM, (3) Composite Manufacturing with in-situ monitoring, (4) Strain Monitoring using tensile testing, and (5) Fracture Monitoring with Mode-I testing, showing crack initiation and propagation. Reproduced from [106] with permission.

semiconductors with bandgaps that range from 0.5 to 3 eV (e.g., $MoSe_2$, HfS_2). TMDs have a variable bandgap depending on their semimetal or semiconducting status, the number of layers, elemental combination, and the presence or absence of a doping atom. The semiconducting properties of TMDs make them attractive for electronics-related applications. The molybdenum (Mo) and tungsten (W) dichalcogenides have received the most attention since they are predominantly semiconducting materials. TMDs have a wide range of applications beyond the electrical and electronic fields. They can be used in polymeric composites and nanocomposites where high performance and engineering behavior are essential [107,108]. TMDs belonging to groups 4–7 (as shown in Fig. 10 are mostly layered, while some TMDs in groups 8–10 are commonly found in non-layered structures. In a layered structure, each layer typically has a thickness of 6–7 Å and consists of a hexagonally packed layer of metal atoms sandwiched between two chalcogen atoms. The intra-layer metal-chalcogen bonds are mostly covalent, while the sandwich layers are held together by weak van der Waals forces, allowing the crystal to cleave readily along the layer surface. Single layers of TMDs are stabilized by developing a ripple structure like graphene.

Considerable efforts have been made to synthesize large-scale, uniform atomic layers of diverse 2D TMDs using various top-down and bottom-up approaches (Fig. 11). Exfoliation is a commonly used approach due to its high quality, but its development beyond fundamental studies has been hindered by critical limitations such as flake size and film uniformity. In contrast, chemical vapor deposition (CVD) has been studied as a scalable and reliable method for producing large area 2D TMDs. However, CVD-grown TMDs exhibit lower quality compared to their exfoliated counterparts (Table 4).

The Internet of Things (IoT) has become increasingly prevalent with the development of energy-efficient chip-scale devices with powerful computing and analytic capabilities for various applications. TMDs have an intrinsic bandgap that can be easily adjusted by changing the number of layers, resulting from quantum confinement effects and other techniques. This feature makes TMDs well-suited for smart sensors and radio frequency tags in space, defense, security, and IoT applications. TMDs such as MoS_2, $MoSe_2$, WS_2, WSe_2, and VS_2 have already demonstrated their usefulness. TMDs possess a large surface-to-volume ratio, which makes them highly sensitive, selective, and energy-efficient as sensors.

TMDs' atomic layers are weakly bonded, which enables easy isolation and stacking with other TMDs to form a variety of van der Waals (vdW) heterostructures without the need for lattice matching. Stacking one-atom-thick layers of different TMDs, such as vertically stacked heterostructures, can result in unique functions and superior properties that are not attainable otherwise. By exploiting the novel properties of these vdW heterostructures, such as band alignment, tunneling transports, and strong interlayer coupling, a wide range of electronic/optoelectronic devices, including tunneling transistors, barristers, photodetectors, LEDs, and flexible electronics, can be developed [110, 111].

Flexible devices have emerged as crucial components in diverse fields such as electronics, industry, healthcare, military, and space exploration. Nevertheless, conventional materials utilized for flexible devices, including silicon, inorganic oxides, and polymers, possess limitations like high stiffness, low electrical conductivity, and high production expenses for large-scale manufacturing. Whereas TMDs exhibit desirable piezoelectric properties, which make them attractive candidates for strain sensors. While TFT-type strain sensors function by gate switching that is controlled by mechanical signals, TMDs can also be directly incorporated into devices or e-skins for detecting pressure. This is feasible due to their inherent tunable mechanical and electrical properties, which depend on the bandgap. The resulting pressure sensor can detect signals such as heartbeats and wrist pulses, as well as more intensive signals such as body motions. TMD-based sensors exploit the exceptional mechanical stability of TMDs, which enables them to respond to large-scale bending and stretching. Chhetry et al. reported the fabrication of a piezoresistive strain sensor through one-step carbonisation of a MoS_2-coated polyimide film, resulting in the formation of MoS_2-decorated laser-induced graphene (MDS-LIG). The MDS-LIG takes advantage of the high mobility of graphene and the structural rigidity of MoS_2, leading to improved electromechanical performance due to the interfacial coupling between neighbouring layers of van der Waals heterostructures (vdWHs). The three-dimensional porous graphene nanoflakes decorated with MoS_2 exhibit stable electrical properties,

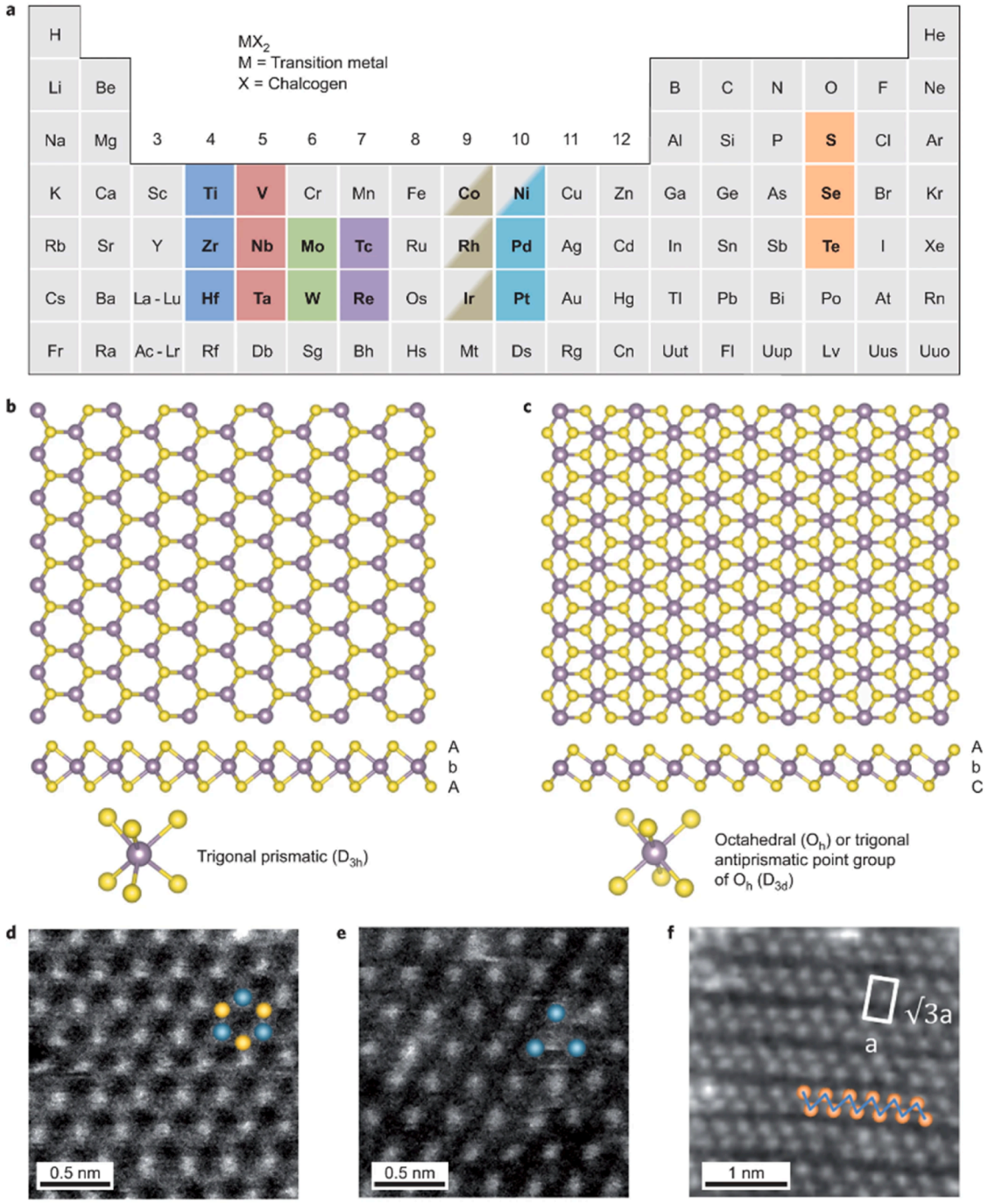

Fig. 10. (a) There are roughly 40 different compounds of layered TMDs. The periodic table highlights the transition metals and three chalcogen elements that typically form these structures. However, not all dichalcogenides exhibit a layered structure, as seen with NiS_2 having a pyrite structure while $NiTe_2$ is layered. (b, c) The c-axis and section view of a single-layer TMD with trigonal prismatic and octahedral coordinations respectively are depicted. Purple atoms represent metal, while yellow atoms represent chalcogen. The labels AbA and AbC indicate the stacking sequence, where uppercase letters signify metal elements and lowercase letters signify chalcogen elements. (d,e) A dark-field scanning transmission electron microscopy image of a single-layer MoS_2 is shown, highlighting the contrast variation of 1H and 1T phases. Mo and S atoms are represented by blue and yellow balls respectively [109]. Reproduced with Permission (f) Single-layer WS_2 exhibits a zigzag chain clusterization of W atoms caused by Jahn-Teller distortion. The clustered W atoms are shown as orange balls. The superstructure's $\sqrt{3}$a x a unit cell is denoted with a white rectangle.

resulting in a reliable output for longer strain/release cycles [112] (Fig. 12).

In a study conducted by Zhu et al., it was demonstrated that incorporating vanadium (V) into MoS_2 films can enhance the sensitivity of strain sensors for various applications. Through the implementation of a four-point bending method, researchers achieved a gauge factor (GF) of approximately 140 for V-doped MoS_2. This successful demonstration of substitutional doping in MoS_2 holds great promise for the development of highly sensitive strain sensing applications. Similarly, in another study by Wang et al., a 2D semiconducting material called Gallium selenide (GaSe) was utilized for fabricating strain sensors with exceptional sensitivity. The fabricated sensors displayed significant changes in electrical resistance in response to applied mechanical strain. Lu et al., developed a wearable piezoresistive-type pressure sensor using

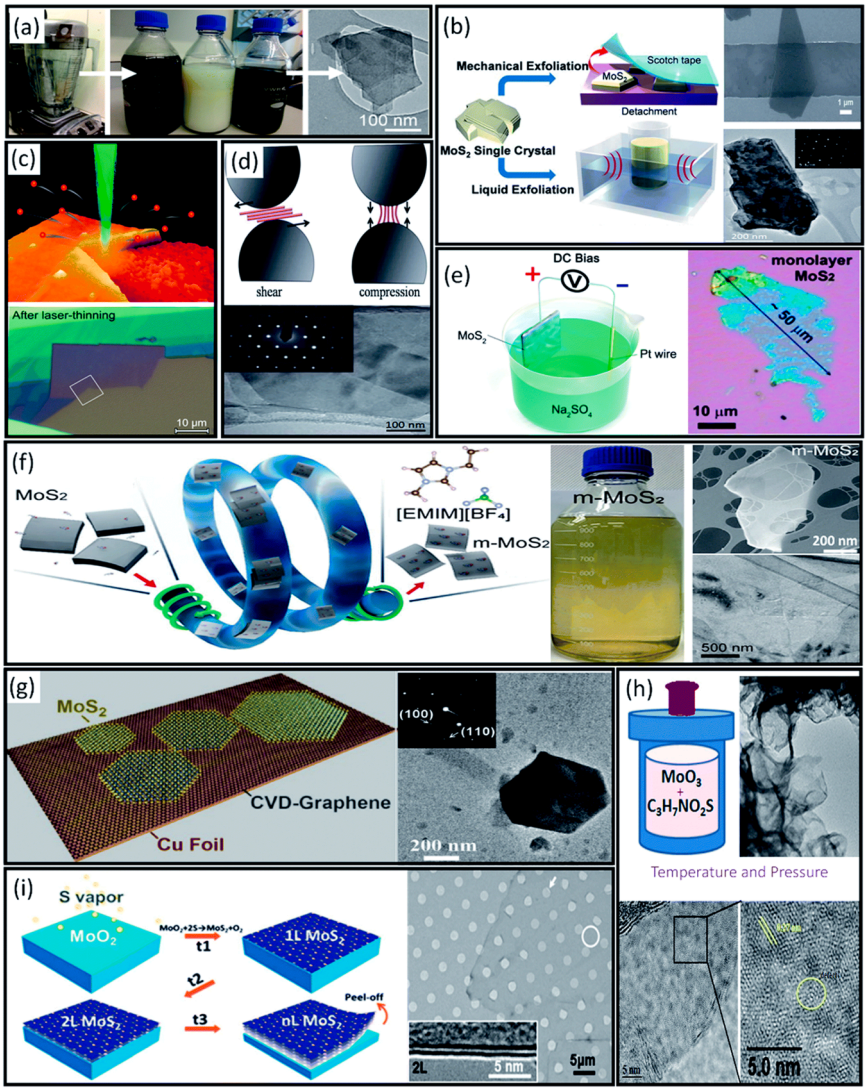

Fig. 11. A brief overview of conventional techniques utilized in synthesizing TMDs. Reproduced with Permission [107] (a) liquid exfoliation approach (b)combination of mechanical and liquid exfoliation approach (c)Laser thermal ablation method (d)Ball milling exfoliation method (e)Electrochemical exfoliation (f)Fluid dynamic exfoliation (g)Van der Waals epitaxial growth (h)hydrothermal method (i)chemical vapor deposition method.

carbonized silk fabric (CSilk) as the substrate and vertically grown MoS_2 on CSilk. The contact resistance between CSilk flakes varies under pressure, leading to sensitivity. The MoS_2/CSilk sensor demonstrated exceptional sensitivities of 11.6, 4.6, and 0.6 kPa^{-1} at pressures of 0.25, 0.25–3, and 3 kPa, respectively. The sensor's longevity is noteworthy as the sensitivity was maintained even after 5000 cycles at 500 Pa and 1 Hz. Additionally, the MoS_2/CSilk sensor operates at a low working voltage of 0.01 V, which is highly favourable for various sensing applications [113–115].

MoS_2 is a highly desirable material in the world of 2d nanomaterials due to its similar structure to graphite. It boasts a remarkable breaking strength of approximately 23 GPa, and a Young's modulus of roughly 300 GPa, which can be compared to that of chemically reduced graphene. As a result, MoS_2 can serve as a reinforcing element in polymer coatings. MoS_2 is also a typical layered inorganic material, which can disperse and exfoliate in polymers, producing a physical barrier effect that hinders the diffusion of heat and decomposition products from the polymer. The addition of MoS_2 as nanofillers in polymer nanocomposites has received significant research attention, and the addition of small amounts of MoS_2 has been found to improve the mechanical, thermal, and fire resistance properties of the nanocomposites [116–118]. $MoSe_2$ has also received significant attention in recent years for its impressive performance in energy storage and conversion applications among all the TMDCs. Conducting polymers are commonly utilized in these applications due to their ability to transfer electrons and holes, fast redox mechanism, and large surface area. Polyaniline is a popular choice due to its low cost, high conductivity, and stability when combined with n-type $MoSe_2$. Huang et al. developed a composite film of $MoSe_2$ nanosheets using a cost-effective drop-coating method as a counter electrode (CE) in a dye-sensitized solar cell (DSSC). The $MoSe_2$ nanosheets have good intrinsic catalytic ability and large active sites, and a flexible $MoSe_2$/PEDOT:PSS CE DSSC achieved a cell efficiency of 8.51 %. MoSe2 has also been combined with other polymers, such as PEDOT:PSS and PPy, to produce flexible energy devices and efficient systems for various applications [119,120].

2.3. MXenes

Since 2011, MXenes have emerged as a novel 2D nanomaterial due to their exceptional electrical conductivity (4600 S cm^{-1}), which is more than ten times higher than rGO the highest among all synthetic 2D nanomaterials. Interestingly, the use of MXene as a functional material in fibre-reinforced polymer composites is still an unexplored area with a lot of potential for further research. MXenes are 2D inorganic

Table 4
Comparing different techniques for producing TMD nanolayers [17].

METHOD	ADVANTAGE	DISADVANTAGE
MECHANICAL EXFOLIATION	Viable and environmentally friendly approach; Long-lasting structural integrity with high crystallinity and large size of up to 10 μm; Less destructive than liquid exfoliation	Inconsistent size distribution with a low yield; Challenging to separate and not scalable;
LIQUID EXFOLIATION	Exfoliation in a single step; Capable of scaling up; Exhibits high crystallinity; Higher production rate compared to sonication	Processing parameters are difficult to control with a kitchen blender; Ultrasonic cleavage using a direct method is time; Organic solvents such as NMP are required; Purification is challenging; More defects compared to micromechanical exfoliation
CHEMICAL EXFOLIATION	High yield; Stable colloidal suspension; Monolayer production is easier compared to liquid exfoliation induced by high shear forces	Intercalation and ion exchange methods require sonication; Intercalating ionic and organic agents or solvents is necessary; Semiconductivity may be altered; Treatment is required to remove Li; Structure is unstable
LASER-INDUCED THERMAL ABLATION	Maintaining optical and electronic properties while controlling the shape or geometry	Process requires a substrate; Scalability is limited; Production rate is low; High processing temperatures are necessary; The process is costly
CHEMICAL VAPOR DEPOSITION	Large nanosheets with uniform thickness; High structural quality	Process is not scalable; Growth control is challenging; Substrate is necessary; High processing temperatures are required; Ultrahigh vacuum conditions are necessary; Costly catalysts are needed; The yield is low
ELECTROCHEMICAL EXFOLIATION	Process is simple and scalable; Larger lateral size; Low level of oxidation; High-quality nanosheet; Holding intrinsic structure	Experiment parameters and conditions require optimization; Surface resistance is non-uniformly distributed.
HYDROTHERMAL REDUCTION	Process is simple and scalable; No tendency for restacking; Surfactants are not required	Process has a low yield; The size of the resulting product is small; The process is time-consuming; Toxic or expensive precursors are necessary; Harsh conditions are required

compounds consisting of metal nitride and carbide, produced through the etching of MAX phase compounds (M-transition metals, A-elements of 13th and 14th group, X-carbide, nitride, or carbonitride). The notation used is $M_{n+1}X_nT_x$, where *T* represents a functional group (e.g., O, F, OH, Cl, -*Sc* or -NH_2), M is an early transition metal (e.g., Ti, V, Mo), and X can be Carbide, Nitride, or Carbonitride ($n = 1$–4) (Fig. 13) [104]. The MAX phases are a fascinating class of machinable, nanolaminated layered solids that combine an unusual, and sometimes unique, combination of properties. Some are stiff and lightweight yet readily machinable, while others exhibit oxidation and creep resistance, metallic conductivity, and exceptional thermal shock resistance. This new group of materials, initially introduced in the 1960s by Novotny et al. as 'H-phase materials,' has since garnered significant interest for its versatile properties [121].

MXenes possess hydrophilic behavior due to their terminal functional groups, making them suitable for synthesis as clay, colloidal, or film-form or use in nanocomposites with polymer matrices. This provides an advantage over carbon-based nanomaterials. Unlike carbon-based nanomaterials, MXenes allow for altering their electronic and chemical properties by modifying their compound chemistry. They provide greater strength and stiffness than other 2D nanomaterials processed through solutions. Additionally, they can be synthesized in scalable batches of up to kilograms and exhibit environmental stability, making them suitable for a variety of applications. Moreover, they are biocompatible and can be processed in aqueous solutions without the need for surfactants. Yan et al. developed a flexible energy storage device using polypyrrole-MXene coated textiles demonstrating an impressive specific capacitance of 343.20 F g^{-1}, highlighting its ability to store energy effectively. The team also constructed a symmetrical solid-state supercapacitor with MXene-PPy textiles, with an energy density yield of 1.30 mW h g^{-1} (with a power density of 41.1 mW g^{-1}). This work introduces a new type of MXene-based textile supercapacitors, which could be ideal for future wearable and flexible energy storage applications [124]. Shibata et al. successfully fabricated $Ti_3C_2T_x$ MXene transparent conductive films. The transferred films exhibited an impressive ~100 times reduction in sheet resistance compared to conventional spray-coated samples and reported the film's transparency and electrical conductivity could be conveniently adjusted by varying the quantity of MXene material used in the process [125].

The group of 2D carbides and nitrides known as MXenes comprises structures of varying numbers of atom layers, including three, five, seven, or nine layers. These structures can exist in an ordered arrangement resulting in numerous compositions with various surface terminations. These MXenes exhibit a diverse of valuable and adjustable properties in electronics, optics, mechanics, and electrochemistry. Consequently, they have found applications in various fields, such as wireless antenna technology, energy storage, catalysis, optoelectronics, shielding against EMI, sensors, and biomedicine (Fig. 14) [122,124,125,127–131].

MXenes can be synthesized using either top-down or bottom-up methods, like most 2D nanomaterials. The top-down approach involves the removal of A atoms from MAX phases that are synthesized by mixing element powders or compounds and heating them at high temperature and pressure to form discs. However, unlike graphene, MXenes require powerful etchants to remove A atoms due to the strong interlayer force between A and M atoms in the MAX phases. Etching techniques such as hydrofluoric acid (HF), electrochemical, alkali, molten salt, and ionic liquid etching can be employed based on the etchant and etching conditions. Although some bottom-up methods have been proposed, they are relatively less common compared to top-down methods, numerous MXene synthesis approaches have been reported in the literature, depending on the precursor material, etchant, and application perspective.

In 2011, Gogotsi et al., pioneered the research on MXenes by selectively etching Ti_3AlC_2 with 50 % HF to obtain a few-layered $Ti_3C_2T_x$ compound. The HF etching process involves the selective etching of Al to form AlF_3, H_2, and accordion-like multi-layered Ti_3C_2. Research indicates that a minimal amount of HF can still selectively etch Al, but a distinct accordion-like shape only appears when the HF concentration exceeds 30 %. When exposed to H_2O and HF, the multi-layered Ti_3C_2 reacts to form multi-layered $Ti_3C_2T_x$ ($Ti_3C_2(OH)_2$ and $Ti_3C_2F_2$), then stripped down to a few layers of $Ti_3C_2T_x$ through ultrasonic vibration.

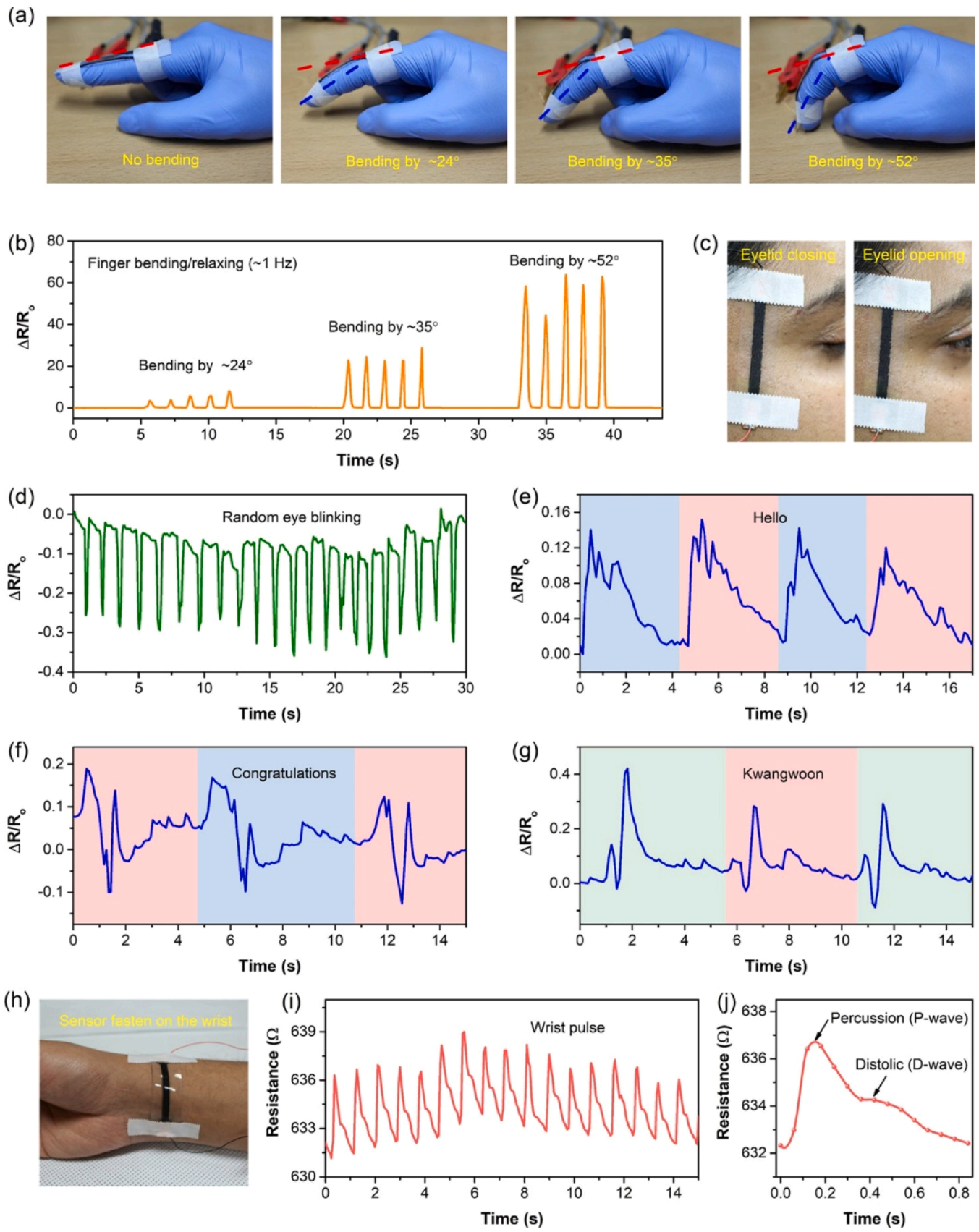

Fig. 12. Real-time signals produced through different applications with the MDS-LIG sensor. Reproduced from [112] with permission.

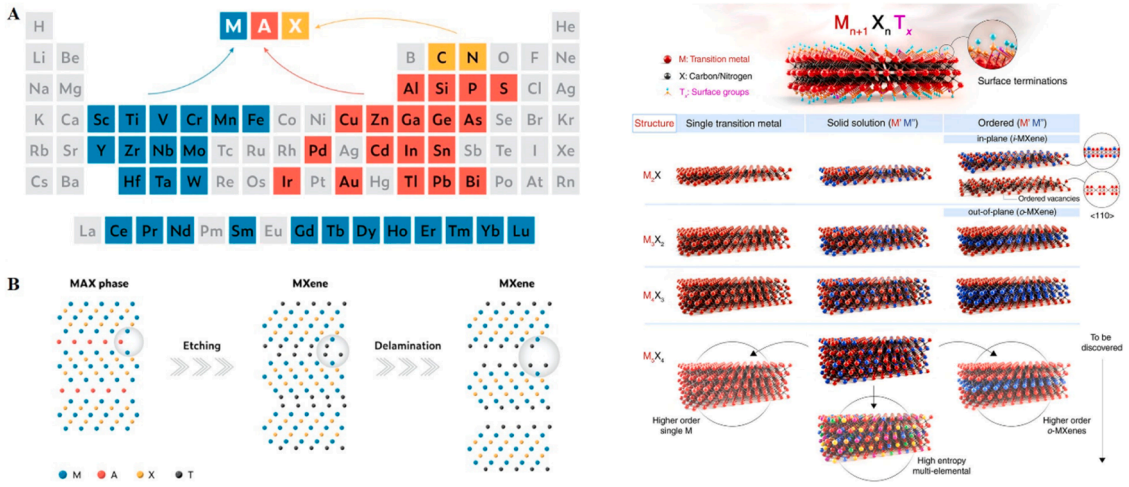

Fig. 13. Periodic table of MXene compositions, with color-coded elements and schematics of the MXene structures. Reproduced with Permission [122,123].

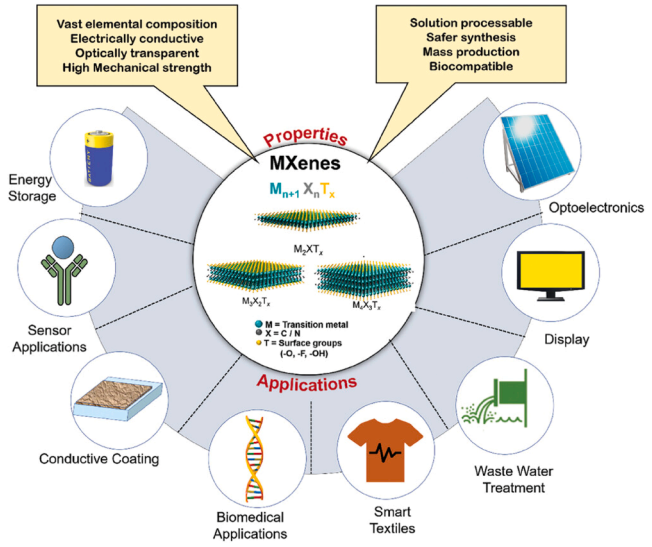

Fig. 14. -Applications of MXenes. Reproduced with permission [126].

The HF etching method is commonly used to prepare various MXenes, such as Ti_2C, V_2C, Nb_2C, Nb_4C_3, Ta_4C_3, Ti_3CN, TiNbC, $(V_{0.5}Cr_{0.5})_3C_2$, and TiVC, $(Ti_{0.5}V_{0.5})_3C_2$, in large quantities. The use of HF for synthesis may be effective, but it comes with significant risks to human health and has corrosive properties. To mitigate these adverse effects, the in-situ HF-forming method is strongly recommended for etching MAX, as it offers a simpler process and higher yield. It must be emphasized that the technique described is unsuitable to produce nitrides due to their low cohesive energy, which causes nitride MXenes to dissolve in HF. However, a new HF-free E-ETCHING technique has been developed for the creation of Ti_2CT_x, which aims to minimize the damage caused by HF. This technique involves the application of voltage to Ti_2AlC in a dilute HCl solution to selectively eliminate Al atoms, leaving behind a monolayer of C atoms. To prevent over-etching, voltage regulation is necessary, and with increased etching time, a multilayer structure is observed. Additionally, the etching rate rises with temperature. Chen et al. also developed the E-etching method in a binary aqueous electrolyte, such as a mixed solution of LiOH and LiCl at constant voltage of 5 .5V. This method has an etching efficiency of 92.2 % and results in a few layers of Ti_3C_2Tx. It is noteworthy that E-etching is a dynamically controlled process that requires careful regulation of voltage, temperature, and solution composition to achieve desired results [132]. Researchers have explored the synthesis of fluorine-free MXenes using *alkaline etching* of MAX phases. One approach involved etching the Ti_3AlC_2 precursor using a mixture of potassium hydroxide and a small amount of water at 180 °C for 24 h in an autoclave. This resulted in the production of single-layered $Ti_3C_2(OH)_2$ without any $-F$ functional groups. During the etching process, the Al layer in the Ti_3AlC_2 structure was replaced by $-OH$ ligands, and $Ti_3C_2(OH)_2$ nanosheets with a thickness of around 1.5 nm was quickly and efficiently obtained through a minimal washing procedure. Another study by Li et al., utilized 27.5 M NaOH to etch the Ti_3AlC_2 precursor at 270 °C in an autoclave, producing fluorine-free surface--terminated $Ti_3C_2T_x$ multilayers with high purity. This was achieved through alkali-etching based on the Bayer process. New research suggests that novel MAX phases can be created by replacing A atoms with other atoms at high temperatures [133]. Huang et al. have introduced a *molten salt etching* technique for synthesizing MXenes by exchanging elements in the A-layer of traditional MAX phases. This method employs late transition metal halides (such as $ZnCl_2$ and $CuCl_2$) that ionize into metal cations in their molten state, acting as electron acceptors, known as Lewis acids, to etch MAX phases and create MXenes. The molten salt etching method produces MXenes with a uniform surface group (-Cl), and by controlling the type of molten salt, MXenes can be doped with different elements. Therefore, this method has become popular in electrochemical applications, second only to HF/in situ HF-forming etching. In addition to the top-down synthesis methods mentioned earlier, other approaches have been developed, including *ionic liquid etching* and *organic solvent* + NH_4HF_2 *etching*. The preparation of nitride MXenes is a challenge due to the instability of nitrides in HF. Urbankowski et al. proposed a *phase transformation* method to address this issue. They were able to convert Mo_2CT_x and V_2CT_x carbide MXenes into nitride MXenes by ammoniating them at 600 °C. This involved replacing C atoms with N atoms from NH_3, resulting in the formation of nitrides [134,135].

Tunable etching methods can control MXenes to synthesize nanoparticles, of a monolayer or multilayer nanosheets with high specific surface areas and amplify sensing capabilities in sensors made of MXenes. Additionally, MXenes can combine with alternative materials, resulting in the formation of composites and exhibit enhanced mechanical flexibility and stretchability through structure design, making them useful in wearable sensors, energy storage, and EMI applications [129,136]. MXenes possess electronic characteristics and equivalent bending strength as graphene, making them ideal for super-sensitive piezoresistive sensors due to their accordion-like structure. They can be blended with other materials to enhance sensor functionality, making them a desirable option in the realm of physical sensors. However, MXenes are fragile, and amalgamation with mechanically robust materials is necessary to endure the sensor's repetitive stress and rebound

cycles. There are two types of MXenes-based flexible piezoresistive sensors: aerogel and MXenes/elastic matrix sensors. Aerogels, due to their high porosity, ultralight weight, and exceptional elasticity, possess desirable attributes for sensor fabrication. However, MXenes lamellae alone cannot form aerogels due to their brittleness, necessitating the inclusion of high-toughness and highly elastic materials to enhance aerogel mechanical strength. Alternatively, MXenes can be directly integrated into a highly elastic substrate, leveraging the conductivity of MXenes and the mechanical properties of the elastic substrate to fulfil the resistance-related requirements and geometric characteristics of flexible piezoresistive sensors [129,137].

Guo et al., have developed a flexible and degradable pressure sensor by incorporating porous MXene-impregnated tissue paper between biodegradable polylactic acid (PLA) thin sheets coated with interdigitated electrodes. This sensor is highly sensitive, with a low detection limit of 10.2 Pa, a broad range of up to 30 kPa, and a fast response time of 11 ms while consuming low power (10^{-8} W) and demonstrating great reproducibility over 10,000 cycles. Moreover, the sensor exhibits excellent degradability. It can be utilized to predict the potential health status of patients, act as an electronic skin for mapping tactile stimuli and has the potential to be used for personal healthcare monitoring, clinical diagnosis, and in the development of next-generation artificial skins. The innovative sensor design demonstrates the potential of MXenes in developing flexible and sensitive sensors with biomedical applications (Fig. 15) [138].

The blend of 2D MXene material and wrinkle structure has led to the development of an ultra-sensitive and flexible piezoresistive sensor, as observed by Yan et al., The sensor was fabricated by spraying the active material onto a pre-stretched polyacrylate tape, a low-cost and efficient method. The MXene composite-based sensor with a wrinkled structure exhibits high sensitivity (148.26 kPa^{-1}), a wide pressure range (up to 16 kPa), a short response time (120 ms), and excellent durability (>13,000 cycles). Due to its exceptional sensing performance and flexibility, the sensor can detect human physiological signals, monitor intelligent robot postures, and map spatial pressure distributions. This makes it suitable for applications in physiological analysis systems, humanoid robotics, and biomedical prostheses [137]. Li et al., developed a flexible pressure sensor by treating a polyurethane sponge with chitosan and dip-coating it with MXene sheets. The resulting MXene@CS@PU sensor has high compressibility, stable piezoresistive response, and can detect small and large pressure signals. It's highly resilient and can handle up to 85 % compressive strains with a rapid response time of 19 ms and a low detection limit of 30 μN. The sensor is promising for detecting human physiological signals and insect movements, and it can detect voices and human breaths by a non-contact detection mode [139].

An ultralight and super elastic aerogel-based piezoresistive sensor has been developed by Ma et al., using MXene/rGO (MX/rGO) hybrid 3D structures, which exhibit better performance than single component rGO or MXene-based sensors. The MX/rGO aerogel combines rGO's large specific surface area and MXene's high conductivity, resulting in a rich porous structure. The sensor shows high sensitivity, fast response time, and good stability over 10,000 cycles and can detect signals below 10 Pa. Its exceptional performance makes it suitable for pressure measurement, strain detection, and health monitoring applications [140]. Irfan et al., conducted a study where they developed MXene-coated glass fabric sensors for in-situ process and structural health monitoring of glass fiber-epoxy aerospace composites manufactured through a resin infusion process. The performance of the MXene-coated sensors was

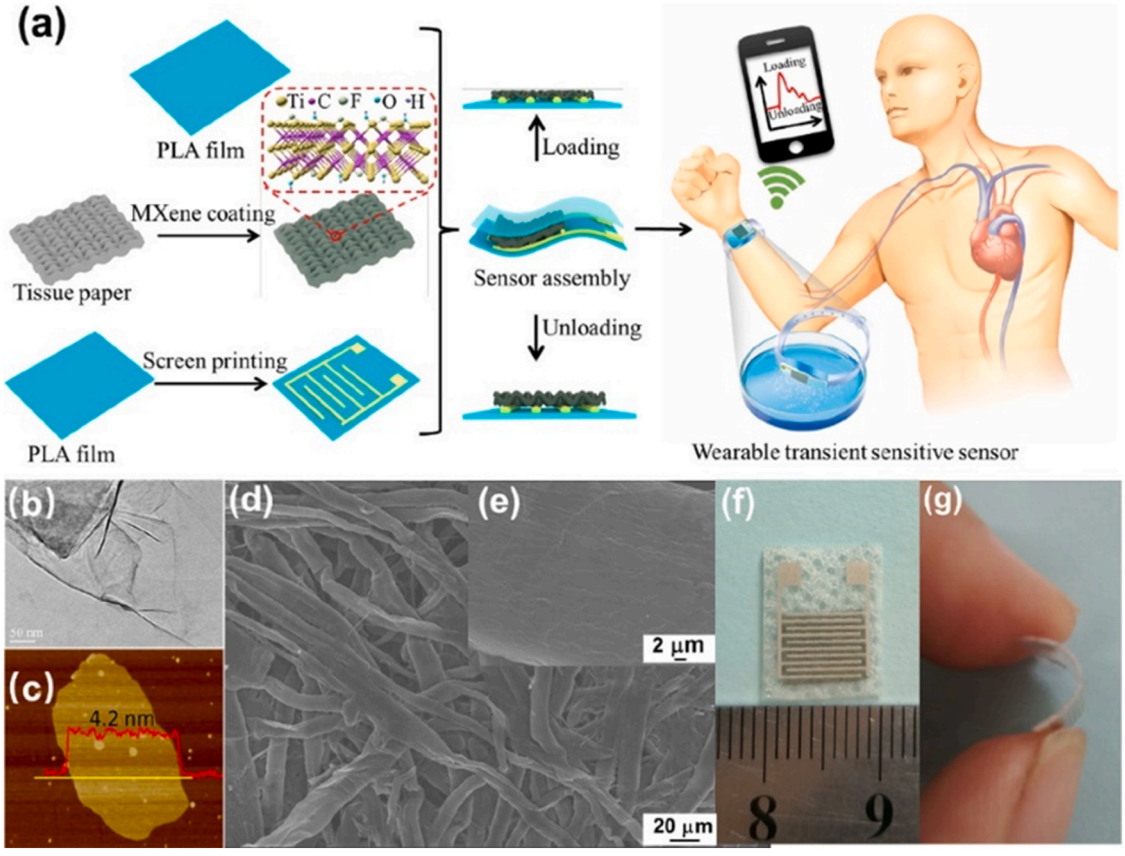

Fig. 15. The fabrication procedure of flexible wearable transient pressure sensors with MXene nanosheets is illustrated in Fig. 1(a). The figure also includes a TEM image of the MXene nanosheets in (b), an AFM image of the MXene nanosheets deposited on a mica plate in (c), and an SEM image of MXene/tissue paper in (d). An enlarged MXene/tissue paper fiber SEM image is shown in (e). Photographs of the flexible wearable transient pressure sensor are presented in (f) and (g). Reproduced with Permission [138].

compared to those coated with thermally rGO. The study found that both coated sensors were suitable for monitoring the process and structural health of the composites. Furthermore, the response of the composites to a dynamic thermomechanical program was evaluated using the embedded sensors for the first time in SHM studies. The MXene-based composites also provided better EMI shielding effectiveness than rGO-based composites. The study concluded that the MXene-based coated fabrics demonstrated excellent sensing capability and multifunctionality for polymer composites [104,130,141].

3. Mechanism of conductivity and sensing

3.1. Conductivity

In today's world, where technology plays a significant role, the demand for high-performance electronic devices and components continues to increase. Conductive coatings have become essential to meet these demands by providing improved electrical conductivity and other desirable properties to various materials. Many materials, such as plastic and glass, are inherently non-conductive. Applying a conductive coating can transform these materials into conductive surfaces, allowing the flow of electric current and facilitating the operation of electronic circuits and devices [142]. Electrical conductivity is the most critical property required for electrical or electromagnetic applications. To achieve this requirement, various conductive additives have been employed to produce novel materials with varying electrical conductivity levels and electromagnetic characteristics. Electrical conductivity can be achieved at the fibre level using intrinsically conducting polymers (ICPs) to form the fibre or by coating conventional insulating fibres with conducting materials. A variety of materials such as ICPs, conducting polymer composites, metals, carbon-based materials like CNTs and graphene, and other emerging 2D nanomaterials like TMDs and MXenes have been used to achieve this. These materials have been applied using coating methods such as electro- and electroless deposition, dip-coating, and CVD to create electrically conductive smart coatings [143]. By carefully selecting and modifying the conductive filler and polymer, smart coatings with a wide range of properties can be fabricated, making them useful for various applications such as sensors, EMI shielding, and energy storage devices [144,145]. The conduction mechanism in these coatings based on conductive fillers is intricate and comprises a fusion of various conduction mechanisms, including contact conduction and tunneling conduction. The conductivity gradually increases with an increase in the filling amount of conductive filler. It sharply increases when the filler content reaches the critical volume fraction, known as the percolation threshold. However, further increases in filler content no longer significantly increase conductivity beyond a certain point. There are two types of conductive filler-based coatings: those with interconnected pathways and those without connection. If the spacing between the conductive fillers is small, the electrons in the fillers gain energy from thermal vibrations and can travel through the thin polymer layer to reach neighbouring fillers. This creates a pathway for electricity through electron tunneling, which is known as the electron tunneling effect [146–148].

The percolation threshold is a fundamental concept in percolation theory that describes the behavior of conductive networks in a material. At a specific concentration, known as the percolation threshold, these materials undergo a metal-insulator-semiconductor transition, significantly changing their electrical conductivity. This concept was first established in 1957 by Broadbent and Hammersley and is used to explain the flow of fluids through a static medium. The percolation threshold was initially determined in 2D geometry and later established in 3D geometry. Understanding the percolation threshold is essential for developing and optimizing novel conductive materials for various applications. This relationship between electrical conductivity and the concentration of conductive filler is expressed through a universal power law equation [149]:

$$\boldsymbol{\sigma_c} = \boldsymbol{\sigma_o}\left(\boldsymbol{\Phi_f} - -\boldsymbol{\Phi_c}\right)^{\mathbf{t}} \tag{1}$$

where σ_c is the conductivity of the material, σ_o is the electrical conductivity of filler content, Φ_f is the concentration of conductive fillers (wt.%), Φ_c is the percolation threshold, and t is the fitting parameter (critical exponent). The critical exponent values depend on the filler's aspect ratio and orientation. The percolation threshold value can be experimentally determined by plotting a graph between electrical conductivity and the volume fraction of filler content. Various factors, such as the type of polymeric materials, preparation technique, and degree of orientation, can affect the percolation threshold value [150].

The phenomenon of percolation theory can be further explained using an example. Fig. 16 illustrates the relationship between the conductivity of a composite and the conductive filler loading. The graph of conductivity versus filler loading typically exhibits three distinct regimes. At low filler loadings, the composite is insulating, and the conductivity is very low. As the filler loading increases, the composite enters the percolating regime, where the conductive fillers start to form a continuous network, resulting in a rapid increase in conductivity. Finally, at high filler loadings, the composite enters the conductive regime where the conductivity reaches a plateau, indicating that the network of conductive fillers is fully formed, and the electrons can flow freely throughout the composite material. The S-shape of the graph is a characteristic feature of percolation behavior and is commonly observed in various composites. The conductive behavior of composites in the three different regimes, namely insulating, percolating, and conductive, can be explained based on the microstructure of the composite. In the absence of a conductive path through the filler, the composite remains insulating because no charges can flow. When the filler forms a directly connected network, electrons can easily move through this network, and the composite becomes conductive [151].

Conductive inks with 2D nanomaterial-based formulations are particularly attractive due to their flake-like shape and different electronic properties, ranging from conductors to insulators. The four-point probe technique can be employed to accurately measure the electrical properties of thin coatings. This technique involves creating equidistant, linearly separated electrical connections with the material surface, where current (I) flows across the outer pair of electrodes, and the voltage drop (V) is measured at high impedance (i.e., at $I = 0$ A) across the inner pair. Determining the electrical conductivity value requires considering the sample's physical dimensions relative to the probe setup, including its thickness (t) and length (l). If the thickness of the sample is ten times smaller than the interprobe spacing ($t/l < 0.1$), the sample can be regarded as "infinitesimally thin" for simplicity, and the sheet resistance (Rs) can be approximated by using:

$$\mathbf{R_s} = \frac{\boldsymbol{\pi}}{\mathbf{ln2}} \times \frac{\boldsymbol{V}}{\boldsymbol{I}} \tag{2}$$

For samples with a thickness greater than ten times the interprobe spacing ($t/l > 0.1$), determining the bulk conductivity (σ) necessitates employing appropriate equations and correction factors that correspond to the sample geometry. Once the bulk conductivity is determined, the sheet resistance can be obtained from it, provided that the thickness is also known:

$$\mathbf{R_s} = \frac{1}{\boldsymbol{\sigma t}} \tag{3}$$

The coating is generally applied as a thin layer on top of sheet substrates, and the sheet resistance is the usual metric reported. In textiles, the coating can penetrate more deeply into the network of fibers, so both sheet and bulk values may be given. However, the 3D structure of foams implies that their electrical properties can only be reported as bulk conductivity [136].

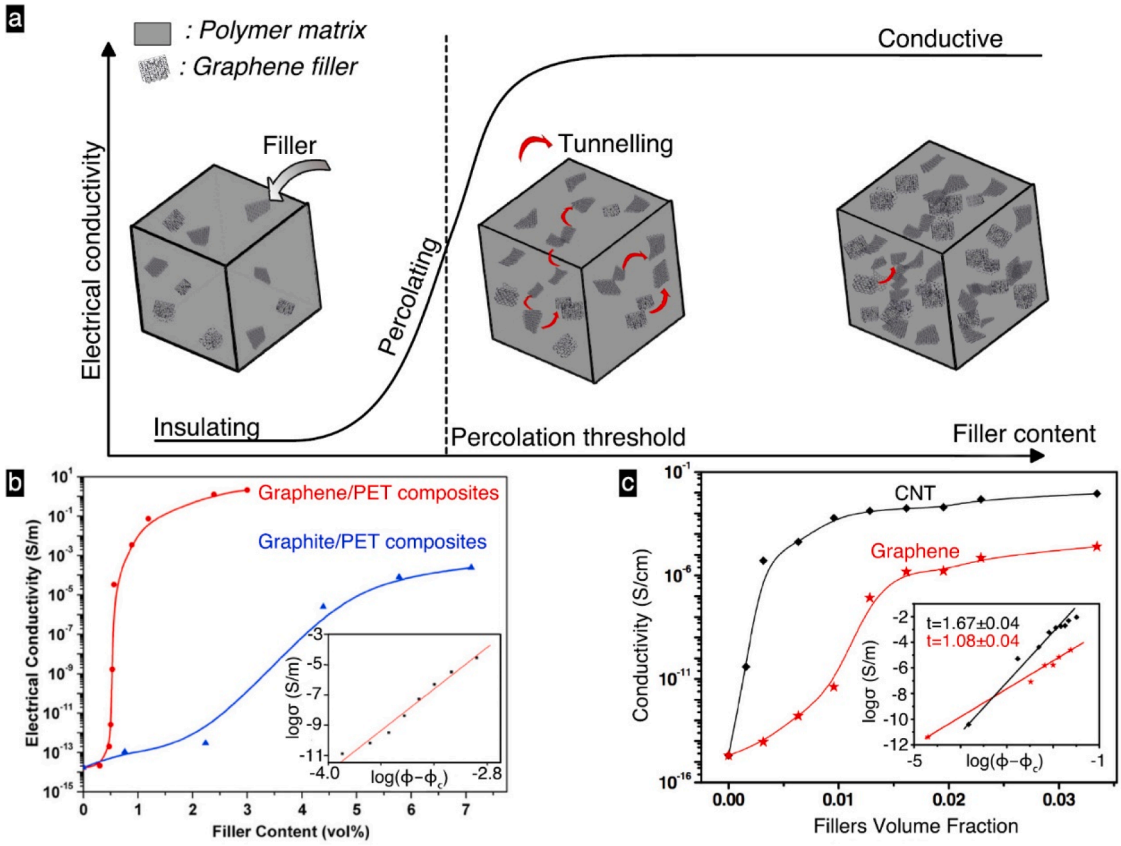

Fig. 16. - a) Diagram illustrating the different conduction mechanisms in a composite material as the filler content increases. b) Comparison of percolation thresholds between graphene and graphite in PET composite c) The conductivity versus filler loading graph illustrates the percolation threshold in high-density polyethylene (HDPE) composites. The black line represents composites formed with (CNTs), while the red line represents composites formed with graphene nanosheets. Reproduced with Permission [152].

3.2. Sensing

In today's world of intelligence, digitalization, and networking, sensors have become the primary way of gathering information. The demand for sensor sensitivity and application range is also on the rise. The sensitive component of a sensor is a crucial factor in its performance as it directly affects its accuracy, sensitivity, and detection range. Physical sensors can be categorized based on their transduction mechanisms, which include piezoresistive, capacitive, iontronic, and piezoelectric transmission. Research into flexible pressure sensors mainly focuses on changing the microstructure of the sensor's conductive layer to enhance its sensing performance. Flexible multifunctional sensors have undergone notable advancements in recent years, particularly in the fields of healthcare, robotics, and biomedicine that requires high sensitivity, accuracy, flexibility, and low-cost sensors. To meet these requirements, sensors must be compatible with large-area processing techniques and easily integrated into flexible devices. Significant efforts have been made in this area, expanding the range of potential applications for these sensors. Examples of multifunctional sensors and mechanisms are illustrated in Fig. 17. Overall, sensors play a critical role in various applications, from monitoring environmental conditions to controlling complex industrial processes, and are an essential component of many modern technological systems [153–156]. Piezoresistive sensors that convert stimuli into resistance changes are widely used due to their simple read-out mechanism, easy fabrication, high linearity, low power consumption, and high pixel density. Piezoresistive sensors operate on the principle of converting an external pressure stimulus applied to the device into a measurable resistance value. This resistance value comprises the contact resistance at the interface between the electrode and sensing material, the interior resistance of the sensing

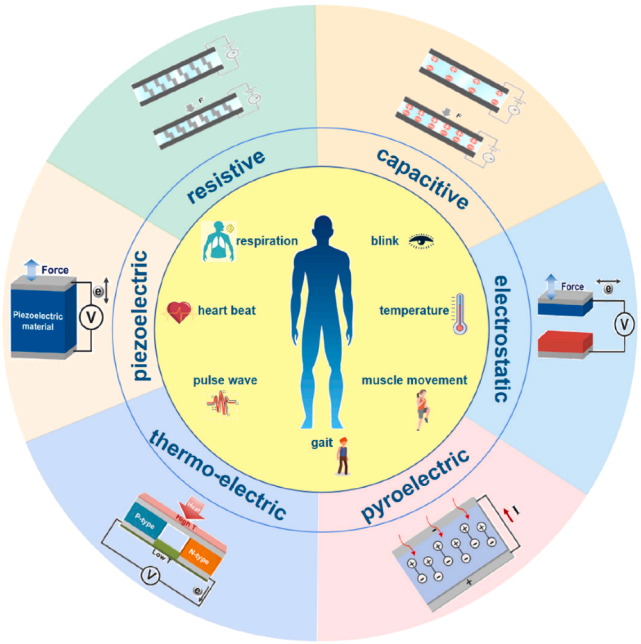

Fig. 17. An illustration depicting multi-functional sensors and mechanisms. Reproduced with Permission [156].

material, and the electrode. A gauge factor (GF) is used to assess the sensitivity of piezoresistive sensors. GF is defined as the ratio of the relative change in resistance (ΔR/R0) to the applied strain (ε) and is a measure of piezoresistive sensitivity. A higher GF value indicates greater sensitivity, while a lower GF value indicates less sensitivity. The sensing performance of piezoresistive sensors is based on the modulation and coupling of conductive paths. For directional sensors, a larger difference in GF values between different directions indicates a better capability to differentiate between multiaxial stimuli. Various criteria are used to evaluate pressure sensor performance, including sensitivity, working range, stability, hysteresis, response time, and recovery time [157–159].

The use of 2D nanomaterials in sensors has increased exponentially in recent years, from environmental monitoring to healthcare, due to their unique properties stemming from their intrinsic structures. Specifically, 2D nanomaterials, such as graphene, TMDs, and MXenes, have garnered substantial attention in various fields, particularly in detection and sensing strategies. The advantages of 2D materials in this includes: 2D nanomaterials are essentially single-layer materials with thicknesses in the range of a few nanometers, resulting in a remarkably high surface-area-to-volume ratio that provides numerous reactive sites between the material and analytes; the conductivity of 2D nanomaterials can be adjusted by controlling structural defects, increasing the number of layers, doping, or even post-functionalizing the material; their mechanical strength and flexibility, are compatible with cutting-edge technologies, such as ultrathin silicon channels, printing methods, metal electrodes, and flexible and wearable electronics (Fig. 18) [160].

4. Future trends in smart coatings

4.1. Artificial intelligence & digitalisation

In today's rapidly evolving technological landscape, there has been a gradual shift from conventional wired technologies to advanced wireless technologies in the past decade. In the context of Industry 4.0, connecting the physical and virtual space is a vital step towards achieving smart operations in material design and manufacturing processes. If we replace devices with smart materials, it will transform the way we approach digital manufacturing. Such materials could sense and send real-time data to the virtual space, making them a game-changer in the field. Integrating smart sensors with Artificial Intelligence (AI) tools such as Artificial Neural Networks, Machine Learning (ML), Deep Learning, and their derivatives like Convolutional Neural Networks, Hybrid Intelligence, and Cloud Computing has led to the development of completely automated monitoring systems. The use of AI in data analytics is now actively driving progress in materials research [161,162].

With the increasing need for repair and rehabilitation, SHM has gained popularity due to technological advancements. Generally, a typical SHM system comprises three major components: data acquisition (including sensing, conditioning, and processing), data communication and storage, and a health evaluation system (which includes data diagnostic algorithms and information management tools). Conventional wired systems use coaxial cables to connect components and transfer data to a central data repository. This type of network is reliable and safe but is only cost-efficient when used on smaller structures or to monitor a localised area in a structure. The cost of the entire network is directly related to the size of the data acquisition system, measured in terms of the number of sensors. Larger structures require a robust and dense sensor network, resulting in high installation and maintenance costs, more labour force, and longer installation times. To overcome these limitations, wireless communication is increasingly being used [163,164]. 2D nanomaterials such as graphene possess superior properties, making them promising materials for various applications, especially electronic devices. Graphene-based devices are versatile and can be used for flexible and transparent electronics, piezo-resistive sensors, and energy storage devices. Amongst different graphene derivatives, rGO-based sensing has gained popularity in polymer composites for SHM and various applications. Fig. 19 illustrates the potential of rGO sensors as an interface between the physical and cyber worlds in the digital manufacturing of FRP composites [162].

Recent advancements in technologies, such as 5 G, wireless sensor networks (WSNs), Internet of Things (IoT), deep learning (DL) algorithms, cloud framework, and high-performance computers, have led to the emergence of a new data-driven paradigm called digital twin (DT). This technology has gained momentum in the engineering community as it allows the integration of physical and digital structures throughout their life cycle. Among these advancements, cloud computing is promising, offering cost-effective, high-performance computing, large-scale storage, and remote access from anywhere. A Digital Twin refers to the computerized and digital representation of a physical object that can simulate how it will operate under different input variables. This can

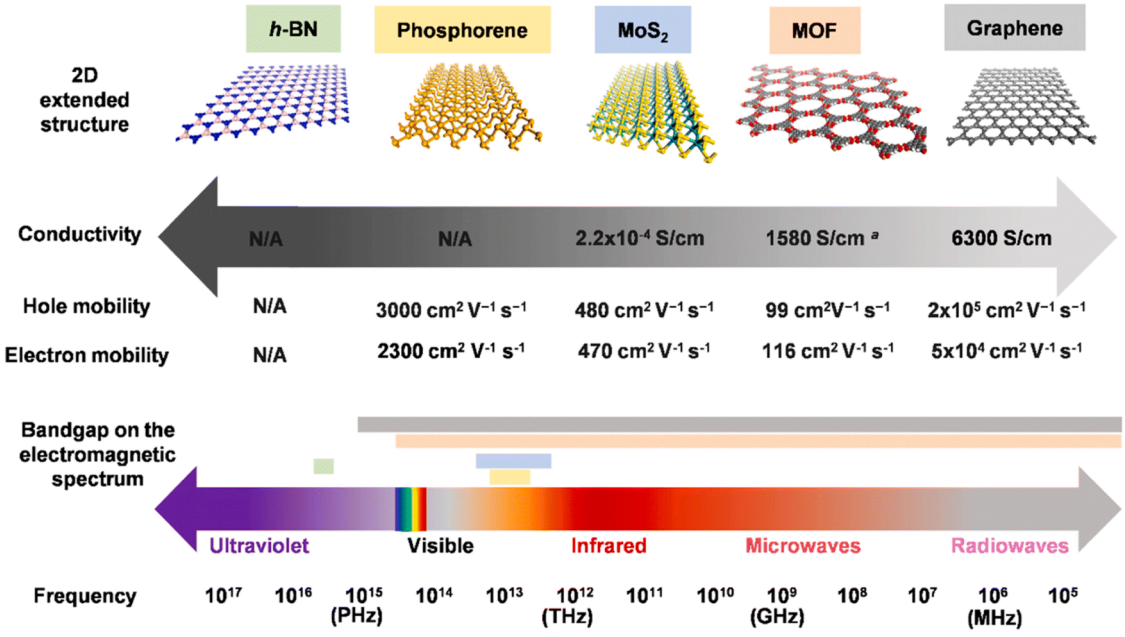

Fig. 18. Properties of 2D nanomaterials enabling their sensing capabilities. Reproduced from [160].

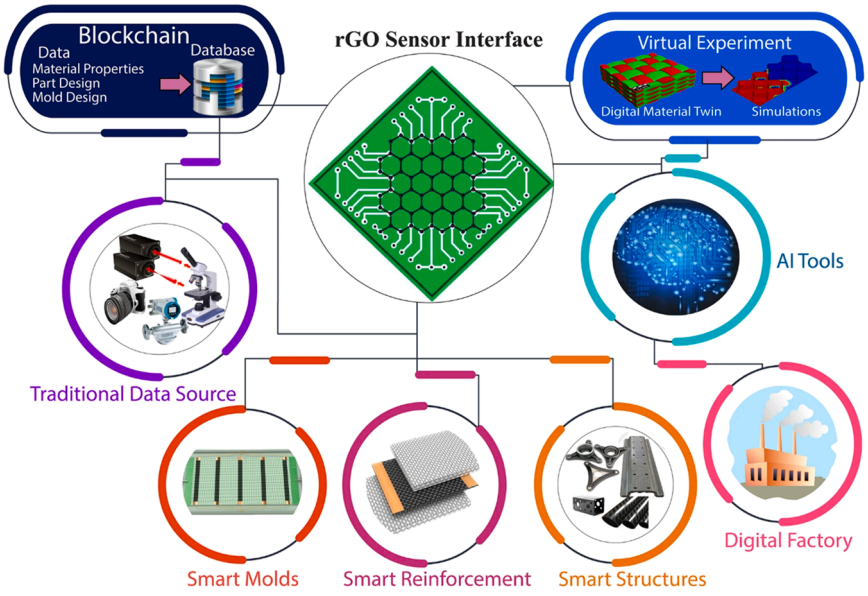

Fig. 19. An illustration of the rGO sensor interface for composite structure digitalisation. Reproduced from [162].

potentially benefit SHM tasks greatly. In a study by Lai X. et al., a digital twin named the measurement-computation combined digital twin (MCC-DT) was proposed. This twin combines measurement and computational data to conduct structural analysis, monitoring, and predictive maintenance [165]. Digital Twin encompasses several components, and its interpretation varies depending on the intended application. Digital Twins have found applications in maintenance strategies where they are used for predicting the state of assets, improving condition monitoring and fault diagnostics, reducing the number of maintenances activities, and formulating optimal maintenance intervals. One application for digital twins is defect detection, in which artificial intelligence algorithms are employed to automatically recognize and evaluate defect regions, such as coating damages [166–168].

In the context of smart coating for wearables, two novel applications including associated signal processing with AI are presented below. a) Measurement of muscle activity and fatigue with force myography (FMG)

Piezoresistive sensors sandwiched between skin and a compression garment or piezoresistive coatings on the skin or the inside of a compression garment experience a higher pressure when a muscle contracts, bulges and compresses the sensor between garment and skin [169,170]. The advantage of this method is that FMG measures the mechanical action of a muscle, in contrast to the EMG (electromyography) which measures its electrical activity. Due to the electro-mechanical delay, the onset of the electrical activity occurs 0.1 0.25 s before the mechanical. FMG is therefore more accurate than EMG, specifically at high-speed movements. The EMG is definitely the gold standard when measuring fatigue, by subjecting the EMG signal to FFT (fast Fourier transform). The median of the FFT power spectrum shifts to smaller frequencies after the onset of muscle fatigue. However, FMG is capable of measuring fatigue too. An AI algorithm based on fractal dimensions of the FMG signal is trained on the signals of fresh and fatigued muscles, by maximally separating the average fractal dimension values of the two conditions. Increasing fractal dimension values indicate growing fatigue. The algorithm is so sensitive that it can even detect alternate fatiguing and recovering of antagonistic muscle groups, e.g., fatiguing quads and simultaneously recovering hamstrings [170] b) Sweet and dead spot analysis, applicable to impacts on smart coatings for sports purposes

Sweet and dead spots on sports equipment are related to advantageous and disadvantageous impact positions, respectively, resulting in effects such as greater energy transfer or minimisation of vibrations. With a pressure sensor array, e.g., in the form of a smart coating on a soccer boot, measuring the magnitude of the ball impact force, as well as the centre of pressure (COP), it is possible to pinpoint the location of sweet and dead spots, and to estimate the chances scoring a goal with a curved kick. The underlying algorithm identifies the characteristics (magnitude peak force, x- and y-coordinate of the COP location) of successful and unsuccessful kicks and assigns a parameter range to these characteristics. When kicking a ball at the sweet spot of the boot with greater force, the chances of scoring a goal are 58 %−86 %; and at the dead spot with lower force only 11 %−22 %. The sweet spot is located more medial and proximal than the dead spot, at an average distance of 21 mm from the dead spot [171].

Another promising avenue for smart coatings is in electronic skin (E-skin) applications to create advanced sensing technologies with applications in fields such as robotics, healthcare, and wearable devices. Flexible E-skins are an increasingly important area of research that has applications in human-robot interactions, human health monitoring, and wearable electronic devices. The field of flexible electronics has made significant progress, with the advancements in smart coatings in recent years, with developments in preparation methods, materials, and potential applications. This progress has laid a solid foundation for further development of electronic skins [172]. There is a growing emphasis on sustainability as the development of smart coatings progresses. The coatings industry is working with industry associations to improve sustainability by researching and using materials that are biodegradable, compostable, recyclable, and sustainably sourced. Incorporating sustainability in developing smart coatings aligns with the broader global efforts to create eco-friendly technologies. It emphasizes the importance of responsible practices in material selection, manufacturing, and application to ensure that the benefits of smart coatings are achieved without compromising environmental considerations [173]. In the following section, we have delved deeply into E-skin and the pivotal role of sustainability in the context of smart coatings. This comprehensive understanding lays the foundation for appreciating the transformative potential of these technologies in shaping a more advanced, responsive, and environmentally conscious future.

4.2. *E-SKIN: an emerging intelligent multifunctional coating*

Electronic skin, or E-skin, serves to detect tactile information and

convert it into electrical signals. Upon touch, the protective layer facilitates the transfer of tactile information to the sensor array, where it undergoes conversion into electrical signals. These signals undergo processing in the signal processing layer, extracting meaningful data [174]. Subsequently, the processed signals are transmitted to the substrate for further conversion, ensuring compatibility with electronic devices. E-skin employs transduction mechanisms such as piezoresistive, capacitance, piezoelectricity, optics, wireless, and triboelectricity to convert external stimuli into electrical signals for subsequent processing and interpretation [174,175]. The advancement of flexible and stretchable sensors is pivotal in the development of E-skin and wearable technologies, holding promise in areas such as digital healthcare, robotics, and Virtual/Augmented Reality (VR/AR). Notably, current trends in wearable sensor and E-skin device development emphasize the utilization of organic and flexible materials, such as polymers and carbon composites, to enhance flexibility and biocompatibility [176]. The applications and systematic history of e-skin is shown in Fig. 20. Early developments integrated flexible sensors to mimic human skin, later advancing to detect pressure, temperature, and strain. This led to the integration of flexible electronic circuitry and energy harvesting, followed by multimodal sensing, data processing, and wireless communication. Biomimetic features enhanced functionality and aesthetics, enabling wearable applications in healthcare, robotics, prosthetics, and virtual reality. Other key trends include the integration of stretchable and conformable sensors for comfortable integration and continuous monitoring, as well as the implementation of multifunctionality to enable comprehensive health monitoring [177].

Nevertheless, challenges persist, including limited sensing range, sensor drift and instability, calibration requirements, limited lifespan, integration complexities, power and energy management, and form factor limitations. Overcoming these challenges necessitates meticulous materials design and the integration of multifunctional flexible sensors, facilitating a new era of highly adaptable and flexible electronics [177]. The incorporation of stretchable materials, including elastomers (e.g., silicone rubber, polyurethane, natural rubber) [180], conductive polymers (e.g., PEDOT:PSS) [181], carbon-based materials (e.g., CNTs, graphene) [182], and metal nanowires (e.g., silver nanowires), play a vital role in E-skin development. Additionally, geometric engineering techniques, such as serpentine patterns for stress distribution, island-bridge designs for independent functional movement, and wrinkled or patterned surfaces to accommodate mechanical deformation while maintaining functionality, enhance the overall stretchability and flexibility of E-skin devices [183,184].

4.2.1. *Characteristics advancements in E-Skin*

A reliable E-skin should possess the following characteristics: self-healable, hydrophobic, stretchable, sensitive, and biocompatible [185, 186]. The self-healing characteristic is inspired by the regenerative properties of human skin and aims to improve the lifespan and functionality of electronic devices. The concept of self-healing E-skin involves incorporating materials and mechanisms that allow the skin to recover from mechanical damage. The mechanism typically relies on two main approaches: the use of healing agents or dynamic reversible bonds [187]. In the healing agent approach, the E-skin is loaded with microcapsules or microvascular networks containing healing agents. When mechanical damage occurs, such as a crack or cut, the capsules rupture, releasing the healing agents that flow into the damaged area [183]. These agents then react and form bonds, effectively repairing the damage and restoring the functionality of the E-skin. The dynamic reversible bond approach utilizes materials with reversible chemical bonds that can break and reform. When the E-skin is damaged, these reversible bonds can dissociate and later re-establish, allowing the material to heal itself [188]. This mechanism is particularly useful for repeated or continuous healing of the E-skin. Peng et al., developed a novel flexible hydrogel by cross-linking polyvinyl alcohol (PVA) and polyethylenimine (PEI) with 4-formylbenzoboric acid (Bn) and incorporated MXene into the network. This Polybutylene terephthalate (PBPM) hydrogel demonstrates exceptional self-healing capabilities (healing time of 0.06 s) and rapid response performance (response time of 0.12 s) due to the combination of reversible dynamic covalent bonds and supramolecular interactions [188].

Several materials are used in the development of self-healing E-skin. Polymer-based materials, such as elastomers, are commonly employed due to their flexibility and ability to withstand mechanical stress. These

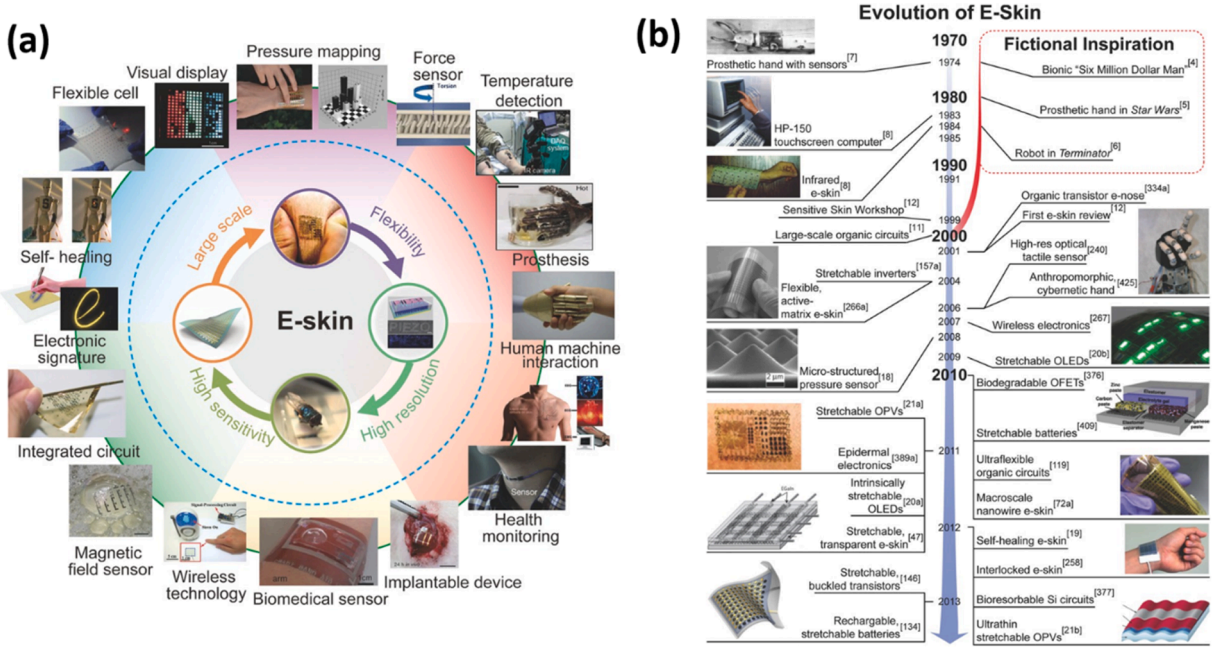

Fig. 20. (a) Exploration of characteristic properties and diverse functions or applications of recently developed devices for e-skins namely, flexibility, stretchability, sensitivity, durability, and biocompatibility, large scale development, high sensitivity and resolution, along with the wide range of applications in fields like healthcare, robotics, human-computer interaction, prosthetics, and visual displays (non-exhaustive)[178](b) A brief chronology of e-skin evolution: [179]. Reproduced with Permission.

polymers can be loaded with healing agents or contain dynamic reversible bonds. Kong et al., reported covalent crosslinked, self-healing polyurethane (PU) polymers which were fabricated as topological structure of covalent network using polytetramethylene glycol (PTMG), and hydroxyethyl disulfide (HEDS), providing stretchability through reversible disulfide bonds and strong intermolecular interactions [191]. The PU layer exhibited 3.8 % hysteresis, 81.2 % stretchability, and ~100 % self-healing efficiency. Combined with a microcrack-based conductive film, it achieves low hysteresis behavior while recording electromyography signals, providing a promising solution for protecting stretchable electronic systems from mechanical damage [191].

Similarly, conductive materials, such as CNTs or metal nanoparticles, and epoxy microcapsules are integrated into the self-healing polymers to maintain its electrical and healing properties. MWCNTs, and nanosilica microcapsules were incorporated into the polymers and found to increase the pristine self-healing properties. Notably, an increase in the volume fraction of microcapsules has been associated with improved healing efficiencies. Conversely, higher mechanical strength of the microcapsules has been found to reduce healing efficiency [192]. Higher volume fractions of microcapsules provide a greater concentration of healing agents, enabling more efficient spreading into the crack. This process fills crack voids, bonds surfaces, and restores mechanical integrity [192]. Scientists have developed a flexible and versatile ferroelectric e-skin that mimics the structural and functional characteristics of human fingertips, as shown in Fig. 21a. The e-skin incorporates piezoresistive, ferroelectric, and interlocked microdome

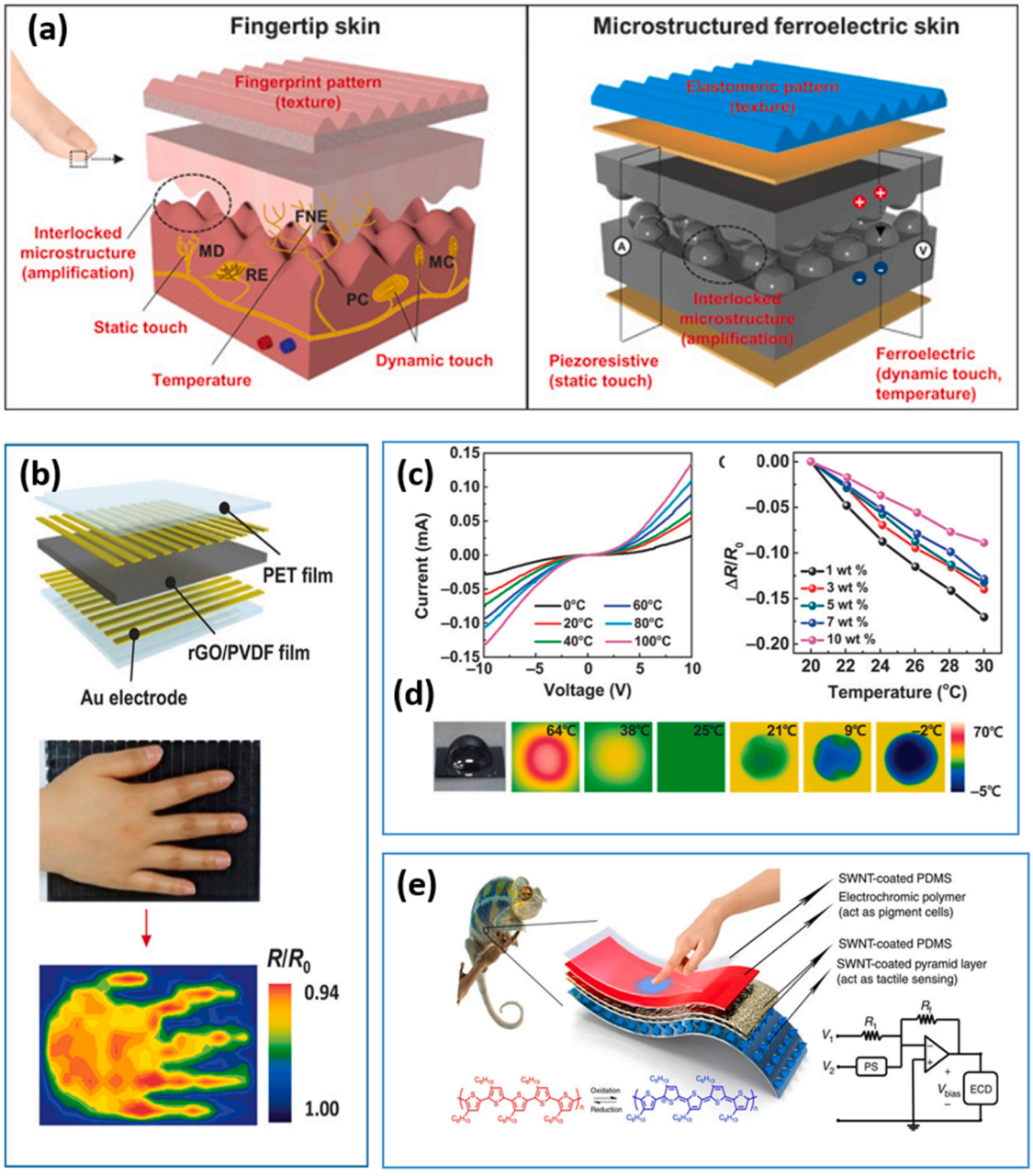

Fig. 21. (a) A flexible and multimodal ferroelectric e-skin replicates human skin functionalities using elastomeric patterns, piezoresistive materials for static pressure sensing, ferroelectric materials for dynamic pressure and temperature sensing, and interlocked micro arrays for tactile signal amplification. (b) Current-voltage curves of 1 wt % rGO/PVDF composite films at different temperatures. (c) Temperature-dependent relative resistance changes of rGO/PVDF composite films with varying rGO concentrations. (d) Visualization of temperature distribution on the human palm [189,17]. (e) Structures of neutral and oxidized states of electrochromic polymer (P3HT). and Schematic of circuit layout (PS: pressure sensor; ECD: electrochromic device)[190]. Reproduced with Permission.

arrays for static and dynamic pressure, temperature, and tactile signal amplification. It features a remarkable negative temperature coefficient of resistance (NTC) due to changes in contact resistance between rGO sheets and intrinsic NTC behavior (Fig. 21a-d). The integration of gold electrode arrays enables flexible temperature-sensitive e-skins capable of mapping temperature variations for medical diagnostics and human-machine interfaces [189].

Others have developed self-healing E-skin based on reversible covalent bonds, such as Diels-Alder reactions or supramolecular interactions [188,192,193]. Self-healing polymers (SHP) employ microencapsulation and reversible bonding through covalent bonds or supramolecular mechanism to achieve autonomous repair and restoration [188]. SHPs can also incorporate a vascular network consisting of microchannels or capillaries filled with healing agents. In the event of damage, the healing agents flow through these channels, effectively filling and repairing the damaged regions. Additionally, certain SHPs exhibit a shape memory effect, allowing them to revert to their original form when deformed or damaged, triggered by external stimuli such as heat or light (power sources)[193]. Reliable power sources are crucial for e-skin to function effectively. They enable sensors to detect and transmit signals, actuators to respond, and electronic circuitry to process data. Moreover, power sources ensure the longevity and continuous operation of e-skin devices. Similarly, Fig. 21e showcases a bio-inspired stretchable e-skin that integrates two functionalities a tunable resistive pressure sensor and stretchable organic electrochromic devices [190]. This combination empowers the e-skin with interactive color-changing and tactile-sensing capabilities, allowing for real-time visible color changes that effectively detect and distinguish varying pressures. The e-skin's tunable resistive pressure sensor enables precise measurement and detection of external pressure applied to its surface, offering a sensitive tactile feedback mechanism. Simultaneously, the incorporation of stretchable organic electrochromic devices allows the e-skin to undergo dynamic color changes, responding visually to the detected pressures. This dual capability makes the e-skin suitable for interactive and intuitive sensing applications [190]. Recently, Zhong et al. demonstrated Bi_2FeMnO_6-based photoelectric synapse that integrates light and electrical pulses for dual neuromorphic control, enhancing hardware potential. Optimized training with UV excitation and ferroelectric enhancement boosts plasticity and reduces pulse requirements, achieving 98.8 % accuracy for sensor-based digit recognition [194]. In another study, Huang et al. developed Au/PHO/FTO synapse demonstrates learning and memory characteristics like biological neurons, facilitated by a convolutional neural network and an enhanced stochastic adaptive algorithm. These findings can be integrated to human-machine interface devices [195].

4.2.2. Energy autonomous E-skin

Energy autonomous E-skin incorporates cutting-edge concepts to create a sophisticated sensing system. It comprises of three primary components: flexible sensors, energy harvesting elements, and energy storage units. By employing various advanced energy harvesting mechanisms, such as photovoltaics, thermoelectrics, piezoelectrics, or triboelectrics, the e-skin becomes capable of harnessing ambient energy to generate electricity.

4.2.2.1. Solar powered E-skin. Solar energy is an increasingly popular and sustainable power source derived from the sun's rays, serving as a clean and efficient alternative to traditional fossil fuels. Solar cells, also known as photovoltaic cells, are pivotal in harnessing solar energy by directly converting sunlight into electricity. These cells come in various types, each possessing distinct characteristics and efficiencies. Among the notable types of solar cells are monocrystalline silicon (Mono-Si) cells, which are fabricated from a single crystal structure, resulting in heightened purity and efficiency. Mono-Si cells exhibit a uniform appearance due to their single crystal structure and boast a notable power conversion efficiency (PCE) ranging from 10 % to 20 %[196,197]. On the other hand, polycrystalline silicon (Poly-Si) cells are made from multiple crystal structures, making them more cost-effective to produce compared to Mono-Si cells. However, Poly-Si cells have a slightly lower PCE, typically ranging from 10 % to 15 %, and display a distinctive bluish hue and speckled appearance [197,198]. Similarly, conductive materials such as CNTs, graphene, MXene, TMDs are strategically integrated into solar cells to enhance their performance. Carrier-selective layers of PEDOT: PSS, MoO_3 WO_3, CNTs optimize energy conversion, achieving >18 % efficiency. Oxide-enhanced CNTs-Si solar cells integrate traditional semiconductor benefits with novel nanostructures, promising high-performance silicon-based photovoltaics [199,200].

Thin-film solar cells consist of exceptionally thin layers of semiconducting materials deposited on various substrates. These cells encompass different variants such as amorphous silicon (a-Si), cadmium telluride (CdTe), and copper indium gallium selenide (CIGS) [201,202]. Their lightweight and flexible nature enables versatile applications. However, thin-film cells generally exhibit lower PCE compared to silicon-based cells, typically ranging from 10 % to 12 %[202]. Despite being in the developmental phase, perovskite solar cells (Sn-Pb) have already demonstrated impressive PCEs exceeding 25 % in laboratory settings, positioning them as promising candidates for future solar technologies [203–205]. Thin-film solar cells, with their flexibility and lightweight nature, are particularly well-suited for integration into e-skin devices. These cells can be printed onto pliable substrates and seamlessly combined with other electronic components, enabling the creation of self-powered e-skin systems.

4.2.2.2.1. DSSCs. Flexible dye-sensitized solar cells (DSSCs) are highly adaptable and lightweight, making them ideal for e-skin applications. Plastic substrates like ITO-PET and ITO-PEN offer flexibility, while metal substrates are preferred for large-scale DSSCs. However, plastic substrates face challenges, resulting in lower conversion efficiency (around 10.28 %) due to limitations in the sintering process at temperatures below 150 °C [206]. To overcome this, researchers have explored alternative materials and fabrication methods, such as binder-added TiO_2 photoanodes and PEI substrates. Recent studies have demonstrated further progress, achieving an impressive conversion rate of 28.9 % by employing the D35 dye, XY1 sensitizer, and the Cu (II/I) $(tmby)_2$ $TFSI_2$/1 redox shuttle under warm white light [207,208]. Architectural improvements have successfully reduced the redox mediator diffusion path, resulting in a remarkable PCE of 32 % under illumination [207,209]. In comparison, a flexible GaAs cell manufactured by Alta devices exhibited a relatively lower conversion efficiency of 21 % under similar illumination conditions [210].

TiO_2 nanoparticles (NPs) are commonly used as photo-anodes in DSSCs due to their optimized bandgap, small particle size, reduced grain boundaries, and significant porosity suitable for efficient charge diffusion. Among the various precursors investigated, titanium isopropoxide (TTIP) has been extensively studied as a precursor for organic metals. TTIP's impact on TiO_2 deposition has been extensively studied. Shuhadah et al., [211,35] investigated TiO_2 particle structure using varying TTIP molarities (0.2 M, 0.3 M, 0.4 M, and 0.5 M). Results show that increasing TTIP concentration reduces rutile phase content, enhances anatase phase crystallization, and reduces crystal size from 21 nm to 17 nm, resulting in improved photocatalytic activity. Some studies suggest an optimal TTIP concentration of 6 mol% for efficient electron transfer, increased current, and enhanced solar cell performance [212]. Moreover, 6 % mol TTIP contributes to improved surface porosity, enhancing dye absorption and photocurrent. UV–Vis analysis confirms the highest UV absorption peak at 6 mol% TTIP [212]. Alternatively, hole-transport materials (HTMs) like redox mediators, electrolytes, solid inorganic materials, and organic polymers have also been explored [213].

Spiro-type HTMs are widely used in solar cells due to their advantageous structures, including nonplanar 3D geometry, high glass-

transition temperature, and good solubility due to weak intermolecular interactions. The cross-shaped configuration of spirobifluorene enhances rigidity and reduces aggregation during film formation [214]. Researchers are exploring other spirobifluorene-based HTMs in organic and hybrid solar cells for improved performance. Iodide/triiodide ($I-/I3-$) in solid polymer, gel, ionic liquid, or plastic crystal systems, Spiro-OMeTAD (2,2′,7,7′-Tetrakis(N,N-di-p-methoxyphenylamine)−9, 9′-spirobifluorene), PEDOT, Poly(3-hexylthiophene) (P3HT), Poly(3, 4-propylenedioxythiophene) (PProDOT), Poly(triarylamine), Copper phthalocyanine (CuPc) and Rubrene are some of the alternatives which increased the PCE [213–216]. Further, packaging technology is crucial for e-skin applications, as it addresses challenges related to hazardous environments and extreme deformation, ensuring the safety and integrity of DSSCs in e-skin devices.

4.2.2.1.2. Organic solar cells. High-performance organic semiconductors like Poly(4,8-bis[5-(2-ethylhexyl)thiophen-2-yl]benzo[1,2-b:4,5-b']dithiophene-2,6-diyl}{3-fluoro-2-[(2-ethylhexyl)carbonyl] thieno[3,4-b]thiophenediyl) (PTB7-Th), Poly(2,7-carbazole-alt-4,7-di (thiophen-2-yl)benzo[c][1,2,5]thiadiazole) (PCE10), Indacenodithieno [3,2-b]thiophene-2,8-dione (ITIC), Poly(3-hexylthiophene) (P3HT), and Poly[[4,8-bis[(2-ethylhexyl)oxy]benzo[1,2-b:4,5-b']dithiophene-2,6-diyl][3-fluoro-2-[(2-ethylhexyl)carbonyl]thieno[3,4-b]thiophenediyl]] (PTB7) were developed, along with promising electron acceptors such as ITIC and ITIC-fluorine, offering improved absorption and charge transport properties [218,219]. Transparent conductive oxides such as ITO and flexible alternatives such as Poly(3,4-ethylenedioxythiophene) PEDOT:PSS were widely employed as electrode materials. The PCE of flexible organic solar cells exceeded 18 % in 2020, with select reports reaching 20 %, while enhanced stability was accomplished through interface engineering, encapsulation techniques, and stable material choices [220,221]. Tandem configurations combining subcells with complementary absorption spectra achieved PCEs exceeding 17 %. Solution-based printing techniques like inkjet, roll-to-roll, and screen printing facilitated large-scale production, and morphology control methods such as solvent annealing and additive engineering optimized the active layer morphology for improved charge transport [210,221]. Flexible substrates like PET, PEN, and metal foils enabled flexibility and conformability, while strategies like stretchable electrodes and encapsulation layers improved mechanical robustness. Arnab et al., introduced a self-powered skin-like sensing device using polymer dots

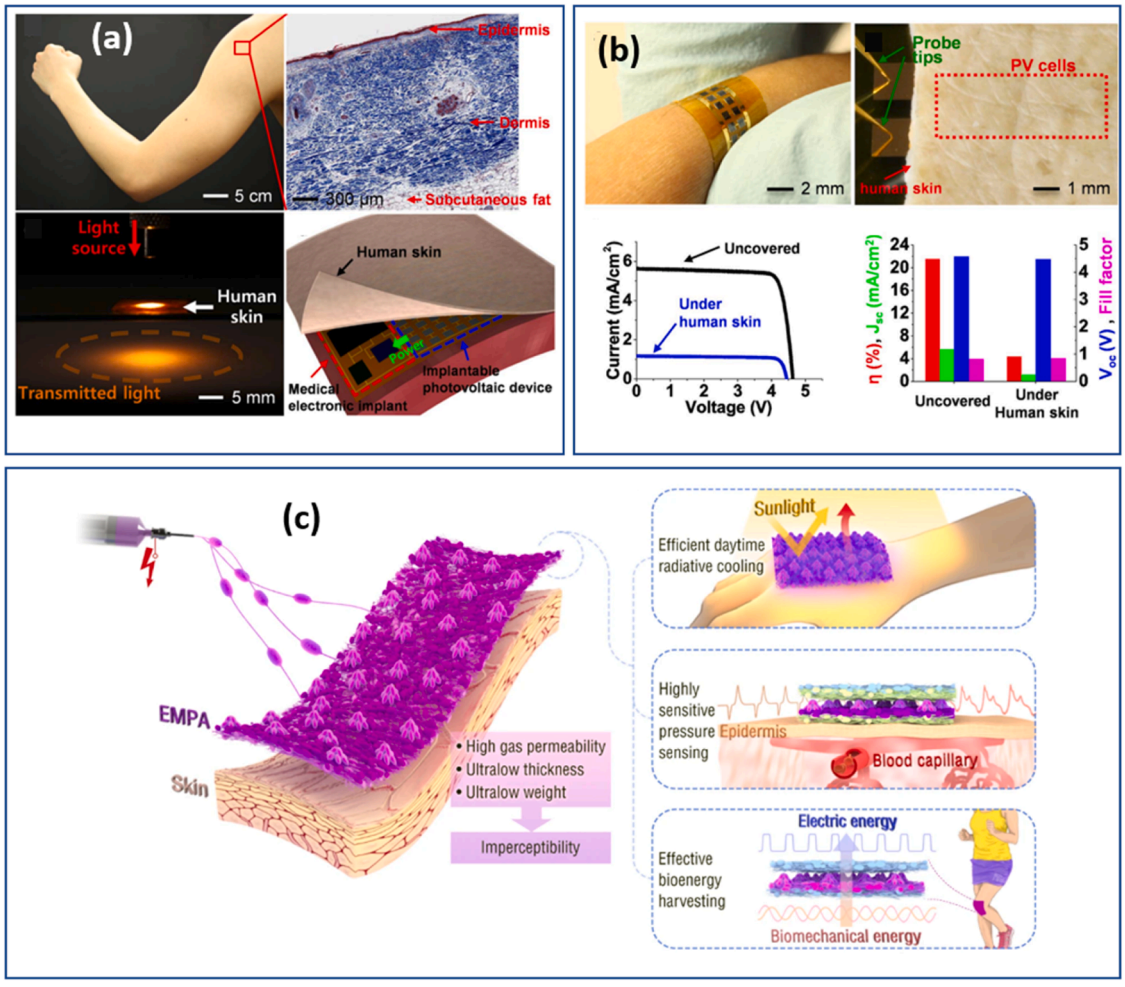

Fig. 22. (a) Human arm with the selected location for the shoulder skin sample, histological microscope image of stained shoulder skin tissue (epidermis: ~32 μm, dermis: ~1.8 mm), demonstration of light transmission through isolated hand dorsum skin (~0.94 mm thickness), and schematic illustration of electrical power generation using an implantable photovoltaic (IPV) device absorbing light transmitted through human skin (b) Electrical properties of a flexible PV device under human skin, including optical image of the device on a forearm, fixed human hand dorsum skin covering the device, current-voltage curves under illumination, and changes in efficiency, short circuit current density, open circuit voltage, and fill factor when uncovered and covered with human skin [217] (c) Fabrication, structure, and application schematic of electrospun micropyramid arrays (EMPAs), Illustration of EMPA growth process showing the dependence of thickness-morphology, with wet heterostructured electrified jets forming inhomogeneously charged microdomains. Electrostatic interaction causes positively charged aerial jets to deposit onto negatively charged microdomains with higher PVDF contents. These microdomains evolve into fibrous domes, representing the embryonic forms of EMPAs, as substrate thickness increases [190]. Reproduced with Permission.

incorporated hydrogel as a capacitive sensor/supercapacitor and a P3TAA/N—CD-based solar cell for energy harvesting [222]. The incorporation of polymer dots improved the mechanical properties of the hydrogel, resulting in enhanced cycling stability and a higher areal capacitance. The device demonstrated high sensitivity in detecting small pressure changes and achieved significant improvements in energy storage efficiency and electrochemical performance [222].

In another work, Song et al., presented the electrical performance of an implantable solar cell array tested on 59 human skin samples (Fig. 22a-b) [217]. The achieved power densities ranged up to 9.05 mW/cm2, with higher power generation observed in thinner and brighter skin. The generated power is sufficient to operate microwatt-level medical electronic implants like pacemakers [217]. Optical properties were measured using a fiber-optic spectrometer with double integrating spheres, revealing light transmission through translucent skin. Current-voltage characteristics were evaluated using a flexible IPV device, showing decreased efficiency (from 21.5 % to 4.3 %) and short circuit current density (from 5.63 mA/cm2 to 1.17 mA/cm2) under human skin, while open circuit voltage and fill factor remained stable. These findings demonstrate the potential of the implantable solar cell array for powering medical implants and offer insights into its electrical performance characteristics under human skin [217]. Another study explores the electrospun micropyramid arrays (EMPAs), beginning with their fabrication, structure, and application schematic. Fig. 22c vividly depicts the EMPA growth process, shedding light on the dependence of thickness-morphology during their formation [190].

During electrospinning, electrified jets emerge, revealing wet heterostructured characteristics as they form inhomogeneously charged microdomains. The interplay of electrostatic forces becomes evident as positively charged aerial jets gracefully deposit onto negatively charged microdomains with higher PVDF contents [190]. Interestingly, the microdomains, with the aid of this electrostatic interaction, evolve into fibrous domes. These fibrous domes, in essence, represent the embryonic forms of the intricate EMPAs. Furthermore, the study uncovers that the thickness of the substrate exerts a profound influence on the final morphology of the EMPAs. As the substrate thickness increases, it orchestrates the evolution of these microdomains into the delicate and precisely structured micropyramid arrays [190].

4.2.2.1.3. Multi junction solid-state solar cells. MJ (multi-junction) solid-state photovoltaics (PVs) represent a class of solar cells that exhibit high conversion efficiencies using multiple semiconductor layers with different bandgaps. This unique design allows each layer to absorb specific portions of the solar spectrum, enabling the capture of a broader range of light wavelengths and maximizing sunlight-to-electricity conversion. III-V compound semiconductors, such as gallium arsenide (GaAs), indium gallium phosphide (InGaP), and indium gallium arsenide (InGaAs), are commonly employed in MJ solid-state PVs [223,224]. These materials possess exceptional electronic properties, high carrier mobility, and efficient light absorption across a wide spectrum. The careful selection of materials and their corresponding bandgaps is crucial for achieving efficient absorption and minimizing energy losses attributed to thermalization processes. The performance traits of MJ solid-state PVs are remarkable, with conversion efficiencies exceeding ~25 % achievable by stacking multiple layers with varying bandgaps. Such efficiencies significantly surpass those of traditional single-junction solar cells. Moreover, MJ solar cells exhibit excellent spectral response, enabling them to maintain high performance even under challenging lighting conditions characterized by low light levels or indirect sunlight [225,226]. The working mechanism of MJ solid-state PVs relies on the absorption of photons in the various layers comprising the cell. Each layer selectively absorbs photons possessing energy levels corresponding to its specific bandgap. The absorbed photons generate electron-hole pairs, thereby creating charge carriers. These carriers are subsequently collected by the respective layers and converted into electrical energy [224].

Advancements in MJ solid-state PVs have been geared toward enhancing efficiency, stability, and scalability. Researchers have explored novel materials, including perovskites (such as methylammonium lead iodide, MAPbI3) and quantum dots (such as colloidal lead sulfide, PbS), as potential candidates for MJ solar cells [223]. Furthermore, advanced fabrication techniques, including epitaxial growth and atomic layer deposition, have been employed to improve layer quality and thickness control. Moreover, efforts have focused on optimizing device structures and interface engineering to minimize energy losses and enhance charge collection efficiency [223,224].

4.2.2.2. Mechanical energy. Mechanical energy harvesting for e-skin applications relies on a range of materials and mechanisms to convert mechanical energy into electrical energy. Triboelectric sensors, as a type of e-skin sensor, can be classified into distinct working modes [227]. The contact-separation (CS) mode detects contact and separation between materials, inducing the generation of positive and negative charges. In the single-electrode (SE) mode, a single electrode collects electric charges generated from the contact and separation between the triboelectric material and another surface [228,229]. The lateral sliding mode detects relative lateral movement, generating charges through friction between different materials. In the freestanding mode, the mechanically responsive triboelectric layers detect touch, pressure, and vibrations experienced through contact and separation, resulting in the generation of electric charges. Triboelectrics, such as polydimethylsiloxane (PDMS), polytetrafluoroethylene (PTFE), and polyimide (PI), generate electrical charges through contact-induced friction, enabling efficient conversion of mechanical energy [230,231]. Qu et al., used triboelectric smart finger that consists of a sensor array, data acquisition module, and OLED display. The sensors use different friction materials and generate voltage signals upon contact and separation [232]. Signals are recorded, transmitted for machine learning, and displayed on a computer or OLED screen. Sensor size and contact/separation distance affect performance. The triboelectric sensor demonstrates fast response, temperature stability, and high detection stability. Integration enables wireless signal transmission, intuitive display, and accurate material recognition. Wireless transmission and display eliminate the need for a data cable, enhancing portability and functionality [231].

Another study (Fig. 23a) reports a CNTs textile, adhering it to a Band-Aid bandage, bonding a spacer with adhesive tape, attaching the FEP film side, and connecting the test electrodes with thin copper wires [233, 59]. The sensor exhibits a signal-to-noise ratio of 23.3 dB, response time of 40 ms, and sensitivity of 0.21 μA kPa^{-1}. It measures systolic and diastolic pressure accurately using machine learning algorithms, validated against a commercial blood pressure cuff. A custom smartphone application facilitates health data sharing and data-driven cardiovascular diagnosis [233].

Researchers developed a fabric belt integrated with sewn triboelectric sensors, allowing for real-time robotic and immersive waist training. Additionally, an insole equipped with TENG sensors was designed to achieve a high level of identification accuracy for rehabilitation plans, Fig. 23b [234]. A pyramid-patterned triboelectric layer was fabricated using a 3D-printed mold and Ecoflex material, employing silicone rubber as the main component. Furthermore, the TPU-coated fabric was composed of PES fabric, TPU film, and Ni-fabric electrodes, resulting in a fabric with a thickness of 0.4 mm. To complete the structure, the silicone layer was carefully attached to the Ni-fabric face, and a thermal sealer was utilized to effectively seal the TPU film and TENG structure [234].

Electromagnets, including ferromagnetic alloys like nickel and iron, operate on the principle of electromagnetic induction, producing an electrical current in nearby coils when mechanical motion induces a change in the magnetic field [235,236]. In self-powered e-skin, the electromagnet's core is made of ferromagnetic materials like iron, nickel, or cobalt, allowing efficient magnetic flux transfer. The coil, usually copper or aluminium, has excellent electrical conductivity to generate the magnetic field. Higher magnetic field strength enhances

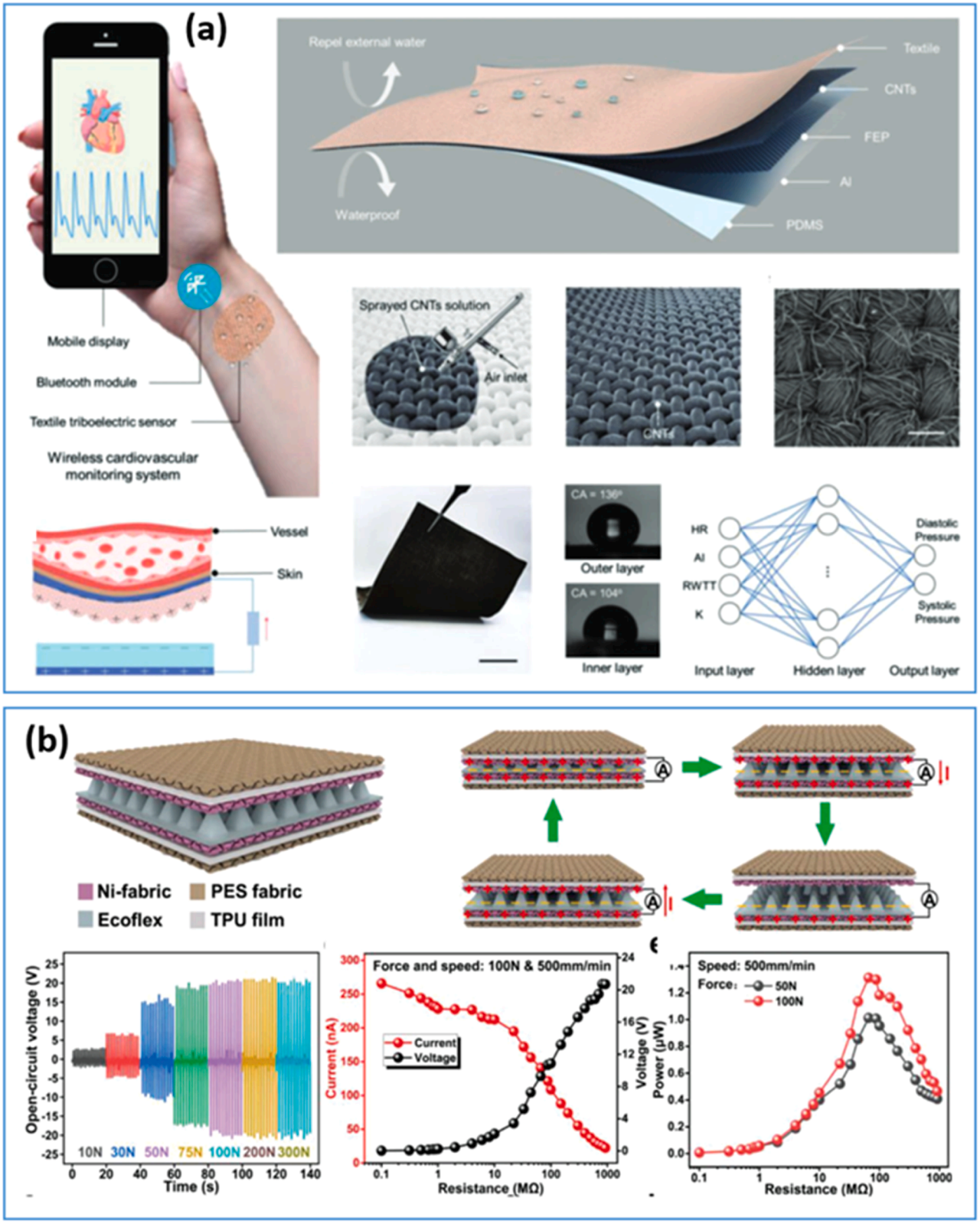

Fig. 23. (a) Design of a self-powered textile triboelectric sensor-based cardiovascular monitoring system with wireless signal transmission, illustrating the response to radial artery pulse for electricity generation, the schematic structure of the textile sensor, spray-coating of monodispersed CNTs onto cotton textile, hierarchically structured CNTs textile, waterproof performance, and the architecture of a supervised feedforward neural network for blood pressure prediction (HR: heart rate, AI: augmentation index, RWTT: reflected wave transit time). (reproduced with permission from [233] (b) Characterizations of a textile-based TENG sensor, including structure, working mechanism, open-circuit voltages under different compressing forces, output characterizations with specific force and speed, and power curves with varying compressing forces (reproduced with permission from [234] Reproduced with Permission.

sensitivity to external magnetic fields. Increasing the coil's turns boosts the field strength. The electromagnet's resonant frequency maximizes sensitivity to external magnetic fields, ensuring optimal performance in self-powered e-skin devices [237–239]. Fabricating electromagnet-based self-powered e-skin involves shaping the ferromagnetic core material through cutting, milling, or lathing into desired forms such as cylindrical or rectangular shapes. The coil is created by tightly and uniformly winding copper or aluminium wire around the core, maximizing current flow and magnetic field strength. Insulation using materials like enamel or tape prevents short circuits and ensures electrical isolation. The electromagnet is then integrated into the e-skin device, alongside other sensing components like temperature and pressure sensors, as well as signal processing circuitry [234,240]. These components are often printed or deposited onto flexible substrates like polyimide or silicone, enabling the creation of flexible and wearable e-skin. Self-powered e-skin devices also incorporate power management circuits and energy harvesting mechanisms, such as piezoelectric materials or triboelectric nanogenerators, which convert mechanical energy (such as pressure or motion) into electrical energy, stored and utilized to power the device [237,239].

Solid-state multifunctional CNTs based nanogenerator was introduced, exhibiting exceptional stretchability of approximately 590 %. This fiber was designed to scavenge both biomechanical energies, generated from body motion, and dissipated electromagnetic energy emitted by nearby electrical appliances. Alongside its energy collection capabilities, the nanogenerator fiber also functioned as a self-powered sensor [241]. Its structure comprised a conducting composite-coated extensible fiber enclosed by a triboelectric elastomer, enabling energy extraction through both triboelectrification (maximum of 424 V m^{-1}) and electromagnetic-induced electrification ($\pm$ 8.8 V m^{-1} at 60 Hz) [241].

The self-powered e-skin system described in this study incorporates an electromagnet to enable its functionality. The electromagnet is composed of a whisker-like magnetized micro-cilia array (MMCA) and flexible coils. The MMCA, known for its exceptional flexibility, allows for adaptive bending of the micro-cilia in response to tactile inputs and surface morphologies [242]. The MMCA is designed with built-in magnetic moments, which play a crucial role in the system's operation. When the MMCA deforms due to external forces, such as pressure or touch, the magnetic flux distribution within the array is altered. This deformation-induced change in magnetic flux induces an electro-motive force (voltage) in the flexible coils integrated beneath the MMCA [242]. The flexible coils are designed to capture the induced voltage and convert it into measurable electrical signals for pressure detection and quantitative recognition of micro-scaled 3D morphologies. The system takes advantage of distinct voltage intensities and waveforms to optimize its performance. These signals are then analyzed to facilitate real-time healthcare monitoring, Braille identification, and reconstruction of relief information. The fabrication process involves customizing the magnetic moment alignments within the MMCA to achieve specific functionalities and generate distinguishable signals. This customization allows the e-skin device to be used for efficient human-machine interaction, including underwater Morse code communication. Additionally, the e-skin system exhibits temperature tolerance and environmental immunity, ensuring its performance and reliability in various conditions [242].

Piezoelectrics, such as lead zirconate titanate (PZT), polyvinylidene fluoride (PVDF), and zinc oxide (ZnO), exhibit the piezoelectric effect by generating electrical charges in response to applied mechanical stress or vibration. PVDF-TrFE, a copolymer of PVDF and trifluoroethylene, provides improved piezoelectric properties, flexibility, and thermal stability, and used in pressure mapping, force sensing, and energy harvesting [243]. PLLA demonstrates potential for biomedical piezoelectric sensors in tissue engineering and implants, while silk fibroin and specific polypeptides offer inherent piezoelectric properties for wearable devices and bioelectronics. Gong et al., combined a high-output voltage meso-PLA triboelectric nanogenerator (NG) with a high-current PLLA-based piezoelectric nanogenerator (PENG) for an E-skin device. The hybrid NG generates 70 V and 25 μA at 19.7 Hz resonance frequency and a 4.71 g tip load. It also produces 0.31 mW output power, 11 % higher than the PLLA-based PENG, and successfully controls a light-emitting diode during a bending test [244]. It has been reported that a lightweight, and wearable piezoelectric e-skin, based on PVDF/MWCNTs, has been developed for monitoring human physiological signals with higher electrical conductivity and mechanical strength when compared to [243]. It has been positioned on the wrist to capture real-time pulse amplitudes and frequencies during rest, typically around 80 bpm. The sensor has been constructed by layering conductive fabrics on PVDF/MWCNTs nanofibers and enclosing them with PDMS. Luo et al. employed the near-field electrohydrodynamic direct-writing method to produce a PVDF/SWCNTs thin film for a piezoelectric pressure sensor [245]. By utilizing a moving rectangle trajectory, they directly write a micro/nano fiber array, leading to a piezoelectric pressure active thin film with enhanced structural consistency and improved piezoelectric performance. The resulting flexible sensor demonstrates a high sensitivity of 15.68 kPa^{-1} and a rapid response time of 66 ms [245].

Advancements in these materials and mechanisms aim to enhance efficiency, durability, and flexibility for e-skin applications. Researchers have explored novel triboelectric and piezoelectric materials with improved charge generation capabilities and mechanical properties. Additionally, efforts have focused on optimizing the design and integration of electromagnetic and piezoelectric materials to enhance energy conversion efficiency and stability. These materials and mechanisms are well-suited for e-skin applications due to their effective harvesting of mechanical energy from the surrounding environment, including subtle movements or vibrations. Their flexibility enables them to conform to the shape of the skin while maintaining their performance even during bending or stretching. Furthermore, they offer self-powered capabilities by generating electrical energy without the need for external power sources, making them highly suitable for wearable devices and e-skin technology [241].

4.2.2.3. Magnetic energy. Magnetic energy harvesting for e-skin is like a dance between electricity and magnetism. It takes advantage of the magnetic fields around us to make useful electricity. Imagine a special wire, like a coil, that touches these magnetic fields. When the magnetic field changes, it makes something called "electromotive force" or EMF in the wire. This EMF creates an electric current, which is a flow of electricity. We then store this electricity in batteries or capacitors. Later, we use this stored energy to power the sensors and parts of the e-skin [240]. Special materials such as amorphous alloys and ferrites were harnessed, leading to enhanced efficiency in energy conversion. Concurrently, researchers innovated by creating coils that could be stretched and bent, aligning them perfectly with the form factor demands of e-skin devices. Furthermore, the study of magnetic bacteria, exemplified by *Magnetospirillum magneticum and Magnetococcus marinus* [246–248]. These bacteria were distinguished by their minute magnetosomes nanoparticles with magnetic properties that aligned with external magnetic fields. By drawing upon the ambient magnetic fields, these magnetic bacteria may introduce novel horizons for wearable technology, suitable for e-skin [249].

Various materials are utilized in magnetic energy storage, each with distinct properties and applications. Permanent magnets, like neodymium-iron-boron (NdFeB) and samarium-cobalt (SmCo) alloys, exhibit enduring strong magnetic properties without external power, finding use in steady magnetic fields for small-scale energy storage and devices like generators [248,250]. Soft magnetic materials, such as iron alloys, enable facile magnetization and demagnetization, crucial for swift magnetic field changes in energy conversion contexts like transformer cores. Nanoscale magnetic materials with amplified surface area, known as magnetic nanoparticles, can be tailored for specific

behaviours, offering versatility in energy storage, including advanced systems like hybrid pseudocapacitors [248]. Magnetic nanocomposites amalgamate nanoparticles with polymers or ceramics, yielding lightweight materials for flexible energy storage, suitable for integration into e-skin. Superconductors, by contrast, devoid of electrical resistance below a certain temperature, store magnetic energy efficiently and are integral in superconducting magnetic energy storage (SMES) systems, serving high-power needs such as grid stabilization through rapid energy discharge, and are less suitable for e-skin.

The researchers explored the inherent potential within 2D nanomaterials. These materials, acknowledged for their exceptional surface activity, were pinpointed as plausible candidates for energy harvesting via flexoelectricity, especially from minor mechanical inputs. The research centred on synthesizing a thin 2D spinel compound $MgCr_2O_4$ using liquid-phase exfoliation, revealing its unique preference for exfoliation along the (111) plane due to low formation energy [251]. The core of the investigation revolved around developing a flexoelectric device driven by the synthesized 2D $MgCr_2O_4$. Remarkably, this device demonstrated a distinctive electrical response, generating voltages of up to ~3 V (peak-to-peak) under a ~0.98 N force during compression and release cycles. This response substantiated the captivating flexoelectric behavior intrinsic to the 2D nanomaterial. Through synergizing its flexoelectric attributes with external energy sources, controlled bending combined with varying magnetic flux (yielding Vmax of ~2.6 V) and fluctuating temperatures while applying a 0.9 N force (resulting in Vmax of ~18 V) unveiled its versatility in energy generation. Importantly, computational analysis played a significant role, revealing a flexoelectric coefficient of 2D $MgCr_2O_4$ approximating $\mu = 0.005$ nC/m. This parameter quantified the material's adeptness in generating electrical potential in response to small mechanical deformations, thus reinforcing its innate suitability for energy generation from e-skin [251].

4.2.2.4. Thermal energy. Thermal energy harvesting is based on the thermoelectric effect or Seebeck effect. This effect states that when a temperature gradient is applied to a thermoelectric material, it generates a voltage difference. Thermoelectric generators (TEGs) can convert this voltage difference into electrical energy. TEGs are typically made of high-efficiency semiconductor materials and consist of p-type and n-type semiconductors connected to form a thermocouple. By exposing one side of the thermocouple to a heat source and keeping the other side at a lower temperature, an electrical potential is generated due to the temperature difference. This potential can power electronic devices or be stored in batteries [252,253]. By introducing nanostructures, such as nanowires or nanograins, the phonon scattering effect can be maximized, thereby reducing thermal conductivity while maintaining electrical conductivity. This leads to improved energy conversion in e-skin [254].

Researchers have been exploring novel materials, such as organic polymers and nanocomposites, that can exhibit thermoelectric properties while maintaining flexibility. These materials can be integrated into flexible substrates or printed onto wearable platforms, enabling the development of conformable and stretchable TEGs. Wu et al., used graphite composite consisting of bonded and aligned graphite nanoplatelets, along with a thin Phase Change Material (PCM) layer, which synergistically enhances thermal conductivity. The resulting PCMs show thermal conductivities ranging from 4.4 to 35.0 W m^{-1} K^{-1} with graphite loadings below 40.0 wt% [255]. These PCCs exhibit uniformity, no leakage, and superior phase change behavior. Aligned graphite sheets are formed by compressing worm-like expanded graphite (WEG) derived from natural graphite flakes. These sheets consist of highly oriented GNPs bonded by van der Waals forces at the micrometre scale, with millimeter-sized lateral dimensions. The van der Waals interactions between adjacent GNPs reduce interfacial thermal resistance, promoting efficient nanoscale thermal conduction. Each graphite sheet acts independently as a conductive chain. Prior to compression, GNPs on WEG are coated with a thin layer of phase change material (PCM), ensuring low junction thermal resistance [255].

In a recent study, a scalable method was presented for creating anisotropically conductive phase change composites (PCCs). The method involves using aligned continuous carbon fibers (CFs) embedded in paraffin wax (PW)/olefin block copolymer (OBC) blends. The aligned CFs establish continuous and directional thermal conduction paths within the PCCs, resulting in a high lengthwise thermal conductivity of 5.63 $W{\cdot}K^{-1}{\cdot}m^{-1}$ and a low transverse thermal conductivity of 0.77 $W{\cdot}K^{-1}{\cdot}m^{-1}$, with a remarkable anisotropic degree of 7.31 (Fig. 24a). Additionally, a carbon black coating is applied to the PCC surface to enhance solar absorption, boosting the full-spectrum solar absorptance to an impressive 0.988.

Kashyap et al., presented an innovative hybrid system that combines molecular energy and latent heat storage for continuous energy delivery. It was explained that this system can achieve high harvesting efficiency during the day, reaching 73 % at small scale and 90 % at large scale (Fig. 24b) [257]. Moreover, it was highlighted that the system demonstrates impressive energy recovery at night, with an efficiency of 80 % at higher temperatures compared to those observed during the day. The hybrid system comprises a molecular storage material (MSM), a localized phase-change material (L-PCM), and a silica aerogel that serves to maintain temperature differences. This combination allows for efficient energy capture and storage [257]. Molecular energy refers to the energy stored within the molecular structure of certain materials, which can be released and harnessed for various applications. Latent heat storage, on the other hand, involves storing thermal energy by utilizing the phase transition of a material, such as from solid to liquid or vice versa. By combining these two storage mechanisms, the hybrid system achieves high harvesting efficiency during the day and energy recovery at night [257].

The development of flexible composite PCMs, which integrated the uniquely constructed CNTs sponge and polyvinylidene fluoride (PVDF), demonstrated efficient performance in thermotherapy [258]. It was further stated that the utilization of $Ti_3C_2T_x$ MXene, polyaniline (PANI), and SWCNTs in thermoelectrochemical cells (TECs) yielded significantly improved performance in comparison to conventional platinum electrodes. The resulting ternary composite electrodes were reported to possess a porous layered structure, enabling extensive electrochemical reactions due to their large surface area [259]. It was pointed out that experimental and simulation data revealed the synergistic effects of $Ti_3C_2T_x$ and PANI, facilitating both mass and charge transport at the interface between the electrolyte and the electrodes. These enhancements were said to result in an impressive output power of 13.15 μW cm^{-1} for the TECs when exposed to a temperature difference (ΔT) of 40 K [259].

Various materials have been explored and studied extensively to enhance thermoelectric performance. One prominent group of materials is the class of skutterudites ($CoSb_3$), which are compounds consisting of rare earth or alkaline earth metals, transition metals, and pnictogens [260]. Another promising class of materials is the group of half-Heusler compounds (ZrNiSn and TiNiSn), which are composed of three different elements, typically a transition metal, a main group element, and a metalloid [261]. By tailoring the composition and manipulating the crystal structure, researchers have achieved improved thermoelectric performance in half-Heusler compounds. Various silicide compounds, such as Mg_2Si, Ca_3Si_2, and $SrSi_2$, have been studied for their thermoelectric properties [262,263].

4.2.2.5. Chemical energy. In addition to thermal and mechanical energies, researchers have started recognizing the untapped potential of chemical energy as a viable power source for electronic skin, or e-skin. Initially overlooked, recent advancements in biofuel cell (BFC) technology have paved the way for harnessing energy from various human body fluids such as saliva, urine, sweat, and blood through

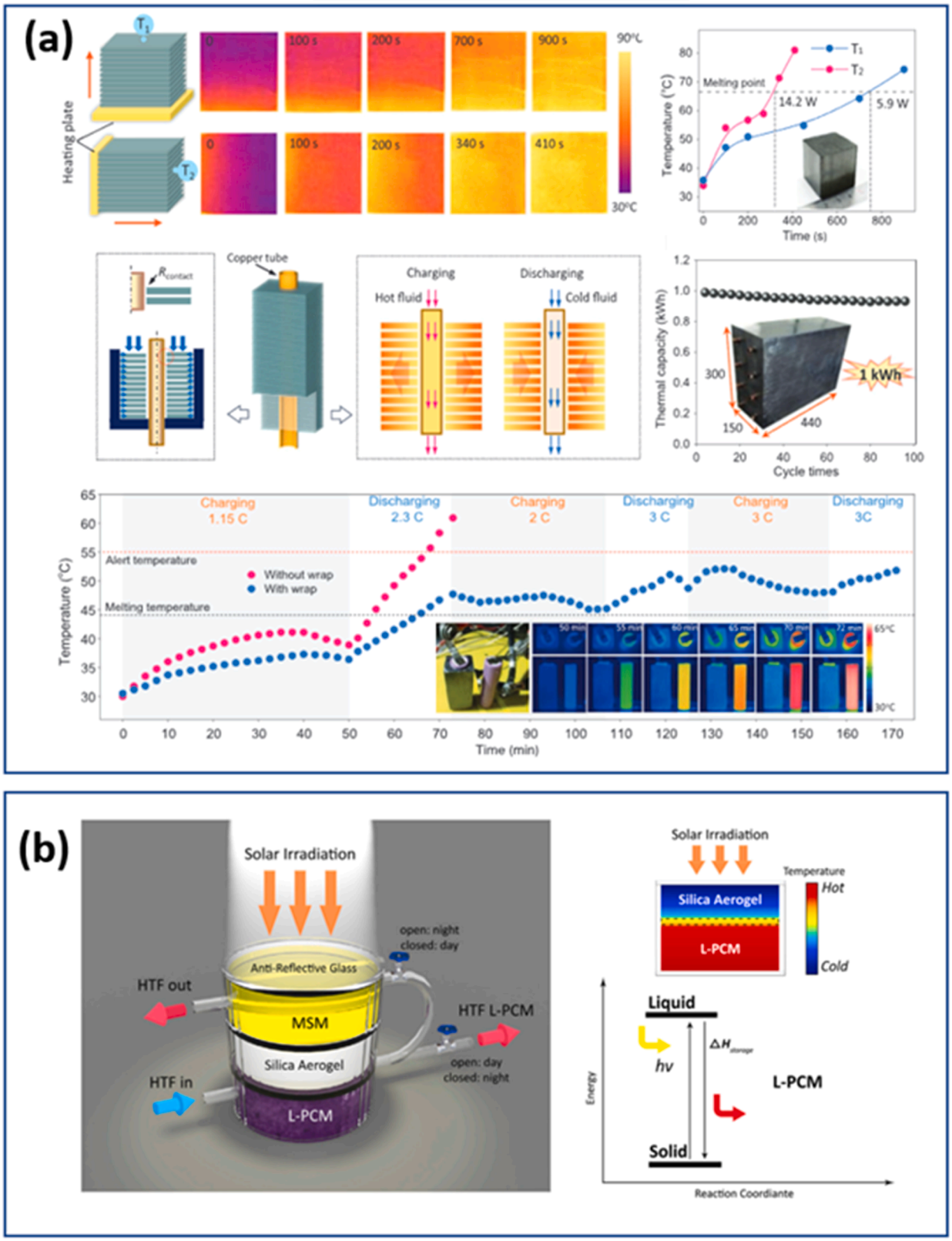

Fig. 24. (a) Thermal management and energy storage applications, featuring a comparison of 1D coordinated and uncoordinated heat conduction, temperature profiles of measured points, schematic diagram of heat design for thermal energy harvesting device, thermal capacity stability of thermal energy harvesting device, and temperature profiles of battery monomers during discharging process (reproduced with permission from [256] (b) Illustration of the molecular and phase-change hybrid, comprising a molecular storage material (MSM) and a localized phase-change material (L-PCM) separated by a silica aerogel to preserve the required temperature difference. The concept of phase-change energy storage is demonstrated, where energy is stored as enthalpy. Reproduced with Permission [257].

electrochemical reactions [264]. Biofuel cells operate by leveraging biocatalytic redox enzyme reactions to convert the chemical energy present in bodily fluids into electricity. These innovative energy-harvesting devices can be categorized based on the types of biochemical reactions they employ and the nature of their electrodes [264].

Microbial BFCs and enzymatic BFCs have emerged as particularly promising approaches in this field. Microbial BFCs utilize living cells to facilitate the oxidation of fuel, thereby providing prolonged lifetimes for the devices. However, they offer limited power densities, meaning they generate relatively low amounts of electrical power. Conversely, enzymatic BFCs have demonstrated higher power densities compared to microbial BFCs, although still lower than conventional fuel cells [264, 267]. For instance, considering a glucose-based bio cell (Fig. 25a), in a biofuel cell, a series of electron transfers occur. At the anode, electrons are transferred from glucose-to-glucose oxidase (GO_x), then from GOx to redox polymer (I), and finally from redox polymer (I) to the carbon nanotube CNTs fiber. On the other hand, at the cathode, electrons are transferred from the CNTs fiber to redox polymer (II), from redox polymer (II) to bilirubin oxidase (BOD), and ultimately from BOD to oxygen [266]. In another study, the schematic configuration of a biofuel cell was presented. It was reported that the anode consisted of magnetic polymeric composite (MPC) nanoparticles, which were capped with glucose oxidase (GOx) and lactate oxidase (LOx). These MPC nanoparticles were modified to enable the oxidation of both glucose and lactate fuels. Conversely, the cathode was loaded with loaded MPC nanoparticles, which were capped with bilirubin oxidase and catalase. These MPC nanoparticles were modified to utilize O_2 and H_2O_2 as oxidizers for the cathodic reactions [249].

Enzymatic BFCs leverage enzymes as biocatalysts, which allows for increased power generation. However, these enzymes are often fragile and prone to degradation over time, resulting in shorter lifetimes for the

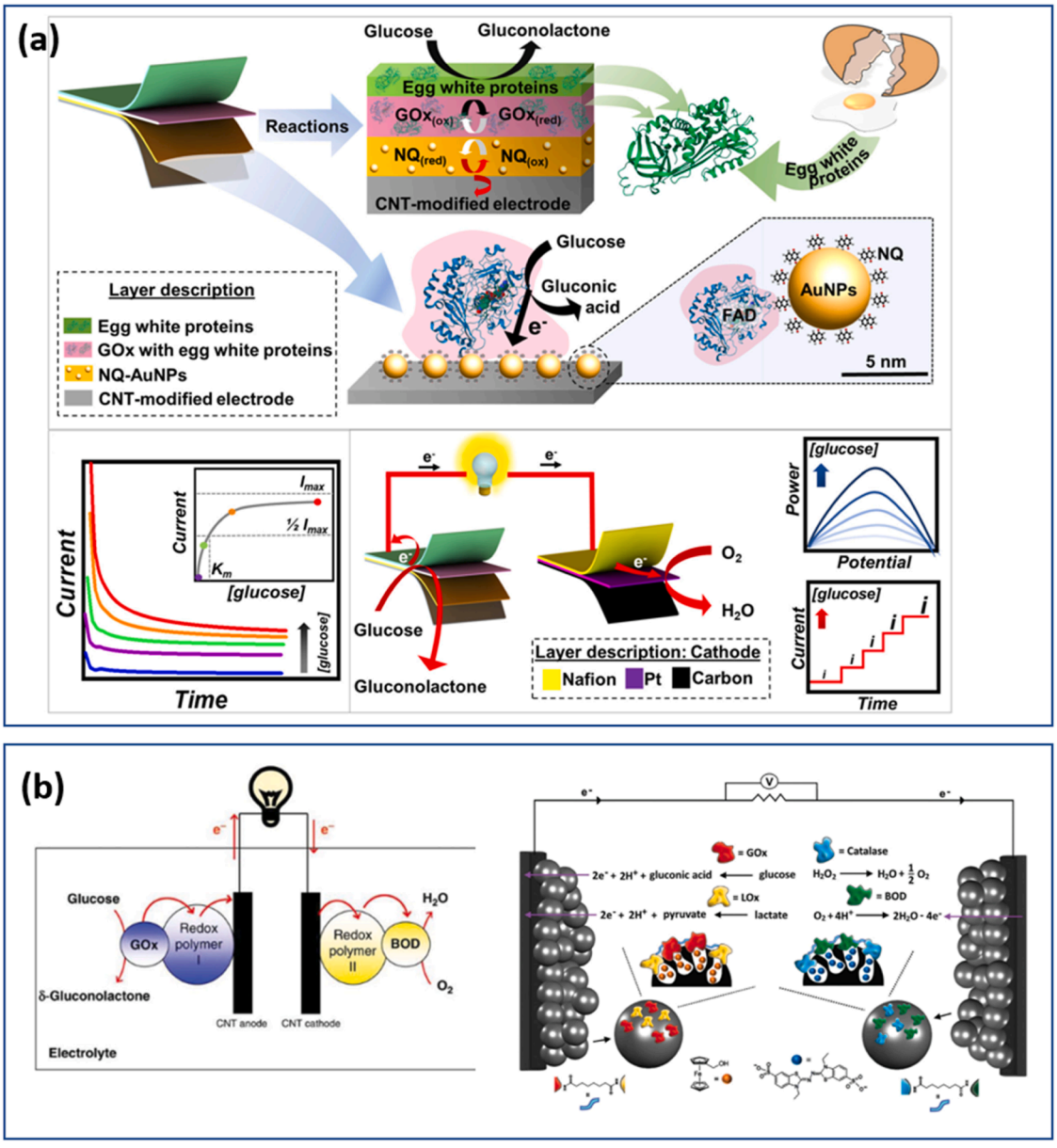

Fig. 25. (a) Conceptual presentation of redox-mediated AuNPs with GOx and egg white proteins for biosensors and BFCs, illustrating the components of a screen-printed bioanode, amperometric responses of the GOx-based electrode to successive glucose additions, and the components and reactions of a glucose BFC for energy-harvesting and self-powered sensing modules Reproduced with Permission [265] (b) Schematic of an enzyme-based fuel cell (EBFC) using CNTs fibers Reproduced with Permission [266,249].

devices. Despite the challenges and limitations associated with chemical energy-based e-skin systems, researchers are actively working on overcoming these hurdles [268]. It was reported in another study, glucose oxidase (GOx) was successfully integrated with egg white proteins on a 5 nm gold nanoparticle (AuNP) functionalized with 1,4-naphthoquinone (NQ) and a screen-printed flexible CNTs-modified electrode (Fig. 25b) [265]. It was noted that this interface facilitated effective enzyme retention and optimized reactions in a biocompatible environment. The bioelectrodes were observed to demonstrate high sensitivity and remarkable stability, indicating their potential promise for biosensors and self-sustaining energy devices [265].

Sun et al., presented the first example of a fully integrated bendable biofuel cell (BFC)-based biomedical nanodevice called iezCard. This palm-sized, pump-free device allows for the point-of-care diagnosis of scurvy using just 0.2 μL of untreated human serum [269]. By incorporating a disposable vitamin C/air microfluidic BFC, a custom mini digital LED voltmeter, and a built-in biocomputing Buffer gate, this nanodevice is cost-saving, easy to use, and satisfies the basic requirements for scurvy diagnosis. The implementation of a cost-effective design strategy reduces the feedstock cost to approximately USD 2.55 per kit, making it suitable for resource-poor settings [269].

In a recent study, Cosnier et al., found that two connected microbial fuel cells (MFCs) generated an open circuit voltage of 1.35 V, while a single MFC produced 0.663 V. The open circuit voltages of screen-printed paper-based MFCs were 0.57 V for a single setup and 1.04 V for a two-series configuration [270]. Another study by Slaughter et al., showcased a self-powered electrochemical lactate biosensor using a charge pump IC and a 10 μF capacitor, resulting in a power range of 1.2 to 1.8 V. This biosensor achieved a linear detection range of 1–100 mM for lactic acid concentration, with a sensitivity of 125.88 Hz mM^{-1} cm^{-1} based on discharging frequency measurements [271]. Recently, Guo et al. designed a scalable, printable nanocomposite film for a high-performance microstructured $BaTiO_3$/Ecoflex triboelectric nanogenerator (MBE-TENG) and examines its use in self-powered sensing and human-machine interaction. The MBE-TENG generates a short-circuit current of 1.46 μA, and a charge density of 6.62 nC/cm^2. Furthermore, a smart tactile sensing glove, developed using the MBE-TENG and neural networks, achieves 96.33 % accuracy in recognizing six different objects [272]. Zhong et al. also developed a Bi2NiMnO6 thin films with a dielectric tunability of up to 92 % that can be applied to wearables [273].

4.2.3. Energy storage

Flexible batteries are a crucial component in the development of e-skin. These batteries are designed to be thin, lightweight, and conformable, allowing them to be seamlessly integrated into flexible and wearable devices. They provide a stable power source for e-skin, enabling it to function independently. Solid-state electrolytes provide stability, wide temperature operation, and minimal self-discharge [274,275]. Gel polymer electrolytes (GPEs) have emerged as a solution, incorporating liquid electrolytes for high ionic conductivity and low flammability [276–278]. Recent advances in GPEs include UV-cured trivalent/monovalent acrylate polymers and the integration of Al_2O_3 nanoparticles to enhance flexibility [279,280]. Plastic crystal electrolytes with polymer matrix integration offer improved mechanical stability, while deformable plastic crystal polymer electrolytes (PCPEs) embedded with compliant frameworks like PET further enhance flexibility and stability [281–283].

Fabrication techniques like vacuum filtration and chemical vapor deposition (CVD) self-assembly have been utilized to create flexible composite electrodes based on CNTs. Furthermore, the incorporation of nanocrystals and metal oxides into CNTs networks has demonstrated enhanced electrochemical performance [284]. Exciting developments involving CNTs-supported materials with high capacity, such as Fe_2O_3 and Cu_2O, offer prospects for lightweight and flexible batteries suitable for e-skin applications. Another intriguing avenue involves the utilization of super-aligned CNTs arrays through dry-drawing, resulting in large-area CNTs membranes that serve as optimal substrates for accommodating nanoparticles [285,286].

Through pulsed laser deposition, researchers have successfully developed a Si/SWCNTs paper by depositing a silicon layer onto an existing SWCNTs paper. This innovative technique has yielded an impressive capacity improvement of over 60 % compared to pure CNTs paper. However, it's worth noting that the Si content in this material is limited to 2.2 wt%, and the loading rate is relatively slow, posing challenges for practical applications as a flexible anode material [287]. Another approach involves incorporating a lightweight carbon nanofiber network as a current collector to facilitate the growth of silicon nanowires (NWs) as a standalone electrode. The porous structure of the carbon nanofiber network enhances the growth of silicon NWs, resulting in a significant increase in specific energy density by approximately 23 % compared to a graphite-based cell that utilizes a heavy copper (Cu) substrate, considering a fixed areal capacity of 4 mA h cm^{-1} [288].

In flexible batteries for e-skin, work function compatibility is crucial for achieving efficient charge transfer at the electrode-electrolyte interface. The work function of the electrode material needs to be properly aligned with the work function of the electrolyte to enable effective electron transfer and maintain good electrochemical performance. The band gaps of the materials used in these batteries should be carefully matched to enable seamless integration with the skin, minimize energy loss, and maintain stable performance. Band gap engineering techniques are employed to select appropriate materials with suitable band gaps for e-skin applications [289,290]. Strategies like alloying Mg with biocompatible metals, surface coating with biomaterials, and design optimization have been proposed to overcome this issue. Biodegradable Mg-air batteries using Mg alloy anodes and cathode materials like Fe, Mo, W, molybdenum oxide, polypyrrole, or Au have been demonstrated [291,292]. Na-ion batteries with aqueous electrolytes and naturally occurring or edible electrode materials have also been developed. Polymer electrolytes and gel electrolytes based on biocompatible ionic liquids embedded in silk have been explored. However, the gel electrolyte's performance declines at high discharge rates due to low ion migration rate.

Advancements in supercapacitors and flexible capacitors have improved their energy storage capabilities and flexibility, making them ideal for e-skin applications. These devices offer quick charging, high power density, and long cycle life compared to traditional batteries. Materials studied for supercapacitors and flexible capacitors include carbon-based materials (activated carbon, CNTs, and graphene), transition metal oxides (ruthenium oxide, manganese oxide, and nickel oxide), conducting polymers (polyaniline, polypyrrole, and poly(3,4-ethylenedioxythiophene)), and nanostructured materials [293]. Capacitive storage mechanisms involve double-layer capacitance and pseudocapacitance, where ions are adsorbed at the electrode-electrolyte interface or undergo reversible redox reactions. Similarly, electrochemical fuel cells, specifically direct ethanol fuel cells (DEFCs) and proton exchange membrane fuel cells (PEMFCs), possess unique characteristics that make them ideal for powering e-skin applications. Firstly, DEFCs and PEMFCs boast high energy densities, outperforming conventional batteries, and enabling prolonged power supply in compact form factors. This is of utmost importance for e-skin devices, which require continuous operation without frequent recharging, ensuring the user experiences uninterrupted functionality and convenience. Secondly, both DEFCs and PEMFCs exhibit rapid startup times, ensuring quick power generation when needed. This feature is particularly valuable for e-skin applications, where instant response and continuous power availability are critical for seamless interaction and real-time sensing capabilities. Moreover, the safe and clean operation of electrochemical fuel cells is a compelling factor for wearable applications like e-skin. Operating at lower temperatures than internal combustion engines, they enhance user safety and comfort. Additionally, fuel cells produce minimal emissions, aligning with environmental

sustainability goals. Furthermore, the lightweight and portable nature of fuel cells, especially PEMFCs, aligns perfectly with e-skin's design requirements. With a favourable weight-to-power ratio, fuel cells enable unobtrusive integration into the e-skin device, ensuring the wearer's comfort and freedom of movement. When selecting fuel cells for e-skin, consider high energy density for longer operation, along with the flexibility of thin PEMFCs for seamless integration. Match the power output to the sensors' needs, prioritize safety with PEMFCs' lower temperatures, and opt for robust cells to endure mechanical stress. Lastly, ensure practical refuelling or recharging options for uninterrupted power supply and enhanced user experience.

Energy harvesting and storage in e-skin holds great promise in advancing the field of wearable electronics and human-machine interfaces. By integrating energy harvesting technologies, such as photovoltaics or triboelectric nanogenerators, with energy storage components like supercapacitors or lithium-ion batteries, e-skin devices can achieve self-sustainability and continuous operation without the need for frequent battery replacements. This concept is particularly relevant for wearable devices that require long-term usage and portability. Moreover, the integration of energy harvesting systems offers the opportunity to harness renewable energy sources, reducing the environmental impact and promoting sustainable energy solutions.

4.3. Sustainability: eco-friendly coating formulations

With increased environmental concerns, the demand for eco-friendly coatings has become the major driving force for new coating technology development in recent years. The new technologies utilize sustainable materials, sustainable production methods and sustainable application practices to minimize the environmental impact of coatings. In one segment, the transition from organic-solvent-based to water-based carrying medium is already accelerating at a fast pace as a response to growing consumer awareness and environmental legislations. The global waterborne coatings market is projected to grow from a market size of US$58 billion in 2022 to US$89 billion by 2030 [294]. The scope can be further expanded by also taking into account the end life of the material and its ability to be recycled or reprocessed creating a circular economy [295,296]. This closed-loop model aims to minimize waste to theoretically zero, with cradle-to-cradle principles integrated in the product or process design (Fig. 26) [297]. Some of the current obstacles include challenges in maintaining or improving performance levels, the feasibility of the process, and the associated cost of changing any infrastructure currently in place for manufacturing. For the last point, the aim is to provide 'drop-in' solutions replacement with minimal changes required [298]. Solvent-based coatings, fluorocarbons, heavy metal salts, as well as materials that would prevent the recycling/biodegradation of the material or bioaccumulate in the environment are areas of concern in regards to sustainable coatings [173]. There have been a few reviews that look at environmentally friendly coatings for various applications such as self-healing coatings [299], anticorrosion [300], use of nanomaterials [301], and coatings on metallic alloys [302].

4.3.1. Reduced environmental impact

The sustainability of coatings can be quantified with methods such as Life Cycle Analysis (LCA), which looks at various data to determine the largest contributing factors to environmental impacts. The scope of the LCA is an important variable when considering circular economy because most LCA studies look at a cradle-to-gate life and do not consider consumer use and end life due to numerous variables that

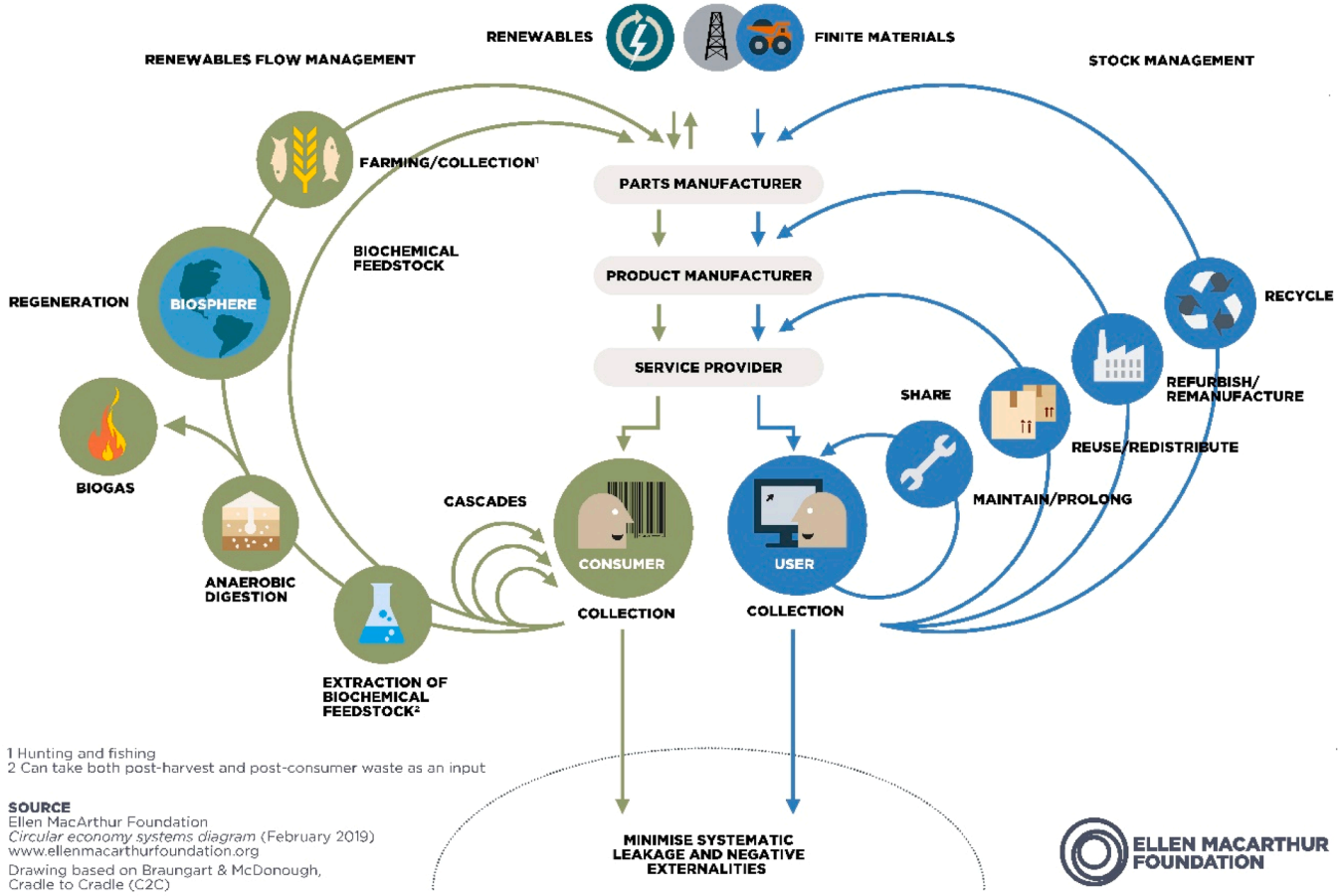

Fig. 26. Graphic representation of Circular Economy. Reproduced with permission from the Ellen Macarthur Foundation [303].

would be difficult to quantify [304]. It is important to note these are the limitations for current modeling techniques, but as more research and information is collected the discrepancies between theoretical and actual implementation will narrow. A LCA was conducted using two industrial anti-fouling coatings to determine where the most impact can be made when designing a sustainable polymer. In this study, they had a cradle to grave scope that was broken down into 4 phases: production, application, use and maintenance, and end of life. Looking at the global warming potential (GWP), photochemical oxidation creation potential (POCP), acidification potential (AP), eutrophication potential (EP), and marine aquatic toxicity potential (MTP) it was shown that outside of MTP, production had the largest impact for both systems due to the high energy processes of both coatings. The use and maintenance of the coating provided the largest contribution to MTP, due to the nature of the coating in which it releases toxic metals into the environment to prevent microbial build-up (Fig. 27) [305].

By using more environmentally friendly resources and methodologies we can have a larger benefit to the overall environmental impact of the system. Another study by Manfredi et al., showed how the use of an antimicrobial coating on milk packaging was able to reduce the environmental impact due to the increase in shelf life of the product. Though assumptions were made regarding how much increasing the shelf life would decrease food waste, it shows the potential that smart coatings can have just by increasing the longevity of a product and therefore minimizing waste production [306]. As well as environmental benefits, smart coatings can have their unique multifunctional applications. Below are some of the fastest growing and emerging areas.

4.3.2. *Sustainable feedstock*

The adoption of natural and renewable raw materials, which can include vegetable oils, cellulose, lignin, tannin, chitosan, protein, and starch not only provide more versatile functional capabilities but also the potential for cost reduction. Vegetable oils such castor oil have been used to produce waterborne polyurethane and self-healing coatings [307,308]. Smart coatings containing benzotriazole (BTA)-encapsulated mesoporous silica nanoparticles has been demonstrated to show passive and active anticorrosion performances by releasing corrosion inhibitors [309]. Waterborne conductive coatings containing multiwall CNTs and carbon black are developed for sensing tensile and impact damages, with potential applications in structural damage monitoring and localization [310].

The utilization of biopolymers in eco-friendly coating formulations is one of the fastest growing areas. When discussing sustainable polymers or plastics, the terminology currently used can be misleading. Terms such as bioplastic, biopolymer, biobased, biodegradable, and green polymer can all give the impression that the material is sustainable, which is not always the case. There are petrochemical based polymers that can be biologically degraded, as well as biobased polymers that are not fully biodegradable. For the purposes of this article the definitions will follow those outlines by Endres in Biorefineries [298]. A polymer to be labelled a biopolymer must have a component that is sourced from biomaterials or be biodegradable as shown in Fig. 28.

Porous coatings of polycaprolactone (PCL), a biodegradable and biocompatible polyester, have shown anti-biofouling properties [312]. One compound that has shown great potential as a green alternative for lubricants used in omniphobic coatings is Polydimethylsiloxane (PDMS). This cyclic siloxane can be molecularly recycled using a reversible ring closing synthesis which allows easy transition between polymeric and monomeric states [296]. Omniphobic coatings tend to use either rough surfaces, which are not suitable for longevity, or fluorinated compounds, which are toxic to the environment and expensive. Chen et al., developed a lignin-based urethane coating with a derivative of PDMS as the dwetting agent. The lignin provided UV resistance due to the presence of phenolic hydroxyl groups and the PDMS provided the omniphobic and anti-smudge properties repelling various low surface energy liquids, water, and oil (Fig. 29) [313].

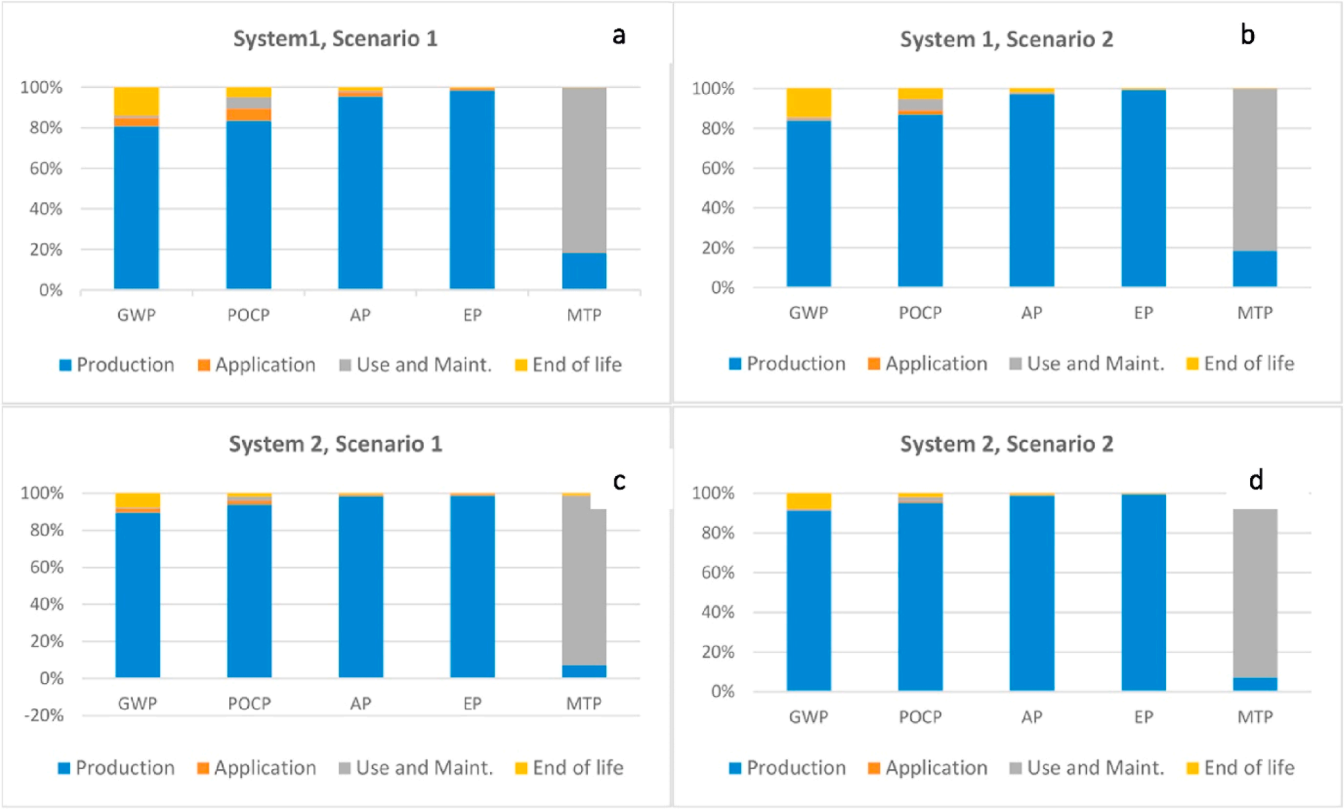

Fig. 27. (A) Scope (cradle-to-grave) for LCA analysis (B) Environmental profile considering transportation (scenario 1) and omitting transportation (scenario 2). Reproduced with permission from [305].

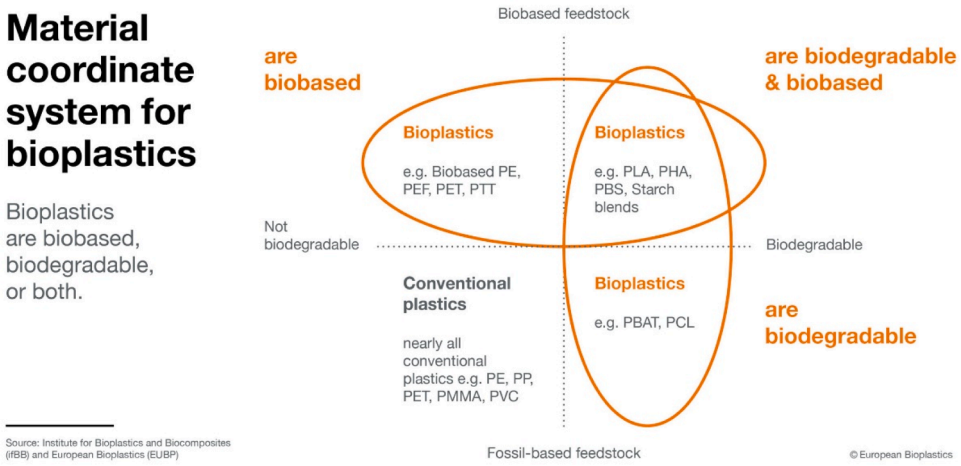

Fig. 28. Bioplastic Classification. Reproduced with permission from European Bioplastics [311].

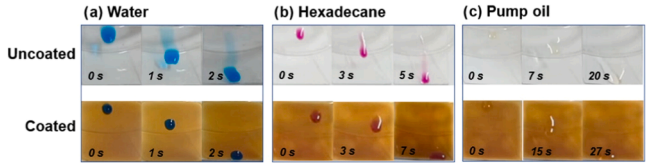

Fig. 29. Surface wettability testing of lignin-polyurethane coating with 3.0 wt. % of PMDS. Reproduced with permission from [313].

PDMS has been used in combination with methyl anthranilate to produce an antifouling coating by Zhang et al., who also saw good repellency for various organic solvents as well as water and oil. These were tested on various substrates such as leather, plastic, and tin with each showing comparable properties. The use of methyl anthranilate provided antimicrobial properties for which the group saw growth inhibition rate of 92.5–96.5 % for E. coli, S. aureus, and Penicillium. The material was tested up to 800 abrasion cycles where it still maintained its repellency properties. Overall, the material showed chemical and thermal stability and was UV resistant, showing progress in the production of environmentally friendly coatings [314].

4.3.3. Carbon materials and nanotechnology

Another area that has seen great improvement towards sustainability is the production of carbon-based materials, which are widely used in smart coatings due to their mechanical, electrical, and optical properties. There are several reviews that outline the various biomass and waste that have been shown to produce carbon-based materials using various methods [312,315–317]. One method that has shown potential recently is Flash Joule Heating, which is used to produce Flash Graphene and can be further processed to yield turbostratic graphene [318]. In this method, direct current is used to quickly heat the material to high temperatures, which avoids the loss of energy from a typical pyrolysis method and removes the volatiles in the process without pre-treatment. Algozeeb et al. have used this method to see its potential for use on plastic waste and were able to see a 22 % yield of graphene starting with mixed plastic waste and increased to 27 % when starting with high-density polyethylene (Fig. 30). This green recycling method does not use any catalysts or solvents and has a low cost for upscale. It was reported that it would cost $124/ ton of plastic waste, which would give a yield of about 180 kg of graphene [318]. This method was also used by Advincula et al., for its potential to recycle rubber waste. They studied two different streams: pyrolyzed rubber tire derived carbon black, and a mixture of carbon black and shredded rubber tires seeing a 70 % and 47 % yield respectively. Further studies are still needed to determine the environmental impact especially in the case of the pyrolyzed rubber tire, which underwent a pre-treatment process so the overall yield for graphene from waste might be lower [319]. Electronic waste is another stream that has shown potential for producing graphene nanosheets. Bajpai et al., used milled printed circuit boards and pulsed laser ablation in de-ionized to produce 3–4 layers of graphene with conducting abilities. The size of the sheet and yield were dependent on the amount of energy used in processing, with higher energies producing larger sheets and therefore higher yields. The yields are lower compared to other methodologies used to produce graphene, with 40.2 % as the highest yield achieved for this method whereas Hummer's method, ball milling, and even the previously mentioned flash heating reporting yields ranging from 65 to 90+. The benefits to this method are its chemical free processing that shows easy scale-up potential [320].

Graphene has also been synthesized from Kraft lignin, which is a by-product from the paper pulping industry. Holding time was an important factor contributing to the structure of the carbon. A sufficient holding time of 75 min was needed to produce the stacked lamellar and prolonged time increased the number of sheets with agglomeration occurring at 105 min and forming CNTs (Fig. 31). Compared to commercial graphene, the lignin-based graphene needs further improvement to optimize the quality and layers that they were able to produce [321]. With the methodology in place to produce biobased carbon, the next step would be incorporating these biobased carbon materials into composites and optimizing properties to produce industry competitive materials. Hsiao et al., developed a graphene polymer composite by first creating a water borne polyurethane matrix through electrospinning, which produces a high surface area. This is followed by a layer-by-layer assembly of the graphene composite allowing for less disruption of electron transmission, which is beneficial for use in EMI shielding.

The researchers were able to see an increase in weight retention and conductivity with increased cycles measuring 34 dB for shielding over a range of 8.2 to 12.4 Hz (Fig. 32). The overall thickness of the material was 1 mm, showing potential for use in flexible electronics [322]. rGO was used in combination with natural jute fibers by Karim et al., showing improved tensile strength and breaking force. The study also looked at the composite for use in EMI shielding, where the reduced graphene improved performance over the pretreated natural fiber but did not reach the same level as graphene-flaked coated jute fibers. The layered structure of graphene flakes helps to improve shielding during internal reflection. The use of natural fibers can have a positive economic impact and considering that jute is biodegradable it provides an environmentally friendly impact as well when compared to glass or carbon fibers (Fig. 33) [309].

Nanofillers are a common technique used to tFilor polymeric properties for wide range applications and therefore used in many surface

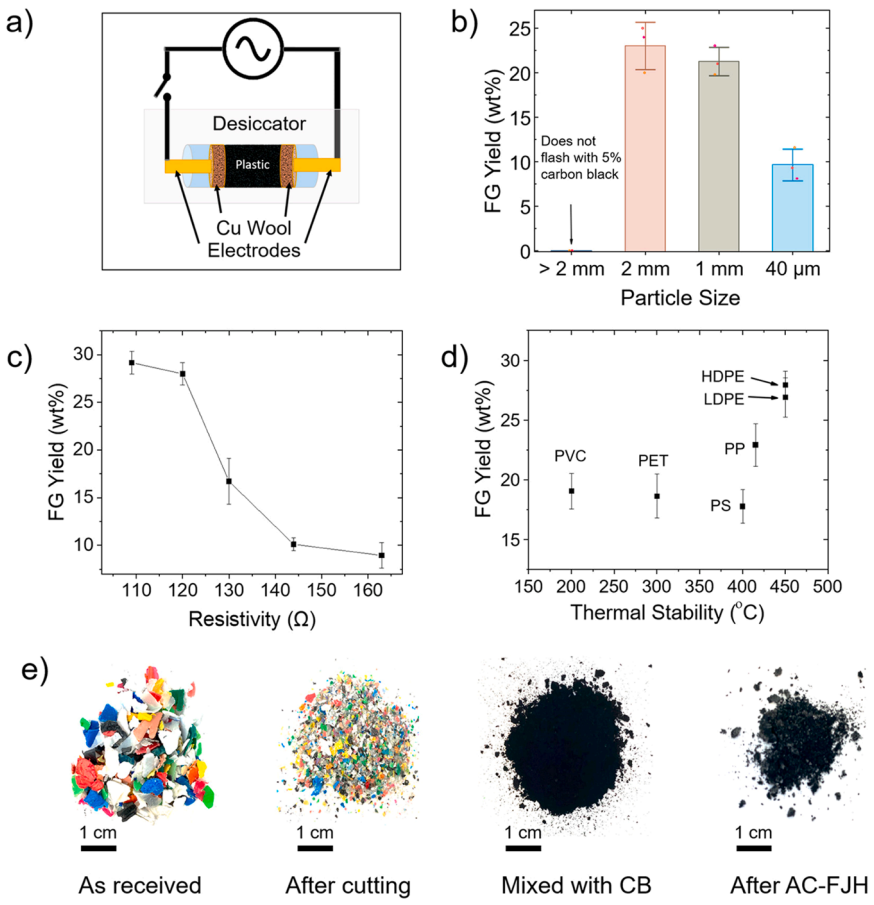

Fig. 30. Overview of graphene production from mixed plastic waste. (a) schematic of the circuit. (b) AC-FG yield from HPE with varying particle size from three sample runs. (c) Effect of initial resistivity on yield. (d) AC-FG yields from different plastics. (d) images of the post-consumer plastic. Reproduced with permission from [318].

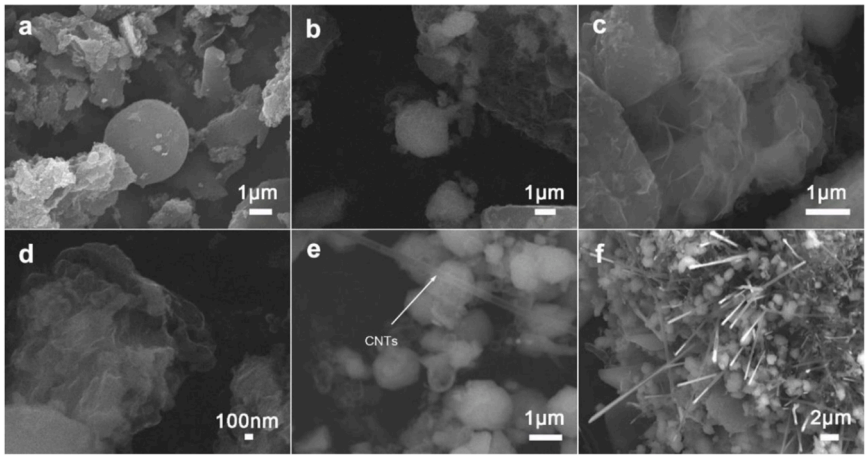

Fig. 31. FE-SEM images of carbon material with increasing hold time (75–120 min). Reproduced from [321].

coatings. Carbon black is widely used to increase electrical conductivity in thermoplastics. One alternative to petroleum based-carbon black is biochar as seen by Arroryo and Ryan who use biochar derived from lignin in a PHBV:PLA blend. These polymers, which are sourced from microorganisms, are typically brittle but the use of a nanofiller as well as an optimized ratio can produce a composite with ideal properties.

The study compared composites formed with the biocarbon as well as carbon black with both showing comparable resistance of $3.34 \times 10^8\Omega$ and $2.99 \times 10^8\Omega$ respectively. The difficulties arise in the processing for the biocarbon, which has a more complex reaction with the blend that increases the solubility of PHA in PHBV and decreases the viscosity significantly with increase in filler whereas the opposite is seen with carbon black. They were able to show a conductive network within a biobased blend of polymers with tailorable properties, but more research is needed to show the potential use of lignin based biocarbon [323]. Attia et al., produced rice husk based-silica nanoparticles and demonstrated use as a coating for various textiles for enhanced properties. When looking at woven and braided polyester and viscose fabrics

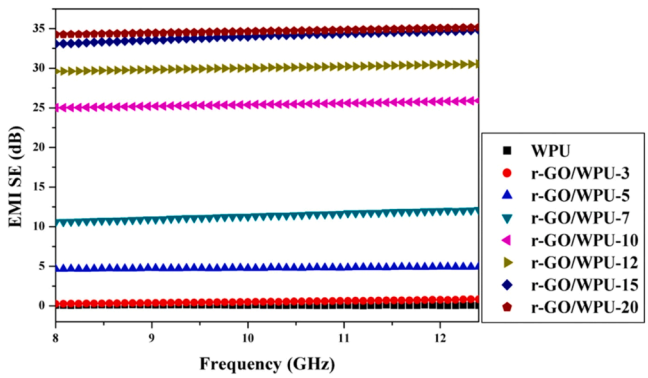

Fig. 32. EMI Shielding of rGO/WPU composites with various l-b-L assembly cycles in X-band range. Reproduced with permission from [322].

the use of nanoparticle coatings increased thermal stability as well as increased tensile strength and UV shielding capabilities [324]. You et al., produced nanosheets from chitin, a nitrogen containing polysaccharide found in crabs. These carbon nanosheets demonstrated a large increase in specific surface area over carbonized chitin powder, and with a N-doped nature makes them highly suitable for electrical applications such as supercapacitor electrodes. The nanosheets were also able to be dispersed in solvents allowing for applications as bio membranes. Tunable conductivity was demonstrated with varying wt% of carbon nanosheets achieving values comparable to industry additives like SuperP and SuperC65. The use of chitin also provides a biocompatible for potential use in biological devices [314].

4.3.4. *Sustainable methods and processes*

Progress has also been made for other coating materials, such as MXenes and metal oxides, as discussed in several reviews [326–328]. Some drawbacks of these compounds and their derivatives are that they tend to use high energy process due to the temperatures needed to form the structure. The other concern stems from the harmful substances typically used for etching, such as hydrogen fluoride (HF). One method that has garnered interest to produce metal oxides is solution combustion synthesis due to its low cost and energy efficient method to produce wide morphology of oxides [329].

Rosa et al., conducted a LCA of 3 different synthesis techniques for TiO_2 nanoparticles: solution combustion synthesis (SCS), hydrolytic sol-gel synthesis (HSGS), and nonhydrolytic sol-gel synthesis (NHSGSC). When looking at two different scales of producing 1 kg vs 1000m^2 surface area, it shows that SCS has the lowest overall impact and NHSGSC has the highest (Fig. 34) [330]. Stieberova et al., conducted a LCA on the use of nanoparticles in self-cleaning coatings. The use of Zinc Oxide nanoparticles in a polyvinylidene fluoride (PVDF) coating was studied for the environmental impacts with and without NPs. The use of NPs increased the cumulative energy demand due to additional energy intensive processing but showed a lower global warming potential due to longevity of the coating, which didn't require maintenance during use and contained a smaller amount of fluorinated compounds [331]. When looking at alternatives to conventional etching techniques used, molten salts have shown potential. Pang et al. developed a molten-salt electrochemical process to produce carbon materials from CaC_2 and $CaCO_3$. They further tested the synthesized Cr_2AlC—CDC for use as an anode in Li-ion batteries, and were able to achieve a discharge capacity of 248 mAh g^{-1} after 100 cycles and indicating good stability [332].

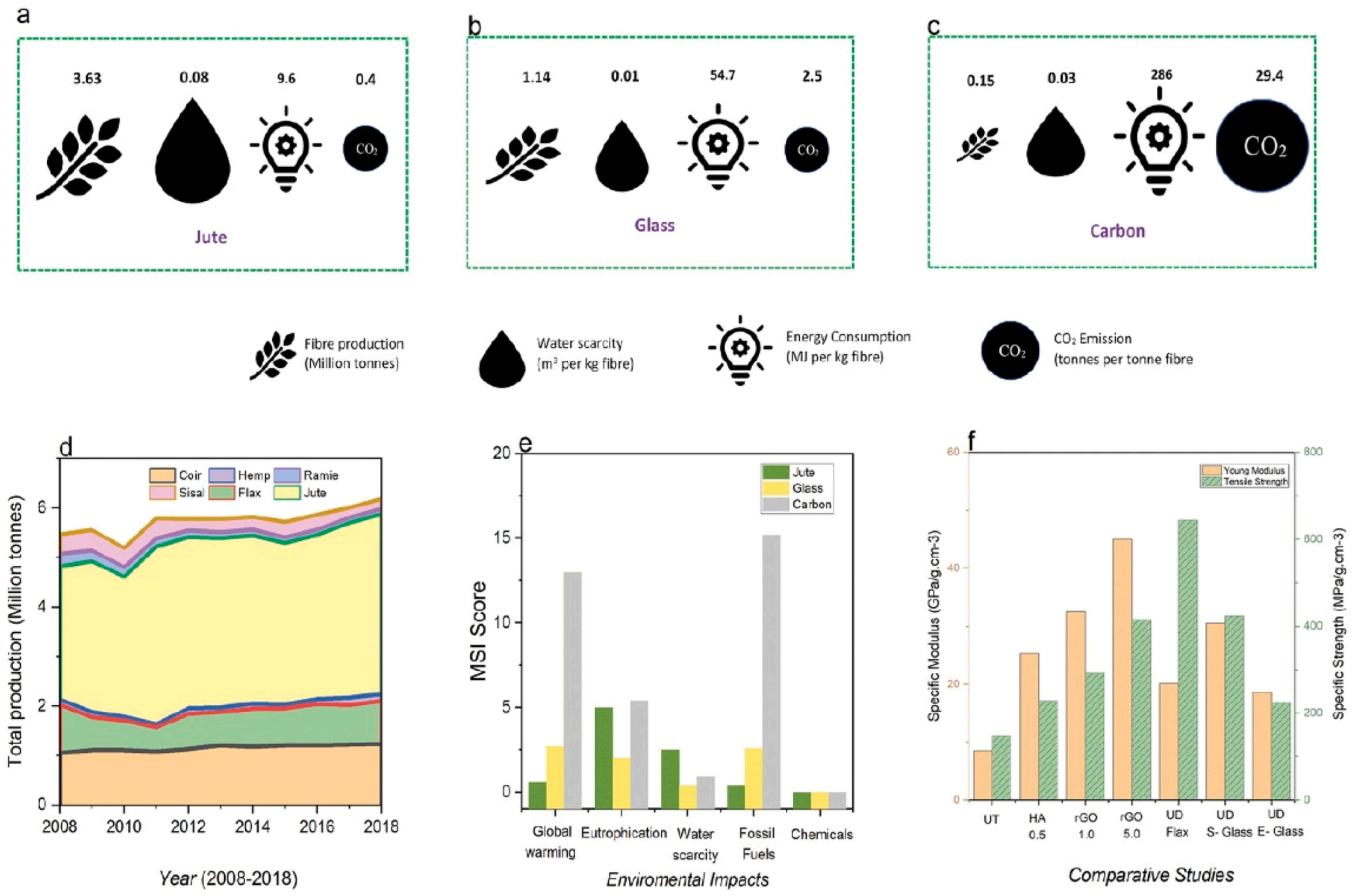

Fig. 33. Environmental impact and comparative study of a) jute, b) glass, and c) carbon fiber; d) total bast fiber production globally (2008–2018) e) Materials sustainability index of fibers and f) comparative properties of fiber composites. Reproduced from [325].

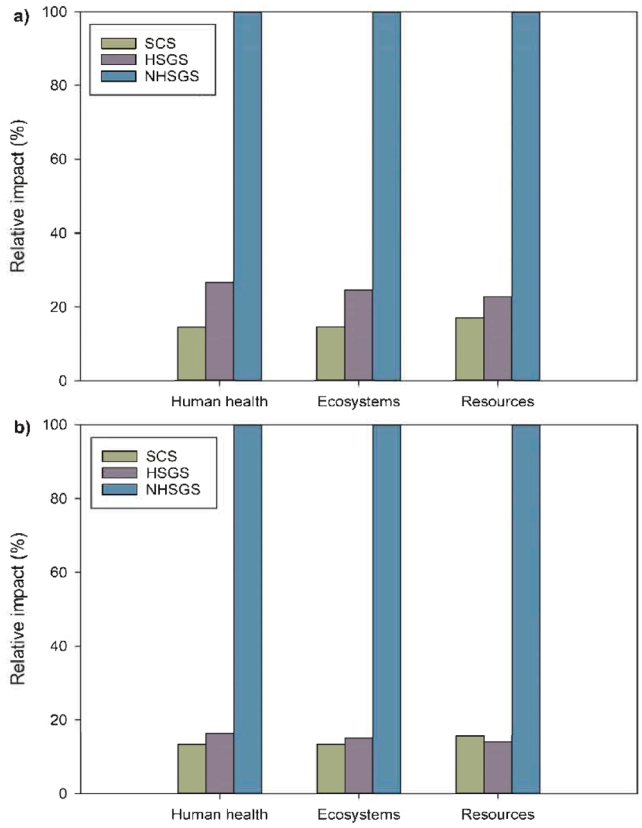

Fig. 34. Relative environmental impact of solution combustion synthesis, hydrolytic sol-gel synthesis, and nonhydrolytic sol-gel synthesis on scale of (a) 1 kg and (b) 1000 m^2 surface area production. Reproduced from [330].

In smart coatings, the implementation of sustainability principles provides exciting win-win opportunities, as the sustainable materials and processes help the coating materials from performing passive to active functions, from matching conventional coating characteristics to achieving enhanced and diversified performances, and from minimizing resource consumption to recycling, repairing, and restoring resources. Active research is being carried out in achieving the functional characteristics at competitive cost while providing environmental and health benefits and meeting the challenges of providing drop-in solutions to minimize the need for infrastructure modification. Progress in these areas will transform the smart coating sector in the years to come.

5. Concluding remarks and perspectives

In this review, we have systematically investigated the potential of nanomaterials such as graphene, TMDs, and MXenes to bring advancements in the coating industry. Graphene stands out for its exceptional conductivity, tensile strength, and flexibility. It is highly adaptable for energy storage, environmental sensing, and biomedical applications, where properties like high surface area and atomic thickness are beneficial. TMDs, particularly in their monolayer form, offer unique advantages with a tunable bandgap and enhanced mechanical stability despite their relatively low conductivity. MXenes, with their unique surface chemistry and high hydrophilicity, excel in applications requiring biocompatibility and conductivity. However, challenges like layer stacking and oxidation remain. This underscores how hybrid structures could address these challenges—for example, combining TMDs and MXenes to enhance conductivity and stability. Understanding the unique challenges of these nanomaterials is crucial, as addressing these issues will guide ongoing research to refine their properties and expand their applicability at an industrial scale. By tackling these material-specific limitations, researchers can better harness the full potential of these 2D structures, especially in fields such as smart coatings, where tailored performance is essential for commercial success. Continued efforts in synthesis and hybridisation promise to advance these materials from laboratory research to impactful, scalable solutions across various industries.

By integrating these materials and utilising their superior characteristics, smart coatings with intelligence capabilities can be developed, which will pave the way for real-time structural health monitoring and next-generation flexible electronics applications. Understanding the mechanism of conductivity and sensing will aid in the quest for novel formulations for smart coatings. Further fundamental research is necessary to advance the Technology Readiness Level (TRL) beyond the current laboratory-scale research for nanomaterials-based smart coatings, particularly for sensing applications. This sector can be transformed by integrating artificial intelligence and machine learning, accelerating the industrialisation of nanomaterials, and making them commercially viable. In addition, we discussed the current research on the energy autonomy of electronic skin and the characteristics required for efficient sensing applications. The prospects of energy harvesting and storage in e-skin are multifaceted and transformative. From enhancing device portability and comfort to enabling real-time energy monitoring and promoting sustainable energy solutions, these integrated systems have the potential to revolutionise wearable electronics and pave the way for more sophisticated and efficient human-machine interfaces. As these technologies continue to advance and become more scalable and cost-effective, energy-harvesting e-skin holds significant promise for a wide range of applications in wearable technology and healthcare. Researchers in material science have paid great attention to e-skins. However, there has been a lack of focus on cost and production efficiency. This has limited the practical applications of e-skins, and therefore, there is a need for further investigation in that direction. It is crucial to evaluate the impact of new coatings on the environment throughout their life cycle. Hence, we have highlighted some recent studies on sustainability measures in selecting materials for smart coating formulations.

The development of smart coatings promises significant advancements across various industries, yet scaling up production presents key challenges. As demand grows, cost-effectiveness becomes a critical concern, with expenses rising in materials, equipment, and labour. To keep these coatings economically viable, manufacturers must streamline workflows, improve material efficiency, and explore energy-saving strategies. Incorporating automation and advanced manufacturing technologies can also enhance efficiency and reduce costs, facilitating broader adoption. At the same time, adapting synthesis methods for large-scale production remains complex, as techniques that work well in labs may face consistency and quality control issues at an industrial scale. Effective monitoring and uniform dispersion across large batches are essential but may require innovative quality assurance solutions to maintain product performance. Another challenge is integrating smart coatings into existing industrial frameworks where traditional coatings have been optimised over the years. Ensuring compatibility with established processes and equipment requires careful adaptation, essential for practical scalability and long-term success. By addressing these cost, quality, and integration challenges, manufacturers can make strides toward realising the full potential of smart coatings, enabling sustainable growth and impactful applications across diverse fields. It is also essential to address the environmental implications associated with the nanomaterials used in smart coatings. Ensuring responsible disposal methods and reducing potential environmental impact are key areas that warrant careful consideration. Furthermore, compliance with evolving environmental and safety regulations is critical for the responsible development and application of these coatings. Researchers can contribute to sustainability efforts by exploring the use of natural raw materials to enhance coating degradability and incorporating non-toxic or low-toxicity additives to minimize environmental harm. With these

considerations in mind, smart coating materials are poised to play a transformative role in the industry, presenting significant growth opportunities and expanding the market potential for innovative, eco-conscious coatings. This review provides readers with a comprehensive understanding of the fundamental characteristics of 2D nanomaterials, offering insights into emerging trends and technologies that are driving the future of smart coatings across diverse industries.

Declaration of generative AI and AI-assisted technologies in the writing process

During the preparation of this work, the author(s) used [CHATGPT] to improve the readability and language. After using this tool/service, the author(s) reviewed and edited the content as needed and took (s) full responsibility for the publication's content.

CRediT authorship contribution statement

Vishnu V. Pillai: Writing – review & editing, Writing – original draft, Visualization, Validation, Methodology, Investigation. **Brindha Ramasubramanian:** Writing – review & editing, Writing – original draft, Methodology. **Olivia Sequerth:** Writing – review & editing, Writing – original draft, Methodology. **Srikanth Pilla:** Writing – review & editing, Methodology, Investigation. **Tao Wang:** Writing – review & editing, Writing – original draft, Methodology. **Amar K Mohanty:** Writing – review & editing, Methodology. **Premika Govindaraj:** Writing – review & editing, Supervision, Methodology, Investigation. **Saeed M. Alhassan:** Writing – review & editing, Methodology. **Nisa Salim:** Writing – review & editing, Supervision, Investigation, Funding acquisition. **Peter Kingshott:** Writing – review & editing, Supervision, Methodology, Funding acquisition. **Franz Konstantin Fuss:** Writing – review & editing, Writing – original draft, Methodology. **Seeram Ramakrishna:** Writing – review & editing, Methodology. **Nishar Hameed:** Writing – review & editing, Supervision, Methodology, Funding acquisition, Conceptualization.

Declaration of competing interest

The authors declare that they have no known competing financial interests or personal relationships that could have appeared to influence the work reported in this paper.

Acknowledgements

The author VP would also like to acknowledge the Australian Research Council (ARC) and Swinburne University for the PhD scholarship. Author PG would like to thank AINSE Limited for financial assistance (PGRA ALNSTU12654). VP, PG, NS, PK, and NH would like to thank the Australian Research Council for the ARC Linkage (LP200301659) research grant. The authors thank all individuals and organisations who permitted us to republish their figures and other relevant information.

Data availability

Data will be made available on request.

References

[1] S. Nagappan, et al., Stimuli-Responsive Smart Polymeric Coatings: An Overview, Springer International Publishing: Cham, 2016, pp. 27–49.
[2] D. Tejero-Martin, et al., Beyond traditional coatings: a review on thermal-sprayed functional and smart coatings, J. Therm. Spray Technol. 28 (4) (2019) 598–644.
[3] A. Balcerak-Woźniak, M. Dzwonkowska-Zarzycka, J. Kabatc-Borcz, A comprehensive review of stimuli-responsive smart polymer materials—recent advances and future perspectives, Materials 17 (17) (2024) 4255.
[4] A.S. Hamdy, et al., Corrosion behavior of electroless Ni–P alloy coatings containing tungsten or nano-scattered alumina composite in 3.5% NaCl solution, Surf. Coat. Technol. 202 (1) (2007) 162–171.
[5] S. Wise, et al., Strength comparison of topology optimized lattice from printed SLA resin, electroplated resin and PBF aluminum alloy, in: 2022 International Solid Freeform Fabrication Symposium, 2022.
[6] A. Aoki, A. Ito, S. Watanabe, Reversible Ag electroplating onto ITO electrode for smart window, Solar Energy Mater. Solar Cells 200 (2019) 109922.
[7] T. Kim, et al., Wearable sensors and supercapacitors using electroplated-Ni/ZnO antibacterial fabric, J. Mater. Sci. Technol. 100 (2022) 254–264.
[8] R.J. Isaifan, et al., Improved self-cleaning properties of an efficient and easy to scale up TiO2 thin films prepared by adsorptive self-assembly, Sci. Rep. 7 (1) (2017) 1–9.
[9] U. Bilal, et al., HfO2-based nanostructured thin-films (i.e., low-e coatings) with robust optical performance and energy efficiency, J. Nanostructure Chem. 12 (6) (2022) 1131–1142.
[10] G. Cui, et al., A comprehensive review on smart anti-corrosive coatings, Prog. Org. Coat. 148 (2020) 105821.
[11] Y. Yuan, et al., Enabling antibacterial and antifouling coating via grafting of a nitric oxide-releasing ionic liquid on silicone rubber, Biomacromolecules. 23 (6) (2022) 2329–2341.
[12] Ulaeto, S.B., et al., Smart Coatings. 2018. p. 341–372.
[13] Z. Wu, et al., Transparent, conductive carbon nanotube films, Science 305 (5688) (2004) 1273–1276.
[14] A.K. Geim, Graphene: status and prospects, Science 324 (5934) (2009) 1530–1534.
[15] A. Synnefa, M. Santamouris, K. Apostolakis, On the development, optical properties and thermal performance of cool colored coatings for the urban environment, Solar energy 81 (4) (2007) 488–497.
[16] Y. Sun, R. Singh Rawat, Z. Chen, Mechanically robust multifunctional antifogging coating on transparent plastic substrates, Appl. Surf. Sci. 580 (2022) 152307.
[17] S. Liu, et al., Self-cleaning transparent superhydrophobic coatings through simple sol–gel processing of fluoroalkylsilane, Appl. Surf. Sci. 351 (2015) 897–903.
[18] J.P. Wang, et al., Smart-Sensing polymer coatings with autonomously reporting corrosion dynamics of self-healing systems, Adv. Mater. Interfaces. 6 (10) (2019), 1900055-n/a.
[19] J. Williams, Military Applications: Development of Superomniphobic Coatings, Textiles and Surfaces, Elsevier, 2018, 1-1.
[20] A. Ali, et al., An overview of controlled-biocide-release coating based on polymer resin for marine antifouling applications, J. Polym. Res. 27 (4) (2020).
[21] X. Li, J. He, W. Liu, Broadband anti-reflective and water-repellent coatings on glass substrates for self-cleaning photovoltaic cells, Mater. Res. Bull. 48 (7) (2013) 2522–2528.
[22] J.H. Lee, et al., Stretchable and recoverable acrylate-based pressure sensitive adhesives with high adhesion performance, optical clarity, and metal corrosion resistance, Chem. Eng. J. 406 (2021) 126800.
[23] V. Kumaravel, et al., Antimicrobial TiO2 nanocomposite coatings for surfaces, dental and orthopaedic implants, Chem. Eng. J. 416 (2021), 129071-129071.
[24] N. Pathan, P. Shende, Strategic conceptualization and potential of self-healing polymers in biomedical field, Mater. Sci. Eng. C 125 (2021), 112099-112099.
[25] V. Orts Mercadillo, et al., Electrically conductive 2D material coatings for flexible and stretchable electronics: a comparative review of graphenes and MXenes, Adv. Funct. Mater. 32 (38) (2022) 2204772.
[26] A. Mirabedini, et al., Evolving strategies for producing multiscale graphene-enhanced fiber-reinforced polymer composites for smart structural applications, Adv. Sci. 7 (11) (2020) 1903501.
[27] R.K. Prusty, et al., Reinforcement effect of graphene oxide in glass fibre/epoxy composites at in-situ elevated temperature environments: an emphasis on graphene oxide content, Compos. Part A 95 (2017) 40–53.
[28] M.S. Irfan, et al., Carbon coated piezoresistive fiber sensors: from process monitoring to structural health monitoring of composites – a review, Compos. Part A Appl. Sci. Manuf. 141 (2021) 106236.
[29] W. Han, J. Zhou, Q. Shi, Research progress on enhancement mechanism and mechanical properties of FRP composites reinforced with graphene and carbon nanotubes, Alexandria Eng. J. 64 (2023) 541–579.
[30] C. Cuellar, K. Watson, E. Smela, Fabrication, characterization, and Repair of Nanocarbon-Loaded Aircraft Paint-Based Sensors For Real-World SHM: Studies At the Laboratory Scale, Structural Health Monitoring, 2023 14759217231198015.
[31] M. Ghaderi, H. Bi, K. Dam-Johansen, Adv. Mater. for smart protective coatings: unleashing the potential of metal/covalent organic frameworks, 2D nanomaterials and carbonaceous structures, Adv. Colloid. Interface Sci. 323 (2024) 103055.
[32] H. Chen, et al., Advances in graphene-based flexible and wearable strain sensors, Chem. Eng. J. 464 (2023) 142576.
[33] K. Baidya, A. Roy, K. Das, A review of polymer-matrix piezoelectric composite coatings for energy harvesting and smart sensors, J. Coat. Technol. Res. 21 (1) (2024) 55–85.
[34] M. Reghat, et al., Graphene as a piezo-resistive coating to enable strain monitoring in glass fiber composites, Compos. Sci. Technol. 211 (2021) 108842.
[35] O.A. Moses, et al., 2D materials inks toward smart flexible electronics, Mater. Today 50 (2021) 116–148.
[36] X. He, et al., MXene and polymer collision: sparking the future of high-performance multifunctional coatings, Adv. Funct. Mater. (2024) 2409675.
[37] M.S. Irfan, et al., Carbon coated piezoresistive fiber sensors: from process monitoring to structural health monitoring of composites – a review, Compos. Part A 141 (2021) 106236.

[38] A. Thakur, A. Kumar, Challenges and opportunities in the development of nano-hybrid smart coatings, Nano-hybrid Smart Coat. (2024) 353–384.
[39] A. Hirsch, The era of carbon allotropes, Nat. Mater. 9 (11) (2010) 868–871.
[40] M.H. Islam, et al., Graphene and CNT-based smart fiber-reinforced composites: a review, Adv. Funct. Mater. 32 (40) (2022), 2205723-n/a.
[41] A. Nag, S.C. Mukhopadhyay, Fabrication and implementation of carbon nanotubes for piezoresistive-sensing applications: a review, J. Sci. 7 (1) (2022) 100416.
[42] J.-C. Charlier, Defects in carbon nanotubes, Acc. Chem. Res. 35 (12) (2002) 1063–1069.
[43] A. Nag, S.C. Mukhopadhyay, Fabrication and implementation of carbon nanotubes for piezoresistive-sensing applications: a review, J. Sci. 7 (1) (2022) 100416.
[44] J. Tang, et al., Flexible strain sensor based on CNT/TPU composite nanofiber yarn for smart sports bandage, Compos. Part B 232 (2022) 109605.
[45] R.K. Prusty, et al., Reinforcement effect of graphene oxide in glass fibre/epoxy composites at in-situ elevated temperature environments: an emphasis on graphene oxide content, Compos. Part a Appl. Sci. Manuf. 95 (2017) 40–53.
[46] R. Yadav, et al., The role of fillers to enhance the mechanical, thermal, and wear characteristics of polymer composite materials: a review, Compos. Part A 175 (2023) 107775.
[47] Y. Yan, et al., Progress and opportunities in additive manufacturing of electrically conductive polymer composites, Mater. Today Adv. 17 (2023) 100333.
[48] D. Mi, Z. Zhao, H. Bai, Effects of Orientation and Dispersion on Electrical Conductivity and Mechanical Properties of Carbon Nanotube/Polypropylene Composite, Polymers 15 (10) (2023).
[49] Y. Su, et al., Carbon nanotube-decorated glass fibre bundles for cure self-monitoring and load self-sensing of FRPs, Compos. Commun. 27 (2021) 100899.
[50] G. Zhao, et al., Glass fibres coated with flame synthesised carbon nanotubes to enhance interface properties, Compos. Commun. 24 (2021) 100623.
[51] S.R. Shahbaz, et al., Fabrication and analysis of integrated multifunctional MWCNTS sensors in glass fiber reinforced polymer composites, Compos. Struct. 260 (2021) 113527.
[52] H. Wang, et al., Multifunctional pressure/temperature/bending sensor made of carbon fibre-multiwall carbon nanotubes for artificial electronic application, Compos. Part a Appl. Sci. Manuf. 154 (2022) 106796.
[53] Y. Liu, et al., Interlaminar properties of carbon nanotubes modified carbon fibre fabric reinforced polyimide composites, J. Compos. Mater. 57 (7) (2023) 1277–1288.
[54] H. Seeli, V.V.S. Prasad, M. Venkatesh, Nano-graphene E-glass fibre epoxy polymer composite thermal and mechanical characteristics study, in: Mater. Today, 2023.
[55] L. Groo, et al., Transfer printed laser induced graphene strain gauges for embedded sensing in fiberglass composites, Compos. B Eng. 219 (2021) 108932.
[56] M.A.A. Ahmad, et al., Effect of water absorption on graphene nanoplatelet and multiwalled carbon nanotubes-impregnated glass fibre-reinforced epoxy composites, J. Inorg. Organomet. Polym. Mater. (2023).
[57] E.C. Senis, et al., Enhancement of the electrical and thermal properties of unidirectional carbon fibre/epoxy laminates through the addition of graphene oxide, J. Mater. Sci. 54 (12) (2019) 8955–8970.
[58] P. Enrique-Jimenez, et al., Nanoindentation mapping of multiscale composites of graphene-reinforced polypropylene and carbon fibres, Compos. Sci. Technol. 169 (2019) 151–157.
[59] N.O. Weiss, et al., Graphene: an emerging electronic material, Adv. Mater. 24 (43) (2012) 5782–5825.
[60] C. Lee, et al., Measurement of the elastic properties and intrinsic strength of monolayer graphene, Science (1979) 321 (5887) (2008) 385–388.
[61] A.A. Balandin, et al., Superior thermal conductivity of single-layer graphene, Nano Lett. 8 (3) (2008) 902–907.
[62] W. Ababay Ketema, A.Delele Worku, Recent advances of graphene-based materials for emerging technologies, Results. Chem. 5 (2023) 100971.
[63] A. Mirabedini, et al., Evolving strategies for producing multiscale graphene-enhanced fiber-reinforced polymer composites for smart structural applications, Adv. Sci. 7 (11) (2020), p. 1903501-n/a.
[64] J.-H. Lee, S.-J. Park, J.-W. Choi, Electrical property of graphene and its application to electrochemical biosensing, Nanomaterials 9 (2) (2019) 297.
[65] L. Zhu, et al., Graphene oxide composite membranes for water purification, ACS. Appl. Nano Mater. 5 (3) (2022) 3643–3653.
[66] H. Wang, et al., MoS2/Graphene composites as promising materials for energy storage and conversion applications, Adv. Mater. Interfaces. 6 (20) (2019) p. n/a.
[67] Y. Hwang, et al., Ag-fiber/graphene hybrid electrodes for highly flexible and transparent optoelectronic devices, Sci. Rep. 10 (1) (2020), 5117-5117.
[68] K.S. Novoselov, et al., Two-Dimensional Atomic Crystals, PNAS 102 (30) (2005) 10451–10453.
[69] F. Liu, et al., Synthesis of graphene materials by electrochemical exfoliation: recent progress and future potential, Carbon Energy 1 (2) (2019) 173–199.
[70] W.S. Hummers, R.E. Offeman, Preparation of Graphitic Oxide, J. Am. Chem. Soc. 80 (6) (1958), 1339-1339.
[71] N. Mishra, et al., Graphene growth on silicon carbide: a review (Phys. Status Solidi A 9/2016), Physica status solidi. A, Applications and materials science 213 (9) (2016), 2269-2269.
[72] S.S. Shams, et al., Synthesis of graphene from biomass: a green chemistry approach, Mater. Lett. 161 (2015) 476–479.
[73] D.A.C. Brownson, C.E. Banks, The electrochemistry of CVD graphene: progress and prospects, PCCP 14 (23) (2012) 8264–8281.
[74] K. Krishnamoorthy, et al., Graphene oxide nanopaint, Carbon (New York) 72 (2014) 328–337.
[75] P. Wick, et al., Classification Framework for Graphene-Based Materials, Angewandte Chemie (International ed.) 53 (n° 30) (2014) 7714.
[76] A.F. Betancur-Lopera, et al., Role of low-dimensional carbon nanostructures in hybrid material as anticorrosive coating, Prog. Org. Coat. 163 (2022) 106682.
[77] D.C. Marcano, et al., Improved Synthesis of Graphene Oxide, ACS. Nano 4 (8) (2010) 4806–4814.
[78] H. Yu, et al., High-efficient Synthesis of Graphene Oxide Based on Improved Hummers Method, Sci. Rep. 6 (1) (2016), 36143-36143.
[79] R. Raccichini, et al., The role of graphene for electrochemical energy storage, Nat. Mater. 14 (3) (2015) 271–279.
[80] J. Xue, Z. Gao, L. Xiao, The application of stimuli-sensitive actuators based on graphene materials, Front. Chem. 7 (2019) 803.
[81] H. Hu, et al., Synergistic effect of functional carbon nanotubes and graphene oxide on the anti-corrosion performance of epoxy coating, Polym. Adv. Technol. 28 (6) (2017) 754–762.
[82] X.W. Yu, et al., Graphene-based smart materials, Nature Reviews Materials 2 (9) (2017) 13.
[83] Y. Lei, G. Zhang, H. Li, Thermal-responsive nanocomposite hydrogel based on graphene oxide-polyvinyl alcohol/poly (N-isopropylacrylamide), Materials Science and Engineering Conference Series (2017).
[84] N.A. Zubair, et al., Production of conductive PEDOT-coated PVA-GO composite nanofibers, Nanoscale Res. Lett. 12 (1) (2017) 113.
[85] H. Yang, K. Paek, B.J. Kim, Efficient temperature sensing platform based on fluorescent block copolymer-functionalized graphene oxide, Nanoscale 5 (13) (2013) 5720–5724.
[86] J. Lee, et al., Colorimetric thermometer from graphene oxide platform integrated with red, green, and blue emitting, responsive block copolymers, Chemistry of Materials 28 (10) (2016) 3446–3453.
[87] T.Q. Trung, et al., High Thermal Responsiveness of a Reduced Graphene Oxide Field-Effect Transistor, Adv. Mater. 24 (38) (2012) 5254–5260.
[88] W. Du, et al., Multifunctional light-responsive graphene-based polyurethane composites with shape memory, self-healing, and flame retardancy properties, Compos. Part A 128 (2020) 105686.
[89] K. Shi, et al., Near-infrared light-responsive poly (N-isopropylacrylamide)/graphene oxide nanocomposite hydrogels with ultrahigh tensibility, ACS. Appl. Mater. Interfaces 7 (49) (2015) 27289–27298.
[90] R. Kurapati, A.M. Raichur, Near-infrared light-responsive graphene oxide composite multilayer capsules: a novel route for remote controlled drug delivery, Chemical Communications 49 (7) (2013) 734–736.
[91] Q. Liu, et al., High-performance strain sensors with fish-scale-like graphene-sensing layers for full-range detection of human motions, ACS. Nano 10 (8) (2016) 7901–7906.
[92] X. Li, et al., Stretchable and highly sensitive graphene-on-polymer strain sensors, Sci. Rep. 2 (2012) 870.
[93] Y. Wang, et al., Super-elastic graphene ripples for flexible strain sensors, ACS. Nano 5 (5) (2011) 3645–3650.
[94] F. Schedin, et al., Detection of individual gas molecules adsorbed on graphene, Nat. Mater. 6 (9) (2007) 652.
[95] F. Zhao, et al., Direct power generation from a graphene oxide film under moisture, Adv. Mater. 27 (29) (2015) 4351–4357.
[96] H. Bi, et al., Ultrahigh humidity sensitivity of graphene oxide, Sci. Rep. 3 (2013) 2714.
[97] J.-Y. Hong, J. Jang, Highly stable, concentrated dispersions of graphene oxide sheets and their electro-responsive characteristics, Soft. Matter. 8 (28) (2012) 7348–7350.
[98] Y.Q. He, et al., A pH and Electric Responsive Graphene Oxide Based Composite hydrogel. in Adv. Mater. Research, Trans Tech Publ, 2012.
[99] J. Liu, et al., A rationally-designed synergetic polypyrrole/graphene bilayer actuator, J. Mater. Chem. 22 (9) (2012) 4015–4020.
[100] C.H. Hong, et al., Fabrication of smart magnetite/reduced graphene oxide composite nanoparticles and their magnetic stimuli-response, J. Colloid. Interface Sci. 481 (2016) 194–200.
[101] V. Chandra, et al., Water-dispersible magnetite-reduced graphene oxide composites for arsenic removal, ACS. Nano 4 (7) (2010) 3979–3986.
[102] S. Perumal, R. Atchudan, I.W. Cheong, Recent studies on dispersion of graphene–polymer composites, Polymers 13 (14) (2021) 2375.
[103] H. Lu, et al., Applications of graphene-based composite hydrogels: a review, RSC. Adv. 7 (80) (2017) 51008–51020.
[104] M.S. Irfan, et al., MXene and graphene coated multifunctional fiber reinforced aerospace composites with sensing and EMI shielding abilities, Compos. Part A 165 (2023) 107351.
[105] F.S. Irani, et al., Graphene as a piezoresistive material in strain sensing applications, Micromachines 13 (1) (2022).
[106] M.S.S. Bathusha, et al., In-situ monitoring of crack growth and fracture behavior in composite laminates using embedded sensors of rGO coated fabrics and GnP paper, Sens. Actuators A 365 (2024) 114850.
[107] M. Ahmadi, et al., 2D transition metal dichalcogenide nanomaterials: advances, opportunities, and challenges in multi-functional polymer nanocomposites, J. Mater. Chem. A Mater. Energy Sustain. 8 (3) (2020) 845–883.
[108] A.T. Hoang, et al., Large-area synthesis of transition metal dichalcogenides via CVD and solution-based approaches and their device applications, Nanoscale 13 (2) (2021) 615–633.
[109] M. Chhowalla, et al., The chemistry of two-dimensional layered transition metal dichalcogenide nanosheets, Nat. Chem. 5 (4) (2013) 263–275.
[110] W. Choi, et al., Recent development of two-dimensional transition metal dichalcogenides and their applications, Mater. Today 20 (3) (2017) 116–130.

[111] R. Kumar, et al., Transition metal dichalcogenides-based flexible gas sensors, Sens. Actuators A 303 (2020) 111875.
[112] A. Chhetry, et al., MoS2-decorated laser-induced graphene for a highly sensitive, hysteresis-free, and reliable piezoresistive strain sensor, ACS. Appl. Mater. Interfaces 11 (25) (2019) 22531–22542.
[113] N. Bokka, et al., A detailed comparative performance analysis of the Transition Metal Di-chalcogenides (TMDs) based strain sensors through experimental realisations and first principle calculations, FlatChem 32 (2022) 100344.
[114] D. Jiang, et al., Flexible electronics based on 2D transition metal dichalcogenides, J. Mater. Chem. A Mater. Energy Sustain. 1 (1) (2021) 89–121.
[115] M. Zhu, et al., High gauge factor strain sensors based on vanadium doped molybedenum disulfide 2D films, in: 2019 IEEE 32nd International Conference on Micro Electro Mechanical Systems (MEMS), 2019.
[116] K. Zhou, et al., A noncovalent functionalization approach to improve the dispersibility and properties of polymer/MoS2 composites, Appl. Surf. Sci. 316 (2014) 237–244.
[117] K. Zhou, et al., In situ growth of 0D silica nanospheres on 2D molybdenum disulfide nanosheets: towards reducing fire hazards of epoxy resin, J. Hazard. Mater. 344 (2018) 1078–1089.
[118] P. Najmi, et al., Design of nacre-inspired 2D-MoS2 nanosheets assembled with mesoporous covalent organic frameworks (COFs) for smart coatings, ACS. Appl. Mater. Interfaces 14 (48) (2022) 54141–54156.
[119] A. Singh, S. Thakur, Recent advancements in the fabrication of transition metal dichalcogenides-polymer nanocomposites: focused on molybdenum diselenide for various applications, Mater. Today Chem. 30 (2023) 101562.
[120] Y.-J. Huang, et al., MoSe2 nanosheet/poly(3,4-ethylenedioxythiophene): poly (styrenesulfonate) composite film as a Pt-free counter electrode for dye-sensitized solar cells, Electrochim. Acta 211 (2016) 794–803.
[121] M. Dahlqvist, M.W. Barsoum, J. Rosen, MAX phases – Past, present, and future, Mater. Today 72 (2024) 1–24.
[122] A. Vahidmohammadi, J. Rosen, Y. Gogotsi, The world of two-dimensional carbides and nitrides (MXenes), Science 372 (6547) (2021) 1165.
[123] Y. Wang, et al., MXenes for energy harvesting, Adv. Mater. 34 (21) (2022) 2108560.
[124] J Yan, et al., Polypyrrole–MXene coated textile-based flexible energy storage device, RSC. Adv. 8 (69) (2018) 39742–39748.
[125] Y. Shibata, et al., Fabrication of MXene transparent conductive films via transfer process, Appl. Phys. Express. 16 (3) (2023) 037001.
[126] S. Kazim, et al., MXene-Based energy devices: from progressive to prospective, Adv. Funct. Mater. (2024) 2315694.
[127] Y. Gogotsi, B. Anasori, The rise of MXenes, ACS. Nano 13 (8) (2019) 8491–8494.
[128] Y. Gogotsi, Q. Huang, MXenes: two-dimensional building blocks for future materials and devices, ACS. Nano 15 (4) (2021) 5775–5780.
[129] M. Xin, et al., MXenes and their applications in wearable sensors, Front. Chem. 8 (2020), 297-297.
[130] K. Grabowski, et al., Recent advances in MXene-based sensors for structural health monitoring applications: a review, Measurement 189 (2022) 110575.
[131] A. Lipatov, et al., High electrical conductivity and breakdown current density of individual monolayer Ti3C2Tx MXene flakes, Matter 4 (4) (2021) 1413–1427.
[132] J. Chen, et al., Simplified synthesis of fluoride-free Ti3C2Tx via electrochemical etching toward high-performance electrochemical capacitors, ACS. Nano 16 (2) (2022) 2461–2470.
[133] T. Li, et al., Fluorine-free synthesis of high-purity Ti3C2Tx (T= OH, O) via alkali treatment, Angew. Chem. Int. Ed. 57 (21) (2018) 6115–6119.
[134] M.S. Bhargava Reddy, et al., A Family of 2D-MXenes: synthesis, Properties, and Gas Sensing Applications, ACS. Sens. 7 (8) (2022) 2132–2163.
[135] J. Chen, et al., Recent advances in 2D metal carbides and nitrides (MXenes): synthesis and biological application, J Mater Chem B Mater Biol Med 11 (4) (2023) 72–715.
[136] V. Orts Mercadillo, et al., Electrically conductive 2D material coatings for flexible and stretchable electronics: a comparative review of Graphenes and MXenes, Adv. Funct. Mater. 32 (38) (2022), p. 2204772-n/a.
[137] J. Yan, et al., Flexible and high-sensitivity piezoresistive sensor based on MXene composite with wrinkle structure, Ceram. Int. 46 (15) (2020) 23592–23598.
[138] Y. Guo, et al., A wearable transient pressure sensor made with MXene nanosheets for sensitive broad-range human–machine interfacing, Nano Lett. 19 (2) (2019) 1143–1150.
[139] X.-P. Li, et al., Highly sensitive, reliable and flexible piezoresistive pressure sensors featuring polyurethane sponge coated with MXene sheets, J. Colloid. Interface Sci. 542 (2019) 54–62.
[140] Y. Ma, et al., 3D synergistical MXene/reduced graphene oxide aerogel for a piezoresistive sensor, ACS. Nano 12 (4) (2018) 3209–3216.
[141] X. Wang, et al., Health monitoring of repaired composite structure using MXene sensor, Compos. Commun. 27 (2021) 100850.
[142] Why Would You Need Conductive Coatings? 2023; Available from: https://diamondcoatings.com/why-would-you-need-conductive-coatings/.
[143] K. Chatterjee, J. Tabor, T.K. Ghosh, Electrically Conductive Coatings for Fiber-Based E-Textiles, Fibers 7 (6) (2019) 51.
[144] W. Daoudi, et al., Introduction to nano-hybrid smart coatings. Nano-hybrid Smart Coat., American Chemical Society, 2024, pp. 1–16.
[145] L. Wu, et al., Durable and multifunctional superhydrophobic coatings with excellent joule heating and electromagnetic interference shielding performance for flexible sensing electronics, ACS. Appl. Mater. Interfaces 11 (37) (2019) 34338–34347.
[146] H. Tang, et al., Electrical behavior of carbon black-filled polymer composites: effect of interaction between filler and matrix, J. Appl. Polym. Sci. 51 (7) (1994) 1159–1164.
[147] J. Zhang, et al., Self-Healing mechanism and conductivity of the hydrogel flexible sensors: a review, Gels 7 (4) (2021) 216.
[148] S.A. Mirmohammadi, S. Sadjadi, N. Bahri-Laleh, 10 Electrical and Electromagnetic Properties of CNT/Polymer Composites, in Carbon Nanotube-Reinforced Polymers, R. Rafiee, Editor, Elsevier, 2018, pp. 233–258.
[149] F.K. FUSS, B. A, J. SIDHU, F MUELLER, Fractal Dimension Analysis of muscle fatigue with muscle surface pressure measures with compression garments. in 2nd International Conference in Sports Science & Technology (ICSST), in: Proceedings of the 2nd International Conference in Sports Science & Technology (ICSST, 2016.
[150] S. Moharana, et al., 8 Synthesis and properties of percolative metal oxide-polymer composites, in: S. Haider, A. Haider (Eds.), Renewable Polymers and Polymer-Metal Oxide Composites, Elsevier, 2022, pp. 253–282. Editors.
[151] A.J. Marsden, et al., Electrical percolation in graphene-polymer composites, 2d. Mater. 5 (3) (2018) 32003.
[152] A.J. Marsden, et al., Electrical percolation in graphene–polymer composites, 2d. Mater. 5 (3) (2018) 032003.
[153] M.V. Sulleiro, et al., 2D Materials towards sensing technology: from fundamentals to applications, Sens. Biosensing. Res. 38 (2022) 100540.
[154] J. Liu, S. Bao, X. Wang, Applications of graphene-based materials in sensors: a review, Micromachines 13 (2) (2022).
[155] Q. Zheng, et al., Graphene-based wearable piezoresistive physical sensors, Mater. Today 36 (2020) 158–179.
[156] X. Zeng, et al., Wearable Multi-Functional Sensing Technology for Healthcare Smart Detection, Micromachines 13 (2) (2022) 254.
[157] F. Zhang, et al., Anisotropic conductive networks for multidimensional sensing, Mater. Horiz. 8 (1) (2021) 2615–2653.
[158] M. Xie, et al., Flexible multifunctional sensors for wearable and robotic applications, Adv. Mater. Technol. 4 (3) (2019) 1800626.
[159] Z. Shi, et al., Morphological engineering of sensing materials for flexible pressure sensors and artificial intelligence applications, Nanomicro Lett. 14 (1) (2022) 141.
[160] J.Z. Hassan, et al., 2D material-based sensing devices: an update, J. Mater. Chem. A (2023).
[161] A.W. Zia, S.A. Hussain, M.M.F.A. Baig, Optimizing diamond-like carbon coatings From experimental era to artificial intelligence, Ceram. Int. 48 (24) (2022) 36000–36011.
[162] M.A. Ali, et al., Graphene nanoparticles as data generating digital materials in industry 4.0, Sci. Rep. 13 (1) (2023) 4945.
[163] M. Kuntoğlu, et al., A state-of-the-art review on sensors and signal processing systems in mechanical machining processes, The International Journal of Advanced Manufacturing Technology 116 (9) (2021) 2711–2735.
[164] A. Sofi, et al., Structural health monitoring using wireless smart sensor network – An overview, Mech. Syst. Signal. Process. 163 (2022) 108113.
[165] X. Lai, et al., Digital twin-based structural health monitoring by combining measurement and computational data: an aircraft wing example, J. Manuf. Syst. 69 (2023) 76–90.
[166] A.W. Momber, et al., A Digital Twin concept for the prescriptive maintenance of protective coating systems on wind turbine structures, Wind Eng. 46 (3) (2022) 949–971.
[167] H.V. Dang, M. Tatipamula, H.X. Nguyen, Cloud-Based digital twinning for structural health monitoring using deep learning, IEEe Trans. Industr. Inform. 18 (6) (2022) 3820–3830.
[168] P. Stavropoulos, Digitization of manufacturing processes: from sensing to twining, Technologies 10 (5) (2022) 98.
[169] A. Belbasis, F.K. Fuss, J. Sidhu, Muscle Activity Analysis with a Smart Compression Garment, Procedia Eng. 112 (2015) 163–168.
[170] A. Belbasis, F.K. Fuss, Muscle performance investigated with a novel smart compression garment based on pressure sensor force myography and its validation against EMG, Front. Physiol. 9 (2018) 408.
[171] F.K. Fuss, P. Düking, Y. Weizman, Discovery of a sweet spot on the foot with a smart wearable soccer boot sensor that maximizes the chances of scoring a curved kick in soccer, Front. Physiol. 9 (2018) 63.
[172] L. Zhan, et al., Additively fabricated electronic skin with high performance in dynamic sensing as human skin, ACS. Appl. Electron. Mater. 5 (4) (2023) 2017–2025.
[173] M.F. Cunningham, et al., Future green chemistry and sustainability needs in polymeric coatings, Green Chem. 21 (18) (2019) 4919–4926.
[174] F. Liu, et al., Neuro-inspired electronic skin for robots, Sci. Robot. 7 (67) (2022), 7344-7344.
[175] J.C. Yang, et al., Electronic Skin: recent Progress and Future Prospects for Skin-Attachable Devices for Health Monitoring, Robotics, and Prosthetics, Adv. Mater. 31 (48) (2019), 1904765-1904765.
[176] Y. Guo, et al., Recent advances in carbon material-based multifunctional sensors and their applications in electronic skin systems, Adv. Funct. Mater. 31 (40) (2021), 2104288-2104288.
[177] Brindha Ramasubramanian, et al., Novel low-carbon energy solutions for powering emerging wearables, smart textiles, and medical devices, Energy Environ. Sci. (2022).
[178] X. Wang, et al., Recent progress in electronic skin, Adv. Sci. 2 (10) (2015), 1500169-1500169.
[179] M.L. Hammock, et al., 25th anniversary article: the evolution of electronic skin (E-Skin): a brief history, design considerations, and recent progress, Adv. Mater. 25 (42) (2013) 5997–6038.

[180] R. Han, et al., Research on the preparation and thermal stability of silicone rubber composites: a review, Compos. Part C 8 (2022), 100249-100249.
[181] X. Fan, et al., PEDOT:PSS for flexible and stretchable electronics: modifications, strategies, and applications, Adv. Sci. 6 (19) (2019), 1900813-1900813.
[182] S.K. Soni, B. Thomas, V.R. Kar, A comprehensive review on CNTs and CNT-reinforced composites: syntheses, characteristics and applications, Mater. Today Commun. 25 (2020), 101546-101546.
[183] D.S. Kim, et al., A stretchable array of high-performance electrochromic devices for displaying skin-attached multi-sensor signals, Chem. Eng. J. 429 (2022), 132289-132289.
[184] Z. Yan, et al., Stretchable micromotion sensor with enhanced sensitivity using serpentine layout, ACS Appl. Mater. Interfaces 11 (13) (2019) 12261–12271.
[185] X. Liu, The more and less of electronic-skin sensors, Science (1979) 370 (6519) (2020) 910–911.
[186] S. Duan, et al., Water-Modulated biomimetic hyper-attribute-gel electronic skin for robotics and skin-attachable wearables, ACS. Nano (2022).
[187] Y. Chen, et al., Energy autonomous electronic skin with direct temperature-pressure perception, Nano Energy 98 (2022), 107273-107273.
[188] W. Peng, et al., A direction-aware and ultrafast self-healing dual network hydrogel for a flexible electronic skin strain sensor, J. Mater. Chem. A 8 (48) (2020) 26109–26118.
[189] J. Park, et al., Nanomaterials: fingertip skin-inspired microstructured ferroelectric skins discriminate static/dynamic pressure and temperature stimuli, Sci. Adv. 1 (9) (2015).
[190] H.H. Chou, et al., A chameleon-inspired stretchable electronic skin with interactive colour changing controlled by tactile sensing, Nature Communications 2015 6:1 6 (1) (2015) 1–10.
[191] W. Kong, et al., An ultra-low hysteresis, self-healing and stretchable conductor based on dynamic disulfide covalent adaptable networks, J. Mater. Chem. A 10 (4) (2022) 2012–2020.
[192] Barbaz-Isfahani, R., S. Saber-Samandari, and M. Salehi, Experimental and numerical research on healing performance of reinforced microcapsule-based self-healing polymers using nanoparticles. https://doi.org/10.1177/07316844221102945, 2022. 42(3–4): p. 95–109.
[193] C.M. Yeh, et al., Disulfide bond and Diels–Alder reaction bond hybrid polymers with high stretchability, transparency, recyclability, and intrinsic dual healability for skin-like tactile sensing, J. Mater. Chem. A 9 (10) (2021) 6109–6116.
[194] W.-M. Zhong, et al., Artificial optoelectronic synaptic characteristics of Bi2FeMnO6 ferroelectric memristor for neuromorphic computing, Mater. Des. 222 (2022) 111046.
[195] W.-Y. Huang, et al., Synaptic properties of a PbHfO3 ferroelectric memristor for neuromorphic computing, ACS. Appl. Mater. Interfaces 16 (18) (2024) 23615–23624.
[196] T.G. Allen, et al., Passivating contacts for crystalline silicon solar cells, Nature Energy 4 (11) (2019) 914–928.
[197] Andreani, L.C., et al., Silicon solar cells: toward the efficiency limits. https://doi.org/10.1080/23746149.2018.1548305, 2018. 4(1).
[198] A. Richter, et al., Design rules for high-efficiency both-sides-contacted silicon solar cells with balanced charge carrier transport and recombination losses, Nature Energy 2021 6:4 6 (4) (2021) 429–438.
[199] L. Wieland, et al., Carbon nanotubes for photovoltaics: from lab to industry, Adv. Energy Mater. 11 (3) (2021) 2002880.
[200] X. Zhao, et al., High-efficiency CNT-Si solar cells based on a collaborative system enabled by oxide penetration, Nano Res. 15 (3) (2022) 2497–2504.
[201] A. Romeo, E. Artegiani, CdTe-Based thin film solar cells: past, present and future, Energies 14 (6) (2021), 1684-1684.
[202] A.K. Gain, et al., A review of primary technologies of thin-film solar cells, Eng. Res. Express 3 (3) (2021), 032001-032001.
[203] G. Kapil, et al., Tin-Lead perovskite fabricated via ethylenediamine interlayer guides to the solar cell efficiency of 21.74%, Adv. Energy Mater. 11 (25) (2021), 2101069-2101069.
[204] Q. Ma, et al., Promoting charge separation resulting in ternary organic solar cells efficiency over 17.5%, Nano Energy 78 (2020), 105272-105272.
[205] C. Li, et al., Low-bandgap mixed tin–lead iodide perovskites with reduced methylammonium for simultaneous enhancement of solar cell efficiency and stability, Nature Energy 5 (10) (2020) 768–776.
[206] M. Kam, et al., Room-Temperature sputtered SnO2 as robust electron transport layer for air-stable and efficient perovskite solar cells on rigid and flexible substrates, Sci. Rep. 9 (1) (2019) 1–10.
[207] R. Carron, et al., Advanced alkali treatments for high-efficiency Cu(In,Ga)Se2 solar cells on flexible substrates, Adv. Energy Mater. 9 (24) (2019), 1900408-1900408.
[208] Surface and interface science. Surface and Interface Science, 2020.
[209] Saygili, Y., Copper Bipyridyl Redox Mediators for High Performance Dye-Sensitized Solar Cells. 2019.
[210] S. Sharma, et al., Novel Epitaxial Lift-Off for Flexible, Inexpensive GaAs Solar Cells, in: Conference Record of the IEEE Photovoltaic Specialists Conference, 2020, pp. 0744–0746, 2020-June.
[211] A.Y. Shuhadah, et al., Influence of water and precursor molarity on the tio2 thin films deposited from solventless sol-gel, JAMT 12 (1(4)) (2018) 125–134.
[212] M.M. Karkare, Choice of precursor not affecting the size of anatase TiO2 nanoparticles but affecting morphology under broader view, Int. Nano Lett. 4 (3) (2014) 1–8.
[213] Y. Wang, et al., Defective MWCNT enabled dual interface coupling for carbon-based perovskite solar cells with efficiency exceeding 22%, Adv. Funct. Mater. 32 (31) (2022), 2204831-2204831.
[214] F. Liu, et al., Hole Transport Materials Based on 6,12-Dihydroindeno[1,2-b]fluorine with Different Periphery Groups: a New Strategy for Dopant-Free Perovskite Solar Cells, Adv. Funct. Mater. 29 (24) (2019), 1901296-1901296.
[215] L. Vaghi, F. Rizzo, The future of spirobifluorene-based molecules as hole-transporting materials for solar cells, Sol. RRL. 7 (7) (2023), 2201108-2201108.
[216] N.A.N. Ouedraogo, et al., Oxidation of Spiro-OMeTAD in high-efficiency perovskite solar cells, ACS Appl. Mater. Interfaces 14 (30) (2022) 34303–34327.
[217] K. Song, et al., Generation of electrical power under human skin by subdermal solar cell arrays for implantable bioelectronic devices, Biosens. Bioelectr. 92 (2017) 364–371.
[218] A. Harillo-Baños, X. Rodríguez-Martínez, M. Campoy-Quiles, Efficient exploration of the composition space in ternary organic solar cells by combining high-throughput material libraries and hyperspectral imaging, Adv. Energy Mater. 10 (1) (2020), 1902417-1902417.
[219] J. Bertrandie, et al., The energy level conundrum of organic semiconductors in solar cells, Adv. Mater. 34 (35) (2022), 2202575-2202575.
[220] K. Dong, X. Peng, Z.L. Wang, Fiber/Fabric-Based piezoelectric and triboelectric nanogenerators for flexible/stretchable and wearable electronics and artificial intelligence, Adv. Mater. 32 (5) (2020), 1902549-1902549.
[221] S.A. Hashemi, S. Ramakrishna, A.G. Aberle, Recent progress in flexible–wearable solar cells for self-powered electronic devices, Energy Environ. Sci. 13 (3) (2020) 685–743.
[222] A. Shit, et al., Mineralized soft and elastic polymer dot hydrogel for a flexible self-powered electronic skin sensor, ACS Appl. Mater. Interfaces 12 (30) (2020) 34105–34114.
[223] Y. Takeda, T. Morikawa, N. Kato, Spectrally robust series/parallel-connected triple-junction photovoltaic cells used for artificial photosynthesis, J. Appl. Phys. 127 (20) (2020).
[224] K. Xiao, et al., Solution-processed monolithic all-perovskite triple-junction solar cells with efficiency exceeding 20%, ACS. Energy Lett. 5 (9) (2020) 2819–2826.
[225] Y. Park, B. Zhao, S. Fan, Reaching the ultimate efficiency of solar energy harvesting with a nonreciprocal multijunction solar cell, Nano Lett. 22 (1) (2022) 448–452.
[226] N. Torabi, et al., Progress and challenges in perovskite photovoltaics from single- to multi-junction cells, Mater. Today Energy 12 (2019) 70–94.
[227] C. Ye, et al., A triboelectric-electromagnetic hybrid nanogenerator with broadband working range for wind energy harvesting and a self-powered wind speed sensor, ACS. Energy Lett. 6 (4) (2021) 1443–1452.
[228] J. Sun, et al., A mobile and self-powered micro-flow pump based on triboelectricity driven electroosmosis, Adv. Mater. 33 (34) (2021), 2102765-2102765.
[229] B. Ghatak, et al., Design of a self-powered triboelectric face mask, Nano Energy 79 (2021), 105387-105387.
[230] B. Dudem, et al., Nanopillar-array architectured PDMS-based triboelectric nanogenerator integrated with a windmill model for effective wind energy harvesting, Nano Energy 42 (2017) 269–281.
[231] L. Wang, et al., A CNT-PDMS wearable device for simultaneous measurement of wrist pulse pressure and cardiac electrical activity, Mater. Sci. Eng. C 117 (2020), 111345-111345.
[232] X. Qu, et al., Artificial tactile perception smart finger for material identification based on triboelectric sensing, Sci. Adv. 8 (31) (2022), 2521-2521.
[233] Y. Fang, et al., Ambulatory cardiovascular monitoring via a machine-learning-assisted textile triboelectric sensor, Adv. Mater. 33 (41) (2021), 2104178-2104178.
[234] Q. Zhang, et al., Wearable triboelectric sensors enabled gait analysis and waist motion capture for IoT-based smart healthcare applications, Adv. Sci. 9 (4) (2022), 2103694-2103694.
[235] M.R. Sarker, et al., Review of power converter impact of electromagnetic energy harvesting circuits and devices for autonomous sensor applications, Electronics 10 (9) (2021), 1108-1108.
[236] P. Maharjan, et al., High-performance cycloid inspired wearable electromagnetic energy harvester for scavenging human motion energy, Appl. Energy 256 (2019), 113987-113987.
[237] N. Zhou, et al., Enhanced swing electromagnetic energy harvesting from human motion, Energy 228 (2021), 120591-120591.
[238] M. Hasani, M.Irani Rahaghi, The optimization of an electromagnetic vibration energy harvester based on developed electromagnetic damping models, Energy Convers. Manage 254 (2022), 115271-115271.
[239] Z. Li, et al., Constituting abrupt magnetic flux density change for power density improvement in electromagnetic energy harvesting, Int. J. Mech. Sci. 198 (2021), 106363-106363.
[240] G. Miao, et al., A low-frequency rotational electromagnetic energy harvester using a magnetic plucking mechanism, Appl. Energy 305 (2022), 117838-117838.
[241] Y. Du, et al., Ultraflexible, highly efficient electromagnetic interference shielding, and self-healable triboelectric nanogenerator based on Ti3C2Tx MXene for self-powered wearable electronics, J. Mater. Sci. Technol. 100 (2022) 1–11.
[242] Q. Zhou, et al., Magnetized microcilia array-based self-powered electronic skin for micro-scaled 3D morphology recognition and high-capacity communication, Adv. Funct. Mater. 32 (46) (2022), 2208120-2208120.
[243] Y. Zhen, et al., Three-dimensional AgNps@Mxene@PEDOT:PSS composite hybrid foam as a piezoresistive pressure sensor with ultra-broad working range, J. Mater. Sci. (2022) 1–20.
[244] S. Gong, et al., Biocompatible poly(lactic acid)-based hybrid piezoelectric and electret nanogenerator for electronic skin applications, Adv. Funct. Mater. 30 (14) (2020), 1908724-1908724.

[245] B. Mahanty, et al., Human skin interactive self-powered piezoelectric e-skin based on PVDF/MWCNT electrospun nanofibers for non-invasive health care monitoring, Mater. Today 21 (2020) 1964–1968.
[246] M. Cai, W.H. Liao, Enhanced electromagnetic wrist-worn energy harvester using repulsive magnetic spring, Mech. Syst. Signal. Process. 150 (2021), 107251-107251.
[247] C. Chen, et al., Smart Magnetotactic Bacteria Enable the Inhibition of Neuroblastoma under an Alternating Magnetic Field, ACS Applied Materials and Interfaces 14 (12) (2022) 14049–14058.
[248] W. Lin, et al., Expanding magnetic organelle biogenesis in the domain bacteria, Microbiome 8 (1) (2020) 1–13.
[249] A. Trifonov, et al., Electrically contacted bienzyme-functionalized mesoporous carbon nanoparticle electrodes: applications for the development of dual amperometric biosensors and multifuel-driven biofuel cells, Adv. Energy Mater. 5 (8) (2015), 1401853-1401853.
[250] Y. Lin, et al., Soft–Hard Composites for Bioelectric Interfaces, Trends. Chem. 2 (6) (2020) 519–534.
[251] P.L. Mahapatra, et al., Energy harvesting using two-dimensional magnesiochromite (MgCr2O4), Mater. Today Nano 23 (2023), 100374-100374.
[252] Y. Cao, et al., Flame-retardant and leakage-proof phase change composites based on MXene/polyimide aerogels toward solar thermal energy harvesting, Adv. Compos. Hybrid. Mater. 5 (2) (2022) 1253–1267.
[253] M. Mehrali, et al., Simultaneous solar-thermal energy harvesting and storage via shape stabilized salt hydrate phase change material, Chem. Eng. J. 405 (2021), 126624-126624.
[254] P. Zhang, et al., Anisotropically conductive phase change composites enabled by aligned continuous carbon fibers for full-spectrum solar thermal energy harvesting, Chem. Eng. J. 461 (2023), 141940-141940.
[255] S. Wu, et al., High-Performance thermally conductive phase change composites by large-size oriented graphite sheets for scalable thermal energy harvesting, Adv. Mater. 31 (49) (2019), 1905099-1905099.
[256] S. Wu, et al., High-performance thermally conductive phase change composites by large-size oriented graphite sheets for scalable thermal energy harvesting, Adv. Mater. 31 (49) (2019) 1905099.
[257] V. Kashyap, et al., Full spectrum solar thermal energy harvesting and storage by a molecular and phase-change hybrid material an integrated hybrid system for simultaneous harvesting and storage of solar thermal energy. full spectrum solar thermal energy harvesting and storage by a molecular and phase-change hybrid material, Joule (3) (2019) 3100–3111.
[258] X. Chen, et al., Carbon nanotube bundles assembled flexible hierarchical framework based phase change material composites for thermal energy harvesting and thermotherapy, Energy Storage Mater. 26 (2020) 129–137.
[259] S. Wei, et al., Constructing flexible film electrode with porous layered structure by MXene/SWCNTs/PANI ternary composite for efficient low-grade thermal energy harvest, Adv. Funct. Mater. 33 (13) (2023), 2209806-2209806.
[260] S. El Oualid, et al., High Power Density Thermoelectric Generators with Skutterudites, Adv. Energy Mater. 11 (19) (2021), 2100580-2100580.
[261] Z. Dong, et al., Half-Heusler-like compounds with wide continuous compositions and tunable p- to n-type semiconducting thermoelectrics, Nat. Commun. 13 (1) (2022) 1–9.
[262] G. Li, et al., Dramatically reduced lattice thermal conductivity of Mg2Si thermoelectric material from nanotwinning, Acta Mater. 169 (2019) 9–14.
[263] D. Shiojiri, et al., Performance comparison of hybrid functionals for describing narrow-gap semiconductors: a study on low-temperature thermoelectric material α-SrSi2, Comput. Condens. Matter 30 (2022) p. e00620-e00620.
[264] I. Shitanda, S. Tsujimura, Toward self-powered real-time health monitoring of body fluid components based on improved enzymatic biofuel cells, J. Phys. 3 (3) (2021), 032002-032002.
[265] N. Rasitanon, et al., Redox-Mediated gold nanoparticles with glucose oxidase and egg white proteins for printed biosensors and biofuel cells, Int. J. Mol. Sci. 24 (5) (2023), 4657-4657.
[266] F. Gao, et al., Engineering hybrid nanotube wires for high-power biofuel cells, Nature Commun. 1 (1) (2010) 1–7.
[267] H. Assad, et al., Insights into the role of nanotechnology on the performance of biofuel cells and the production of viable biofuels: a review, Fuel 323 (2022), 124277-124277.
[268] J. Wang, et al., Flexible biofuel cell-in-a-tube (iezTube): an entirely self-contained biofuel cell for wearable green bio-energy harvesting, Adv. Funct. Mater. 32 (48) (2022), 2209697-2209697.
[269] M. Sun, et al., A bendable biofuel cell-based fully integrated biomedical nanodevice for point-of-care diagnosis of scurvy, ACS. Sens. 6 (1) (2021) 275–284.
[270] I. Shitanda, et al., A screen-printed circular-type paper-based glucose/O2 biofuel cell, J. Power Sources 360 (2017), 516-519.
[271] A. Baingane, G. Slaughter, Self-Powered electrochemical lactate biosensing, Energies 10 (10) (2017), 1582-1582.
[272] W.-T. Guo, et al., Printed-scalable microstructure BaTiO3/ecoflex nanocomposite for high-performance triboelectric nanogenerators and self-powered human-machine interaction, Nano Energy 131 (2024) 110324.
[273] W.-M. Zhong, et al., Ultra-high dielectric tuning performance and double-set resistive switching effect achieved on the Bi2NiMnO6 thin film prepared by sol–gel method, J. Colloid. Interface Sci. 606 (2022) 913–919.
[274] M. Ragupathy, et al., Electrocatalytic response of the modified ZnO-G electrodes towards the oxidation of serotonin with multi metallic corrosion protection, J. Indian Chem. Soc. 99 (11) (2022), 100768-100768.
[275] R. Brindha, et al., Hybrid electrochemical behaviour of La1-xCaxMnO3 nano perovskites and recycled polar interspersed graphene for metal-air battery system, J. Electrochem. Soc. 167 (12) (2020), 120539-120539.
[276] J. Kowal, et al., Towards sustainable fuel cells and batteries with an AI perspective, Sustainability 14 (23) (2022), 16001-16001.
[277] B. Ramasubramanian, et al., Growth mechanism of micro/nano metal dendrites and cumulative strategies for countering its impacts in metal ion batteries: a review, Nanomaterials 11 (10) (2021), 2476-2476.
[278] D. Deng, Li-ion batteries: basics, progress, and challenges, Energy Sci. Eng. 3 (5) (2015) 385–418.
[279] K. Wu, et al., Recent advances in polymer electrolytes for zinc ion batteries: mechanisms, properties, and perspectives, Adv. Energy Mater. 10 (12) (2020), 1903977-1903977.
[280] J. Lai, et al., Electrolytes for rechargeable lithium–air batteries, Angew. Chem. Int. Ed. 59 (8) (2020) 2974–2997.
[281] D. Campanella, D. Belanger, A. Paolella, Beyond garnets, phosphates and phosphosulfides solid electrolytes: new ceramic perspectives for all solid lithium metal batteries, J. Power Sources 482 (2021), 228949-228949.
[282] Reddy, M.V., et al., Sulfide and oxide inorganic solid electrolytes for all-solid-state Li batteries: a review. Nanomaterials 2020, Vol. 10, Page 1606, 2020. 10(8): p. 1606-1606.
[283] O.M. Leung, et al., Review—progress in electrolytes for rechargeable aluminium batteries, J. Electrochem. Soc. 168 (5) (2021), 056509-056509.
[284] Y. Zeng, et al., Dendrite-Free zinc deposition induced by multifunctional CNT frameworks for stable flexible Zn-Ion batteries, Adv. Mater. 31 (36) (2019), 1903675-1903675.
[285] M.V. Reddy, et al., Brief history of early lithium-battery development, Materials 13 (8) (2020).
[286] E.I. Shkolnikov, et al., Carbon materials as a cathode for aluminum-ion battery, Mater. Today 5 (12) (2018) 26073–26077.
[287] T Ould Ely, et al., Synthesis and Characterization of Silicon Based Anode Materials, Mater. Today 4 (3) (2017) 4502–4511.
[288] P.C. Chen, et al., Hybrid silicon-carbon nanostructured composites as superior anodes for lithium ion batteries, Nano Res. 4 (3) (2011) 290–296.
[289] A. Jaradat, et al., High performance air breathing flexible lithium–air battery, Small. 17 (42) (2021), 2102072-2102072.
[290] P. Wang, et al., A flexible aqueous Al ion rechargeable full battery, Chem. Eng. J. 373 (2019) 580–586.
[291] K. Chayambuka, et al., From Li-Ion batteries toward na-ion chemistries: challenges and opportunities, Adv. Energy Mater. 10 (38) (2020), 2001310-2001310.
[292] L.F. Zhao, et al., Hard carbon anodes: fundamental understanding and commercial perspectives for Na-Ion batteries beyond Li-Ion and K-Ion counterparts, Adv. Energy Mater. 11 (1) (2021), 2002704-2002704.
[293] M. Gao, et al., (Invited) a nature-inspired porous electrode for flexible, stretchable supercapacitors and lithium-ion batteries, ECS Meeting Abstracts (2018). MA2018-01(26)1539-1539.
[294] Waterborne Coatings Market Size, Share & Trends Analysis Report By Resin (Acrylic, PU, Epoxy, Polyester), By Application (Architectural, General Industrial, Marine), By Region, And Segment Forecasts, 2023 2030. Available from: https://www.grandviewresearch.com/industry-analysis/waterborne-coatings-market.
[295] R. Balu, N.K. Dutta, N.Roy Choudhury, Plastic waste upcycling: a sustainable solution for waste management, product development, and circular economy, Polymers 14 (22) (2022) 4788.
[296] C.G. Schirmeister, R. Mülhaupt, Closing the carbon loop in the circular plastics economy, Macromol. Rapid. Commun. 43 (13) (2022) 2200247.
[297] L.L. Guarieiro, et al., Reaching circular economy through circular chemistry: the basis for sustainable development, J. Braz. Chem. Soc. 33 (2022) 1353–1374.
[298] H.-J. Endres, Bioplastics, Biorefineries (2019) 427–468.
[299] S. He, et al., Advance of design and application in self-healing anticorrosive coating: a review, J. Coat. Technol. Res. 20 (3) (2023) 819–841.
[300] P. Singh, et al., Sustainable smart anti-corrosion coating materials derived from vegetable oil derivatives: a review, RSC. Adv. 13 (6) (2023) 3910–3941.
[301] S. Sfameni, G. Rando, M.R. Plutino, Sustainable secondary-raw materials, natural substances and eco-friendly nanomaterial-based approaches for improved surface performances: an overview of what they are and how they work, Int. J. Mol. Sci. 24 (6) (2023) 5472.
[302] R. Nartita, D. Ionita, I. Demetrescu, Sustainable coatings on metallic alloys as a nowadays challenge, Sustainability 13 (18) (2021) 10217.
[303] Hopkinson, P., et al., Accelerating the transition towards a net zero NHS: delivering a sustainable and resilient UK healthcare sector. 2022.
[304] M. Dieterle, P. Schäfer, T. Viere, Life cycle gaps: interpreting LCA results with a circular economy mindset, Procedia CIRP. 69 (2018) 764–768.
[305] P. Rossini, L. Napolano, G. Matteucci, Biotoxicity and life cycle assessment of two commercial antifouling coatings in marine systems, Chemosphere 237 (2019) 124475.
[306] M. Manfredi, et al., Environmental assessment of antimicrobial coatings for packaged fresh milk, J. Clean. Prod. 95 (2015) 291–300.
[307] H. Liang, et al., Aqueous anionic polyurethane dispersions from castor oil, Ind. Crops. Prod. 122 (2018) 182–189.
[308] X. Wei, et al., Bio-based self-healing coating material derived from renewable castor oil and multifunctional alamine, Eur. Polym. J. 160 (2021) 110804.
[309] N. Karim, et al., Sustainable and multifunctional composites of graphene-based natural jute fibers, Adv. Sustain. Syst. 5 (3) (2021) 2000228.

[310] J. Wei, et al., MWCNTs/CB waterborne conductive smart coating for damage monitoring of composites: design, fabrication, characterization, and verification, Prog. Org. Coat. 172 (2022) 107136.
[311] Bioplastic materials.
[312] M.T.-u. Safian, U.S. Haron, M.M. Ibrahim, A review on bio-based graphene derived from biomass wastes, BioResources 15 (4) (2020) 9756.
[313] J. Chen, et al., Translucent lignin-based omniphobic polyurethane coating with antismudge and UV-blocking dual functionalities, ACS. Sustain. Chem. Eng. 11 (6) (2023) 2613–2622.
[314] X. Zhang, et al., Facile fabrication of fluorine-free slippery antifouling coatings with self-cleaning and anti-microorganism properties, J. Mater. Sci. (2023) 1–12.
[315] N. Balqis, et al., An overview of recycling wastes into graphene derivatives using microwave synthesis; trends and prospects, Materials 16 (10) (2023) 3726.
[316] C. Ungureanu, I. Fierascu, R.C. Fierascu, Sustainable use of cruciferous wastes in nanotechnological applications, Coatings 12 (6) (2022) 769.
[317] O. Vieira, et al., A systematic literature review on the conversion of plastic wastes into valuable 2D graphene-based materials, Chem. Eng. J. 428 (2022) 131399.
[318] W.A. Algozeeb, et al., Flash graphene from plastic waste, ACS. Nano 14 (11) (2020) 15595–15604.
[319] P.A. Advincula, et al., Flash graphene from rubber waste, Carbon 178 (2021) 649–656.
[320] A. Bajpai, et al., Conducting graphene synthesis from electronic waste, ACS. Sustain. Chem. Eng. 9 (42) (2021) 14090–14100.
[321] F. Liu, Y. Chen, J. Gao, Preparation and characterization of biobased graphene from Kraft lignin, BioResources 12 (3) (2017) 6545–6557.
[322] S.-T. Hsiao, et al., Lightweight and flexible reduced graphene oxide/water-borne polyurethane composites with high electrical conductivity and excellent electromagnetic interference shielding performance, ACS. Appl. Mater. Interfaces 6 (13) (2014) 10667–10678.
[323] J. Arroyo, C. Ryan, Incorporation of carbon nanofillers tunes mechanical and electrical percolation in PHBV: PLA blends, Polymers 10 (12) (2018) 1371.
[324] N.F. Attia, et al., Influence of textile fabrics structures on thermal, UV shielding, and mechanical properties of textile fabrics coated with sustainable coating, J. Nat. Fibers 18 (12) (2021) 2189–2196.
[325] N. Karim, et al., Sustainable and multifunctional composites of graphene-based natural jute fibers, Adv. Sustain. Syst. 5 (3) (2021), p. 2000228-n/a.
[326] T. Amrillah, et al., Towards Greener and More Sustainable Synthesis of MXenes: a Review, Nanomaterials 12 (23) (2022) 4280.
[327] M. Rezakazemi, et al., Sustainable MXenes-based membranes for highly energy-efficient separations, Renew. Sustain. Energy Rev. 143 (2021) 110878.
[328] J. Singh, et al., Green'synthesis of metals and their oxide nanoparticles: applications for environmental remediation, J. Nanobiotechnol. 16 (1) (2018) 1–24.
[329] E. Carlos, et al., Solution combustion synthesis: towards a sustainable approach for metal oxides, Chemistry 26 (42) (2020) 9099–9125.
[330] R. Rosa, et al., Life cycle impact assessment of solution combustion synthesis of titanium dioxide nanoparticles and its comparison with more conventional strategies, ChemSusChem. 16 (8) (2023) e202202196.
[331] B. Stieberova, et al., Application of ZnO nanoparticles in a self-cleaning coating on a metal panel: an assessment of environmental benefits, ACS. Sustain. Chem. Eng. 5 (3) (2017) 2493–2500.
[332] Z. Pang, et al., Sustainable synthesis of Cr7C3, Cr2AlC, and their derived porous carbons in molten salts, ACS. Sustain. Chem. Eng. 6 (12) (2018) 16607–16615.